

# Accretion disc winds in X-ray binaries

Teo Muñoz-Darias<sup>1,2\*</sup>, María Díaz Trigo<sup>3†</sup>, Chris Done<sup>4†</sup>,  
Gabriele Ponti<sup>5,6,7\*†</sup>, Ryota Tomaru<sup>8†</sup>

<sup>1\*</sup>Instituto de Astrofísica de Canarias, Via Lactea s/n, La Laguna,  
E-38205, Tenerife, Spain.

<sup>2</sup>Departamento de Astrofísica, Universidad de La Laguna, La Laguna,  
E-38206, Tenerife, Spain.

<sup>3</sup>European Southern Observatory (ESO), Karl-Schwarzschild-Str. 2,  
Garching bei München, 85748, Germany.

<sup>4</sup>Centre for Extragalactic Astronomy, Department of Physics, University  
of Durham, Durham, DH1 3LE, UK.

<sup>5</sup>INAF–Osservatorio Astronomico di Brera, Via Emilio Bianchi 46,  
Merate, I-23807, Italy.

<sup>6</sup>Max-Planck-Institut für Extraterrestrische Physik, Gießenbachstraße 1,  
Garching, 85748, Germany.

<sup>7</sup>Como Lake Center for Astrophysics (CLAP), DiSAT, Università degli  
Studi dell’Insubria, via Valleggio 11, Como, I-22100, Italy.

<sup>8</sup>Department of Earth and Space Science, Graduate School of Science,  
Osaka University, 1-1 Machikaneyama, Toyonaka, Osaka, 560-0043,  
Japan.

\*Corresponding author(s). E-mail(s): [teo.munoz-darias@iac.es](mailto:teo.munoz-darias@iac.es);  
[gabriele.ponti@inaf.it](mailto:gabriele.ponti@inaf.it);

†These authors contributed equally to this work.

## Abstract

Despite early theoretical expectations that large-scale, massive outflows would be triggered by accretion onto black holes and neutron stars, their presence was not firmly established until the 2000s. Since then, they have been recognised as a common, perhaps ubiquitous, feature of accretion discs in X-ray binaries. Over the past two decades, our understanding of these outflows has expanded significantly, with their associated phenomenology now observed across the X-ray, ultraviolet, optical, and near-infrared regimes.

In this review, we provide a comprehensive summary of the observational properties of both low- and high-ionisation winds, treating each separately as well as part of a broader phenomenon, and place these findings in the context of current theoretical modelling. We discuss their close connection with disc atmospheres, their impact on the accretion process, and their role within the broader framework that includes the radio jet and the different accretion flow configurations and states. We also address current challenges and outline some of the anticipated developments, particularly those linked to upcoming observational facilities.

**Keywords:** Black holes, neutron stars, accretion, outflows, winds

## 1 Introduction

The association between accretion onto compact objects and the production of outflows was recognised from the early stages of accretion theory. In fact, these are already described in the model by [Shakura and Sunyaev \(1973\)](#), where a strong outflow of matter is expected to occur at high accretion rates. At that stage, the local accretion rate approaches the Eddington limit and, consequently, radiation pressure due to electron scattering surpasses the gravitational force, leading to the launch of ejecta. Such high accretion rates and ensuing luminosities (approaching the Eddington Luminosity, hereafter  $L_{\text{Edd}}$ ) are possible if the accretor is a neutron star (NS) or a black hole (BH), and thus the presence of massive outflows was naturally anticipated under these critical conditions. However, as we will see, additional launching mechanisms are required to explain the broad observational evidence available today.

In this review, we will present the current observational and theoretical evidence for the presence of non-collimated outflows – hereafter referred to as winds – associated with accretion discs onto stellar-mass BHs and NSs, a topic that we will generally refer to as accretion disc winds in low-mass X-ray binaries (LMXBs). In these stellar systems (see [Bahramian and Degenaar 2022](#) for a recent review), a low-mass star, typically less massive than our Sun, transfers material onto a BH or a NS via an accretion disc, making LMXBs excellent laboratories to simultaneously study accretion and its associated outflow processes. Galactic LMXBs can be bright targets evolving over timescales from milliseconds to years, which makes them particularly well suited for detailed observational studies within human timescales. The same is true for some systems with high-mass companions (i.e. high-mass X-ray binaries), which are also referred to in this review, although in many of them accretion takes place via stellar winds from the massive donor star. Additionally, qualitatively similar winds are also observed, to some extent, in accreting white dwarfs and quasars, and will be briefly mentioned in several sections of the text.

Winds are, together with jets, the two generic classes of outflows observed in LMXBs. The presence of jets associated with X-ray binaries was discovered already in the 1970s (e.g. [Spencer 1979](#)), as they can be spatially extended and are bright in the radio band, where the rest of the components of an LMXB do not emit significant radiation. Jets are collimated outflows, often reaching relativistic speeds (e.g. [Mirabel](#)

and Rodriguez 1999). They can extract a significant amount of energy from the system, although they are not expected to carry away much mass. In contrast, winds typically have lower velocities (up to a few thousand  $\text{km s}^{-1}$ ) and kinetic luminosities, but can carry substantial mass – sometimes even exceeding that ultimately accreted by the BH or the NS (see Fender and Muñoz-Darias 2016 for a review on the mass and energetic balance of jets and winds). Winds, therefore, can have a strong impact on the accretion process itself (e.g. Neilsen et al 2011; Muñoz-Darias et al 2016). In addition, winds might carry away a large amount of angular momentum (e.g. Tetarenko et al 2018), which is key to understanding how matter is ultimately accreted, and more generally, how BH accretion discs operate.

BH LMXBs are, in general, transient sources that go into outburst with recurrence times of years to decades. Their transient nature results from a combination of their relatively long orbital periods – a few hours to several days – and their masses, typically in the range of  $\sim 6 - 12 M_{\odot}$  (e.g. Corral-Santana et al 2016). As a consequence, they tend to have larger accretion discs than their NS counterparts. This implies that higher accretion rates are required to keep the entire disc fully ionised and, therefore, to remain in the active state according to the disc instability model (Lasota, 2001). For this reason, NS LMXBs account for the vast majority of persistent systems (i.e. systems permanently in outburst). During outburst, BH systems are known to show two distinctive accretion states (Miyamoto et al 1992, 1993; see Done et al 2007; Belloni 2010 for reviews). The hard state is displayed at the beginning and end of the outburst. It is characterised by the presence of a relatively cold, likely truncated accretion disc emitting seed photons that are up-Comptonised in a corona of hot electrons, producing hard X-ray emission with a power-law shape (e.g. Gilfanov 2010). In contrast, during the soft state, the X-ray spectrum is dominated by a thermal component, which can, in many cases, be well fitted by a multicolour disc following the Shakura–Sunyaev prescription. These two states are observed following a relatively precise hysteresis pattern, in which a q-shaped track is described in the hardness–intensity diagram (e.g. Homan et al 2001; Belloni et al 2005). The presence of jets is tightly correlated with these accretion states, with a compact jet being a defining property of hard accretion states, and more extended jet ejections, observed during the transitions between hard and soft states (e.g. Fender et al 2004). Phenomenology is arguably more complex in systems harbouring NS accretors, at least regarding spectral analysis, due to the additional emission from the NS surface (and/or boundary layer; e.g. Lin et al 2007; Armas Padilla et al 2017). However, when considering the accretion phenomenology as a whole, including jets (e.g. Migliari and Fender 2006) and fast variability properties, a similar accretion scheme – which also includes hysteresis patterns – can be built (e.g. Muñoz-Darias et al 2014).

Winds entered the accretion-ejection picture in the late 1990s, with the discovery of X-ray absorption features by the *ASCA* mission (Ueda et al, 1998; Kotani et al, 2000). While these early detections hinted at the presence of ejecta, it was only with the advent of higher resolution spectroscopy from *Chandra* and *XMM-Newton* that significant line blueshifts were securely measured and attributed to material being expelled from the system (e.g. Miller et al 2006). In the following years, X-ray signatures of these winds were detected in over twenty systems (see e.g. Ponti et al 2016;

Díaz Trigo and Boirin 2016; Neilsen and Degenaar 2023; Parra et al 2024). This effort has entered a new phase with the advent of the *X-Ray Imaging and Spectroscopy Mission (XRISM)*, whose microcalorimeter (*Resolve*) delivers unprecedented spectral resolution in the X-ray band.

Observations at lower energies – initially in the optical, and increasingly in the near-infrared (NIR) and ultraviolet domains – have opened a new window into the study of BH winds. This progress followed the 2015 outburst of V404 Cyg, during which prominent wind signatures (see Sec. 2) were detected in a dozen optical lines, including a conspicuous nebular phase (Muñoz-Darias et al, 2016). However, wind signatures, although more subtle, were also seen in individual lines during the 1989 outburst of the same source (Casares et al, 1991), and in the BH transient V4641 Sgr (Lindstrøm et al, 2005).

In this review, we approach accretion disc winds as a multiwavelength phenomenon, observed from the X-ray to the NIR. Since the spectral range does not necessarily reflect the physical state of the ejecta responsible for a given transition, we classify winds into two categories based on their ionisation parameter ( $\xi$ ), defined as:

$$\xi = \frac{L}{nR^2} \quad (1)$$

where  $L$  is the source luminosity,  $n$  is the wind density, and  $R$  is the distance of the wind from the illuminating source.

In this context, we consider low-ionisation winds as those with  $\log \xi \lesssim 1.5$  (detected in optical, NIR, and ultraviolet lines), while high-ionisation winds refer to those detected through X-ray lines tracing ejecta with  $\log \xi \gtrsim 1.5$ . We note, however, that this division in  $\log \xi$  is only approximate and should be treated with caution (see Kallman and McCray 1982 for a detailed description of ionic species and the ionisation parameter). To better organise the observational evidence within each category, we often chose to divide low-ionisation winds into *cold* and *cool* types, and high-ionisation winds into *warm* and *hot*, reflecting the different degrees of ionisation inferred from the data.

This review is organised as follows. Sec. 2 describes the main observational signatures from which the presence of low- and high-ionisation winds can be inferred, whose main properties are presented and discussed in Sec. 3 and 4, respectively. Theoretical background and modelling efforts are presented in Sec. 5. Finally, accretion disc winds in X-ray binaries are globally discussed in Sec. 6, while a broad summary and a look at expected developments during the next decade are provided in Sec. 7.

## 2 Observational signatures

Accretion disc winds are revealed by a plethora of characteristic spectral features, primarily emission and absorption line profiles or a combination of both. These features are not necessarily weak; however, they coexist with other spectral components that veil and contaminate them, as we will see below. Additionally, their correct identification, as well as the extraction of key encoded information, such as kinematic properties, requires velocity resolutions of a few hundred  $\text{km s}^{-1}$  at most, ideally less.

This level of precision is achievable at low energies (ultraviolet, optical and NIR; see Sec. 3), typically in combination with the largest ground-based telescopes [e.g. the *Gran Telescopio Canarias (GTC)*, the *Very Large Telescope (VLT)*, and the *Southern African Large Telescope (SALT)*] and space-based facilities such as the *James Webb* and *Hubble* space telescopes. However, achieving this in the X-ray regime has traditionally been challenging, with only *Chandra* and, to some extent, *XMM-Newton* providing relatively precise measurements (see Sec. 4). Fortunately, the recent advent of *XRISM* is enabling, for the first time, X-ray studies at resolutions comparable to those at lower energies.

The observational signatures of disc winds are broadly similar across the different spectral regimes, although, as we will see below, the combination of physical conditions, atomic properties, and observational limitations makes some signatures more frequent or easier to detect in certain spectral domains.

## 2.1 P-Cygni line profiles

P-Cygni (P-Cyg) line profiles are arguably the most reliable indicators of wind-type outflows. These features, named after the supergiant star where they were first observed (Maury and Pickering, 1897; Menzel, 1929; Beals, 1929), are common in massive stars and have been extensively studied in various astrophysical contexts. A P-Cyg profile consists of a blueshifted absorption feature overlapping with a broad emission component (see Fig. 1). Their detection is often considered a definitive signature of an outflowing wind.

Taking the simplest case – photon scattering in a spherically symmetric outflow composed of two-level atoms – regions outside our line of sight absorb photons from the central source and re-emit them in different directions. Some of these photons reach the observer, producing broad emission lines centred around zero velocity. The blueshifted absorption occurs when approaching gas scatters photons out of the observer’s line of sight. The blue-edge of this absorption is usually taken as the characteristic outflow velocity, sometimes referred to as the wind terminal velocity.

The balance between absorption and emission determines the final shape of the P-Cyg profile, which in turn reflects the physical properties of the ejecta. In this simplified scenario, altering the line opacity and plasma conditions can produce profiles without absorption components, flat-top emissions, and other types of distorted profiles, such as skewed ones (e.g. Castor 1970; Proga et al 2002; see also Fig. 2). As already shown by these early works, it is clear that a physically motivated fit to recover the parameters of the outflow is not possible without additional constraints on the properties of the ejecta and the irradiation field. Moreover, assuming scattering of photons by two-level atoms may be valid for resonance lines (i.e., transitions from a ground to an upper level; resonant scattering), such as those associated with some metallic ions in the ultraviolet (e.g., C IV and N V). However, wind-related profiles are frequently observed in recombination lines, making their modelling significantly more complex (see Sec. 3.1).

Things become even more complicated when considering the geometry of the outflow. In the context of LMXBs and other compact binaries, the primary mass source is an accretion disc. Consequently, line-of-sight effects are expected to play a crucial

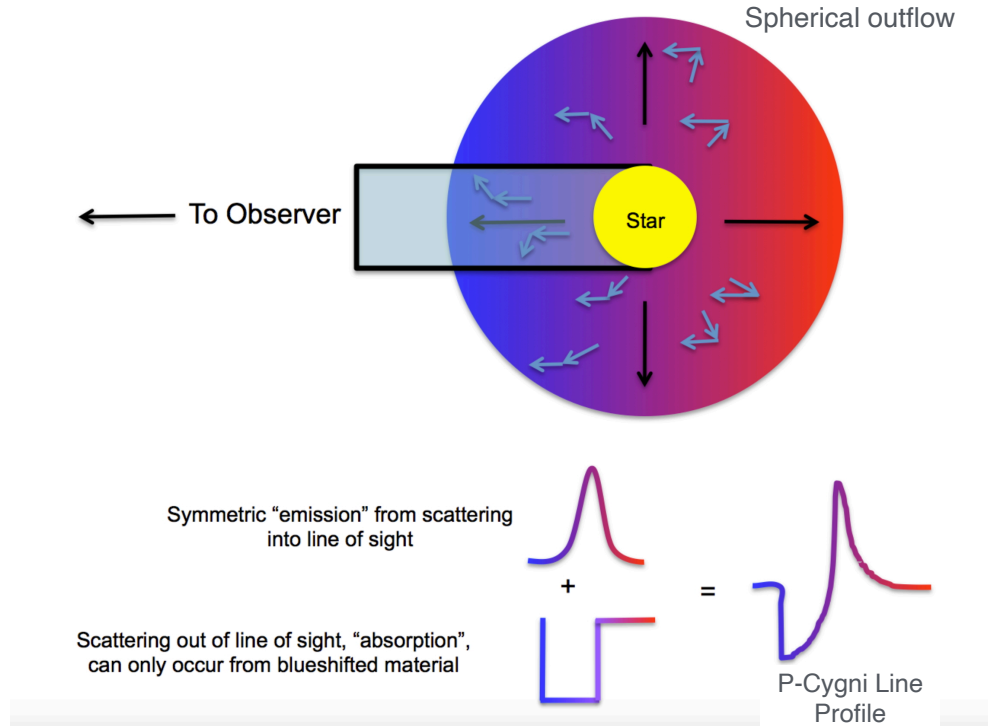


**Fig. 1** Diagram showing the spectral signatures from an expanding spherical wind. The outflow presents significant line opacity around a continuum source (a star in this case, but it can also be a disc), leading to the formation of P-Cygni profiles (sketched at the bottom in an intensity-versus-wavelength representation). These are characterised by an emission component superimposed on a blue-shifted absorption. Black arrows indicate the direction of the outflow, while blue arrows illustrate typical scattering interactions. Adapted from [Matthews \(2016\)](#).

role. The orbital inclination ( $i$ ), defined as the angle between the orbital plane and the observer, strongly impacts the wind's observational signatures. For example, equatorial outflows (e.g. bi-conical winds from the disc) should produce stronger blueshifted absorptions in systems observed close to edge-on ( $i \approx 90^\circ$ ), while the absorption weakens or even disappears at lower inclinations ( $i \approx 0^\circ$ ).

In addition, interpreting wind-related profiles is further complicated by the presence of emission from other spectral components, and in particular the accretion flow itself. In X-rays, the strong disc continuum veils any emission feature, which are often revealed during dips and eclipses (Sec. 4), when part of the disc's emission is blocked by the bulge<sup>1</sup> or the companion star, respectively. In the optical, strong emission lines originating in the disc atmosphere are commonly observed (see also Sec. 6.1). These take the shape of double-peaked lines and are relatively well understood ([Marsh and Horne, 1988](#); [Casares, 2015](#)). However, when combined with P-Cyg profiles, this can

<sup>1</sup>The region of the disc where the incoming stream of material impacts, increasing its vertical size.

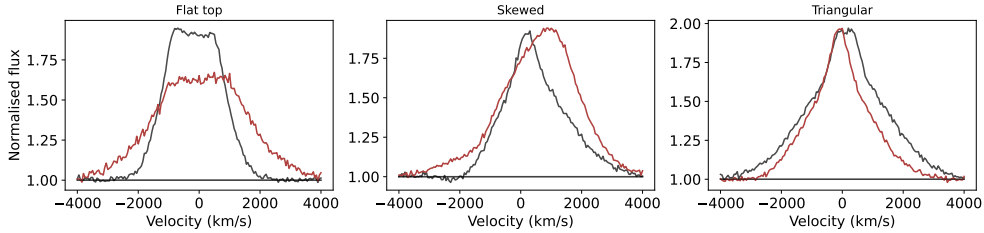


**Fig. 2** Simulated line profiles, distinct from P-Cyg profiles, resulting from the combination of (non-physical) absorption, emission, and double-peaked components expected to play a role in outflows arising in accretion discs. Adapted from [Mata Sánchez et al \(2023\)](#).

result in complex line shapes. A similar situation occurs in the NIR, with an additional challenge: the presence of jet continuum veiling during the hard state, which dilutes – and in some cases completely overshadows – any spectral feature arising from the disc wind or atmosphere. (e.g. [Ambrifi et al 2025](#) and references therein). Nevertheless, conspicuous examples of P-Cyg line profiles have been observed in X-rays (e.g. [Brandt and Schulz 2000](#)), ultraviolet (e.g. [Castro Segura et al 2022](#)), optical (e.g. [Muñoz-Darias et al 2016](#)), and the NIR (e.g. [Sánchez-Sierras et al 2023b](#); see Fig. 3).

## 2.2 Additional wind signatures

As described above, the actual shape of a P-Cyg line profile depends on many factors, including (but not limited to) the geometry, density, and velocity of the expanding outflow (e.g. [Castor and Lamers 1979](#)), as well as possible additional contributions from the accretion flow. Thus, extreme variations of the P-Cyg profile – particularly when one of the components is absent or overwhelmingly dominant – naturally result in characteristic wind signatures. These wind profiles, which we label as ‘additional’ to P-Cyg profiles, can be grouped into the categories described below, with some representative examples shown in Fig. 2. It is worth mentioning that, already in the early days of spectroscopic studies of P-Cygni and other massive stars, up to eight different classes of wind-related profiles were identified. These ranged from the ‘standard’ P-Cyg line profile to those completely dominated by either an emission or an absorption component ([Beals, 1953](#)). Therefore, it is not surprising that similar, if not more complex, phenomenology is also present in LMXBs.

- **Absorption profiles:** The presence of a blueshifted absorption feature can be taken as solid proof of the existence of a wind. This is especially true if two or more lines are detected at a consistent blueshift, allowing for a confident identification of the spectral transitions involved. This is the signature observed in some of the most reliable detections in the X-ray regime (e.g., [Miller et al 2006](#)).

In particular, the presence of Fe XXV and Fe XXVI blueshifted absorptions within the Fe complex at  $\sim 6.7\text{--}7$  keV has been the most prolific method for detecting high-ionisation winds (see Sec. 4). These detections are associated with systems seen at high inclination ([Díaz Trigo et al 2006](#); [Ponti et al 2012](#)) and generally lack the (redshifted) emission component. This may be related to an equatorial wind geometry, which

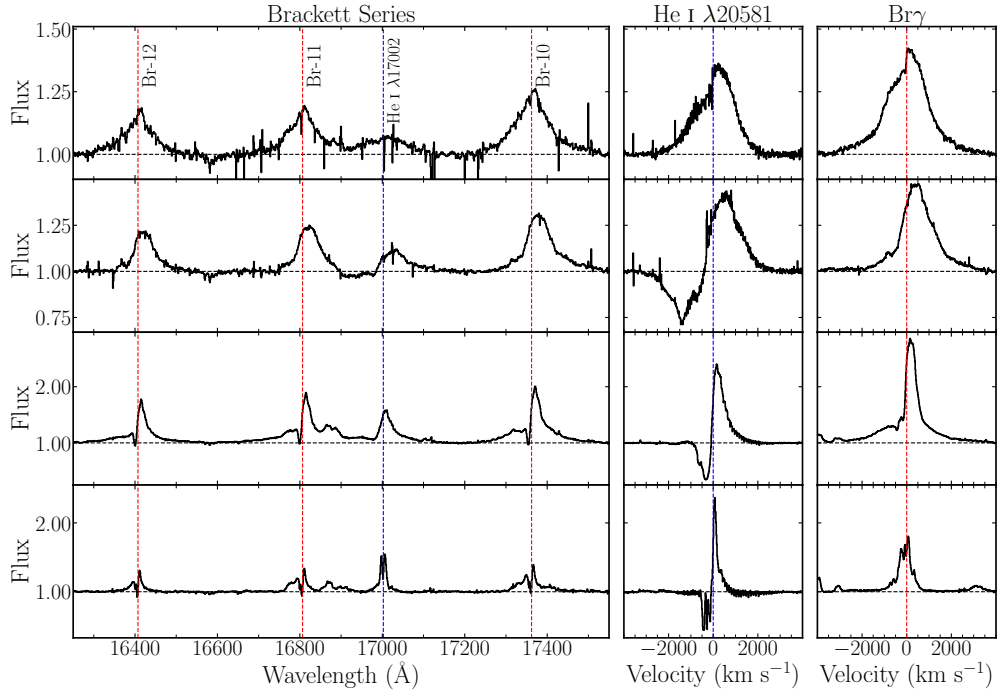


**Fig. 3** NIR wind signatures in GRS 1915+105. Each row corresponds to a different observing epoch, taken from top to bottom in 2019 (19A and 19C) and 2023 (23A and 23D; see [Sánchez-Sierras et al 2023b](#)). Dashed vertical lines mark the rest positions of the different helium (blue) and hydrogen Brackett (red) lines. Different wind signatures are observed depending on the epoch and the specific transition. Brackett lines (left and right columns) are more prone to show emission components (top two panels), which are sometimes accompanied by sharp absorption troughs (bottom two panels). In contrast, He I  $\lambda 20581$  (and  $\lambda 10830$ , not shown) have (typically) higher optical depth and often display strong P-Cyg profiles (middle column; see Sec. 3.1). Adapted from [Sánchez-Sierras et al \(2023b\)](#).

reduces the scattering of photons moving away from the orbital plane. However, the mere fact that the material originates from a disc geometry can explain stronger blueshifts at edge-on lines of sight (e.g., [Higginbottom et al 2019](#)).

Blueshifted absorptions with no associated emission component (i.e. the equivalent of a P-Cyg line profile lacking its emission component; see Fig. 1) are rare in the optical and NIR domains. This can be explained by several factors. On the one hand, emission lines from the disc atmosphere are strong, and when observed together with a blueshifted absorption, they can mimic a P-Cyg profile. Indeed, there are cases of ‘P-Cyg line profiles’ with double-peaked emission, as well as evidence for multiple emission components ([Muñoz-Darias et al 2016, 2020](#)). On the other hand, optical and NIR spectroscopy can be highly sensitive, making it possible to detect emission just a few percent above the continuum level. Additionally, most of the relevant lines in these domains are recombination transitions between excited levels of hydrogen, which are prone to strong emission components (see Sec. 3.1).

- **Emission profiles:** In massive stars, broad emission components are often detected in the ultraviolet and optical domains simultaneously with P-Cyg profiles in other spectral transitions (e.g., [Beals 1953](#); [Prinja and Fullerton 1994](#)). These are also common during certain phases of nova evolution (e.g., [Iijima and Esenoglu 2003](#)). As discussed above, these components can be accounted for by the same principles as P-Cyg profiles (e.g., [Castor 1970](#); see Fig. 2).

Clear examples of this phenomenon are also found in LMXBs, particularly in the optical and NIR regimes (see Fig. 3 and Sec. 3). These lines have full widths at zero intensity of several thousand  $\text{km s}^{-1}$  and are approximately at their rest wavelength, as expected for a P-Cyg profile lacking the blueshifted absorption. Likewise, P-Cyg profiles and broad emission components are seen to alternate in the same spectral transitions over time-scales of just a few days. In these cases, the broad emission profiles meet the blue continuum at roughly the same velocities as those indicated by the blue-edge of the P-Cyg profile (e.g., [Mata Sánchez et al 2022](#)).

An interesting feature often observed in these optical and NIR broad components is the presence of an extended blue wing (or a lack of flux in the red wing). Interestingly, this feature is commonly found in the ionised (e.g., C IV) emission of luminous quasars and is generally thought to be associated with the ubiquitous presence of winds (e.g., [Richards et al 2002, 2011](#); [Matthews et al 2023](#)).

- **Nebular phase:** An extreme example of broad emission lines occurs during the so-called nebular phase. This is characterised by intense emission components with equivalent widths of several hundred to a few thousand Å and high Balmer decrement ( $H\alpha$ -to- $H\beta$ ) values, typically  $\gtrsim 5$ .

This phase was first identified during the 2015 outburst of V404 Cyg ([Muñoz-Darias et al 2016](#); see Fig. 4) and was associated with a cooling, expanding nebula created by a previously launched wind. It was observed after the sudden drop in luminosity that marked the end of the outburst (see also [Casares et al 2019](#); [Rahoui et al 2017](#)), although scaled-down versions of this phenomenon seem to be present in earlier stages ([Mata Sánchez et al, 2018](#)). A similar phase, though much less extreme, was observed in V4641 Sgr ([Chaty et al 2003](#); [Muñoz-Darias et al 2018](#)) and tentatively in the NS transient Aql X-1 ([Panizo-Espinar et al 2021](#)).

- **Flat-top emission profiles** Flat-top, or box-like, emission profiles are commonly observed in outflowing stellar objects, particularly in Wolf-Rayet stars and novae (e.g., [Payne 1930](#)). These broad profiles exhibit nearly constant intensity around their central wavelengths and can be reproduced by considering an optically thin spherical shell of plasma moving at a constant velocity (or with a small spread that avoids zero velocities; [Beals 1931](#)). As such, and in the absence of contamination, they should be considered a reliable signature of the presence of an outflow. These features have also been found in the optical and NIR spectra of LMXBs, particularly in sources with intermediate inclination and sometimes accompanied by blueshifted absorption features (e.g., [Cúneo et al 2020](#); [Panizo-Espinar et al 2022](#); [Ambrifi et al 2025](#)).
- **Distorted and single-peaked emission profiles:** The wind and disc line profiles discussed above can be considered *clean profiles*. However, a greater variety of wind-related profiles can be obtained simply by combining them, even empirically (e.g., [Mata Sánchez et al 2023](#); See Fig. 2). This includes red-skewed profiles and fully

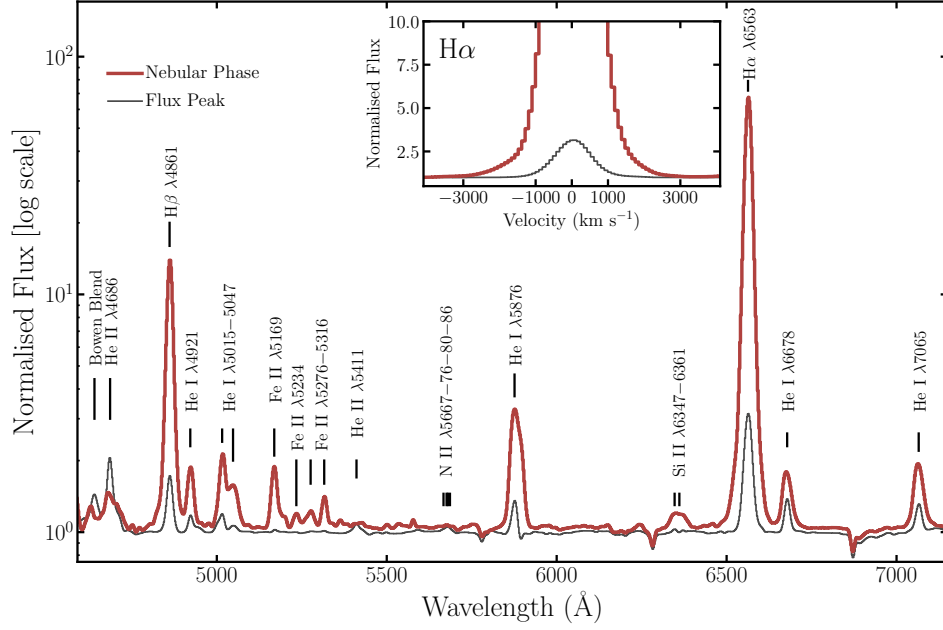


**Fig. 4** The nebular phase of V404 Cyg. Normalised spectra corresponding to the flux peak (black) and the maximum intensity of the nebular phase (red), two days later and following an abrupt drop in the X-ray, OIR and radio fluxes. During this phase, He I and Balmer lines become intense and broad, while additional transitions such as Si II and Fe II emerge. A logarithmic scale is used to represent the intense H $\alpha$  emission, which reached an equivalent width of  $\sim 2000$  Å. A vertical offset of 0.1 has been added to the nebular phase spectrum for clarity. The inset shows the H $\alpha$  region, where broad wings extending to  $\pm 3000$  km s $^{-1}$  are visible. Adapted from [Muñoz-Darias et al \(2016\)](#).

redshifted emission lines, which can be attributed to absorption of the blue part of the emission feature, though not enough to dip below the continuum level. Some clear cases have been detected in LMXBs in the optical regime, appearing simultaneously with P-Cyg profiles (e.g., [Muñoz-Darias et al 2020](#)), the latter occurring in transitions more prone to blueshifted absorption due to atomic properties (see Fig. 3 and Sec. 3.1).

### 3 Low ionisation winds

Over the last decade, and in particular since the 2015 outbursts of the BH transient V404 Cygni, high-quality spectroscopy – mainly at optical wavelengths but increasingly in the NIR and ultraviolet – has revealed signatures of accretion disc winds in LMXBs (see Table 1 and Sec. 3.2). However, earlier detections exist (see Sec. 1), although in some cases they are either restricted to a single transition or the signatures were inconclusive.

Low ionisation winds are primarily detected in transitions of hydrogen and helium, which trace cold gas. Including the detections in He II, as well as the resonance lines

in the far-ultraviolet (e.g. C IV and N v) we can ascribe these low-ionisation winds to *cold-to-warm* (i.e. low-ionised) gas with  $\log \xi \lesssim 1.5$  (e.g. [Kallman and McCray 1982](#)).

### 3.1 Main spectral lines for low-ionised winds

Most low-ionisation wind signatures are found in a common set of spectral transitions. In the optical, the range with the highest number of detections, the strongest signatures are observed in He I at 5876 Å (hereafter He I  $\lambda 5876$ ) and H $\alpha$ . However, additional features, particularly in sources with strong P-Cyg profiles, are also seen in other He I lines such as He I  $\lambda 6678$  and He I  $\lambda 7065$ , as well as in other Balmer transitions. Weak Fe II P-Cyg profiles have also been reported in V404 Cyg ([Muñoz-Darias et al, 2016](#)) and V4641 Sgr ([Lindstrøm et al, 2005](#)).

The NIR has been less explored, with significantly fewer observational campaigns. In addition, some sources exhibit very weak NIR lines during the hard state, particularly at the reddest wavelengths. This is likely due to contamination from a strong jet continuum, which can dilute emission features originating in the disc or disc wind (e.g. [Rahoui et al 2012](#); [Ambrifi et al 2025](#)). Focusing on P-Cyg line profiles in the NIR, the best case study is, by far, that of GRS 1915+105 ([Sánchez-Sierras et al 2023b](#)). In addition to these optical and NIR diagnostics, there are some examples of wind detections on classical ultraviolet resonance lines such as C IV and N v (e.g. [Castro Segura et al 2022](#)), which trace more ionised gas. Likewise, there are a handful of detections in optical and NIR transitions of He II (see Table 1), which also require higher excitation conditions and are typically associated with hotter gas.

#### 3.1.1 Lines tracing cold winds

Balmer, Paschen and Brackett hydrogen lines, together with optical and NIR He I transitions, trace relatively cold gas and often coexist in LMXBs and in other wind-relevant objects such as massive stars. However, not all lines are equally sensitive to outflows. The NIR transitions He I  $\lambda 10830$  ( $2^3S-2^3P$ ) and He I  $\lambda 20581$  ( $2^1S-2^1P$ ) originate from the two  $2s$  levels of the triplet and singlet systems of He I, respectively. These long-lived lower levels can accumulate significant populations, analogous to ground-state levels in ultraviolet resonance lines, making the corresponding transitions particularly responsive to outflows. Of the two, the  $2^3S$  level is much more long-lived and is effectively metastable.

The influence of these metastable levels extends to other transitions connected to them. Combined with the typically higher population of the triplet system compared to the singlet, this helps explain why He I  $\lambda 5876$  ( $2^3P-3^3D$ ) often displays the strongest optical blueshifted absorption features. In contrast, the analogous singlet transition He I  $\lambda 6678$  ( $2^1P-3^1D$ ) is generally weaker due to the lower population and the shorter effective lifetime associated with the  $2^1S$  level.

Hydrogen lines (particularly the Paschen, transitions to  $n = 3$ , and Brackett, transitions to  $n = 4$ , series), while commonly observed as strong emission features, are typically less sensitive to wind-driven absorption than their He I counterparts. This is primarily because they originate from higher- $n$  atomic levels, which are less populated and therefore yield lower line opacity. By contrast, the Balmer series remains

an excellent wind tracer because the  $n = 2$  level is often overpopulated. Under suitable conditions this level can effectively act as a ground state, allowing  $H\alpha$  ( $n = 3 \rightarrow 2$ ) to mimic, to some extent, the behaviour of a resonance transition, as observed in winds from massive stars (e.g. Puls et al 1998; Petrov et al 2014). In this regard, Sánchez-Sierras and Muñoz-Darias (2020) showed that the emission profiles of  $H\alpha$  and He I  $\lambda 10830$  are often similar in BH transients, as both transitions originate from highly populated lower levels and trace overlapping regions of either the disc wind or the disc atmosphere.

### 3.1.2 Lines tracing cool winds

Low-ionisation wind signatures in cool material have been detected via the He II  $\lambda 4686$  line and ultraviolet resonance lines (e.g. C IV and N V; Castro Segura et al 2022; Fijma et al 2023) in a few objects (see Table 1). Ultraviolet resonance lines are primary wind tracers in massive stars (e.g. Kudritzki and Puls 2000) and cataclysmic variables (e.g. Drew and Verbunt 1988; Prinja et al 2000). These lines are formed by resonant scattering – that is, they involve a ground-state lower level – and are particularly sensitive to outflows via blueshifted absorption, often producing conspicuous P-Cyg profiles.

In contrast, the He II  $\lambda 4686$  line is formed by recombination from  $n = 4$  to  $n = 3$  and tends to have lower optical depth, making it less prone to absorption. It primarily traces dense, ionised gas and typically appears in pure emission. However, although rare, P-Cyg profiles in He II  $\lambda 4686$  have also been reported in massive stars (e.g. Herrero et al 2012). In LMXBs, the best example is Swift J1357.2–0933, where the modelling by Charles et al (2019) supports the presence of a hot, dense outflow, possibly favoured by the highly equatorial line-of-sight (see Sec. 3.2.4).

## 3.2 Observations of low-ionised winds

Table 1 presents the list of systems in which observational signatures consistent with the presence of winds have been detected in transitions associated with low ionisation gas. We have divided them into two groups, confident and tentative, according to the typology and confidence we assign to these detections.

In general, we consider confident detections to be those associated with the presence of wind signatures in multiple transitions, especially those that include P-Cyg line profiles or blueshifted absorptions. In total, twelve sources meet these criteria and can be subdivided according to their observed phenomenology.

### 3.2.1 Strong P-Cyg profile sources

Four sources have shown blueshifted absorptions deeper than 10 per cent of the continuum level. These are found across multiple transitions and observing epochs. The sample includes three BH systems (V404 Cyg, V4641 Sgr, and GRS 1915+105), with variable associated velocities reaching up to  $3000 \text{ km s}^{-1}$ , and the NS transient Swift J1858.6–0814, which exhibited blue-edge velocities exceeding  $2000 \text{ km s}^{-1}$ . Thus, these sources have not only shown the strongest P-Cyg profiles but also the highest velocities (see below for the case of Swift J1357.2–0933). These systems have long

**Table 1** Low-ionisation winds: observational evidence

Source (nature)	Signature <sup>a</sup>	Cold <sup>b</sup>	Cool <sup>c</sup>	Vel <sup>d</sup> (km s <sup>-1</sup> )	References
<b>Confident detections</b>					
V404 Cyg (BH)	P-Cyg (>10%), Emi	Optical		1500–3000	1–1e
V4641 Sgr (BH)	P-Cyg (>10%) Emi	Optical Optical		900–1600 ~3000	2–2c
GRS 1915+105 (BH)	P-Cyg (>10%), Emi	NIR		1000–3000	3
Swift J1858.6–0814 (NS)	P-Cyg (>10%)	Optical	UV	1700–2400	4, 4b
MAXI J1820+070 (BH)	P-Cyg Emi	Optical, NIR Optical, NIR		1200–1800 ~1800	5–5c
GRS 1716–249 (BH)	P-Cyg	Optical	He II(?)	~2000	6
Swift J1727.8–162 (BH)	P-Cyg	Optical	He II(?)	1150	7
MAXI J1803–298 (BH)	P-Cyg	Optical		~1250	8
MAXI J1348–630 (BH)	Emi Abs	Optical, NIR Optical, NIR		1500–1700 500–900	9
GX 339–4 (BH)	Emi, Other	Optical, NIR		~1000	10–10c
Swift J1357.2–0933 (BH)	P-Cyg	Optical	He II	1600–4000	11, 11b
UW CrB (NS)	P-Cyg	Optical (?)	UV	1500	12–12c
<b>Tentative detections</b>					
GX 13+1 (NS)	P-Cyg [SL]	NIR		~2400	13
Sco X-1 (NS)	P-Cyg [SL]	NIR		~2600	14
GRO J1655–40 (BH)	Other [T]	Optical			15
4U 1543–47 (BH)	Other [T]	NIR			16
Aql X-1 (NS)	Emi [SL]	Optical		800	17

**Notes.** Horizontal lines separate sources according to the wind detection categories described in Sec. 3.2. **(a)** P-Cyg line profiles, indicating whether the blue-shifted absorption dips below 10% the continuum level (> 10%); Broad emission components, including flat-top and nebular phases (Emi); blue-shifted absorption troughs (Abs.). ‘Other’ refers to skewed profiles, asymmetries in several emission lines. In cases of tentative detections, the reason is indicated in brackets: SL (single line) and T (the features themselves are only tentative or there are alternative explanations). These are further explained in Sec. 3.2.5. **(b)** Detection of cold winds [mainly H (Balmer, Paschen, Brackett series) and He I transitions]. The detection’s spectral range (optical, NIR or both) is indicated. **(c)** Detection of cool winds [He II and ultraviolet (UV; mainly C IV and N V) transitions]. **(d)** Outflow velocity (blue-edge for P-Cyg and Emi).

**References.** (1) Muñoz-Darias et al (2016); (1b) Muñoz-Darias et al (2017); (1c) Mata Sánchez et al (2018); (1d) Rahoui et al (2017); (1e) Vincentelli and Muñoz-Darias (2025); (2) Muñoz-Darias et al (2018); (2b) Lindstrøm et al (2005); (2c) Chaty et al (2003); (3) Sánchez-Sierras et al (2023b); (4) Muñoz-Darias et al (2020); (4b) Castro Segura et al (2022); (5) Muñoz-Darias et al (2019); (5b) Sánchez-Sierras and Muñoz-Darias (2020); (5c) Baglio et al (2025) (6) Cúneo et al (2020); (7) Mata Sánchez et al (2024); (8) Mata Sánchez et al (2022); (9) Panizo-Espinar et al (2022); (10) Ambrifi et al (2025); (10b) Rahoui et al (2014); (10c) Soria et al (1999); (11) Jiménez-Ibarra et al (2019); (11b) Charles et al (2019); (12) Fijma et al (2023); (12b) Kennedy et al (2025); (12c) Fijma et al (2025); (13) Bandyopadhyay et al (1999); (14) Bandyopadhyay et al (1999); (15) Soria et al (2000); (16) Sánchez-Sierras et al (2023a); (17) Panizo-Espinar et al (2021).

orbital periods ( $\gtrsim 1$  day) and are seen at relatively high orbital inclinations ( $\gtrsim 60^\circ$ ). They also display complex outburst evolutions characterised by strong variability as well as variable, intrinsic X-ray absorption (e.g. Motta et al 2017, 2021; Miller et al 2020).

All sources except GRS 1915+105 show these P-Cyg profiles in the optical (hydrogen and He I lines). The latter is well known for its X-ray winds (see Sec. 4), but high extinction prevents optical observations. However, the source is accessible in

the NIR, where wind signatures have been seen simultaneously in multiple lines during the radio-loud, X-ray-obscured stages displayed since 2018 (Fig. 3; Motta et al 2021; Sánchez-Sierras et al 2023b). The deepest blueshifted absorptions appear in He I  $\lambda$ 10830 and He I  $\lambda$ 20581 (i.e. the strongest NIR He I transitions) reaching down to 40 per cent of the continuum.

Finally, in all cases winds are observed simultaneously (or contemporaneously) with radio jets (e.g. Muñoz-Darias et al 2016, 2018; Sánchez-Sierras et al 2023b; see Sec. 6.3). Additional wind features (see Sec. 2), often observed simultaneously with P-Cyg profiles but in different transitions, have also been recurrently detected in these sources.

### 3.2.2 Sources with multiple detections across the accretion states

The BH transients MAXI J1820+070, GRS 1716–249, Swift J1727.8–162 and MAXI J1803–298 have exhibited P-Cyg profiles along with broad emission profiles and other wind-related features in several optical transitions and across multiple observing epochs. The blueshifted absorptions have depths lower than 10 per cent the continuum level (typically between 2 and 5 per cent) and show (blue-edge) velocities between  $\sim$  1000 and 2000 km s $^{-1}$ . With the exception of GRS 1716–249, these systems displayed outburst with both hard and soft states allowing to search and study winds across the different accretion regimes (Muñoz-Darias et al 2019; Sánchez-Sierras and Muñoz-Darias 2020). The overall picture that emerges is that low-ionisation winds are best detected in optical and NIR transitions during the hard state, while these signatures become much weaker or absent during the soft state. However, wind signatures with similar kinematic properties can still be found in NIR transitions during the latter (see Sec. 3.3 below).

### 3.2.3 Lower inclination sources

This group includes two BH transients, MAXI J1348–630 and GX 339–4, which exhibited a roughly similar outburst evolution and observational properties to the previous group. However, they show a different wind phenomenology, and substantial evidence suggests that they are seen at lower inclinations than most, if not all, systems in the previous group (e.g. Muñoz-Darias et al 2013; Carotenuto et al 2021).

MAXI J1348–630 and GX 339–4 have shown compelling evidence for the presence of low-ionisation winds. These signatures primarily include broad and flat-top profiles in multiple transitions across different epochs, as well as red-skewed line profiles. Additionally, MAXI J1348–630 exhibited blueshifted absorption simultaneously detected in several optical and NIR emission lines during the hard-to-soft transition; this feature was also observed in the NIR during the soft state.

This component has a low velocity (centred at  $\sim$  500 km s $^{-1}$ ) and was seen to either dip below the continuum level (i.e. a classical P-Cyg profile) or appear as an absorption trough on the blue wing of emission components, depending on the transition (Panizo-Espinar et al, 2022). The system also shows broad lines with a prominent blue emission wing, which meets the continuum at a larger velocity, comparable to those seen in the previous group (up to 1700 km s $^{-1}$ ).

GX 339–4 has exhibited similar phenomenology to MAXI J1348–630 (e.g. broad, flat-top, and asymmetric profiles; e.g. [Ambrifi et al 2025](#)) in several outbursts, albeit without any blueshifted absorption.

### 3.2.4 Very high inclination sources with distinct detections

Two sources have shown confident detections associated with unique properties. Interestingly, both have short orbital periods and are observed at very high orbital inclination ( $i \gtrsim 80^\circ$ ).

Swift J1357.2–0933, a BH transient with a 3-hour orbital period, is best known for its optical dips, which recur on minute time-scales (e.g. [Corral-Santana et al 2013](#); [Paice et al 2018](#); [Panizo-Espinar et al 2024](#)). Dip-resolved optical spectroscopy has revealed strong blueshifted absorptions associated with these dips. They indicate blue-edge velocities up to  $4000 \text{ km s}^{-1}$  (e.g. [Jiménez-Ibarra et al 2019](#)).

UW CrB (1E 1603.6+2600) is one of the shortest-period LMXBs, with an orbital period of 111 minutes ([Morris et al, 1990](#); [Armas Padilla et al, 2023](#)). This eclipsing NS system has exhibited transient ultraviolet P-Cyg profiles (Si IV and N V) with blue-edge velocities of  $\sim 1500 \text{ km s}^{-1}$ . While possible hints of similar signatures have been reported at optical wavelengths, wind detections remain unconfirmed outside the ultraviolet domain (see [Fijma et al 2023](#); [Kennedy et al 2025](#); [Fijma et al 2025](#)).

Interestingly, both sources exhibit wind signatures in lines tracing warmer material (i.e. cool winds). Swift J1357.2–0933, in particular, has provided the clearest examples of He II P-Cyg profiles during dips. The modelling by [Charles et al \(2019\)](#) suggests that these detections favour hotter and denser ejecta than that typically associated with cold winds. Given the high inclinations of these sources, it is tempting to associate these detections with the high densities expected in equatorial winds, particularly when the line of sight is nearly parallel to the orbital plane. In this context, the high velocities observed in Swift J1357.2–0933 could be better understood as part of an equatorial wind component.

It is worth mentioning that the other LMXB that has shown cool winds, the NS transient Swift J1858.6–0814 (detected in ultraviolet lines by [Castro Segura et al 2022](#)), is also an eclipsing source. However, its orbital period is 21 h ([Buisson et al 2021](#)), much longer than that of UW CrB.

### 3.2.5 Tentative detections

At least five additional sources have shown signatures that we qualitatively classify as tentative. We note that in the case of low-ionisation winds, detections labelled this way do not generally mean that the observed features are non-significant or caused by artifacts, but rather that there are other, plausible interpretations.

- **GX 13+1 and Sco X-1:** Strong Br $\gamma$  P-Cyg profiles were reported in these two luminous NS X-ray binaries ([Bandyopadhyay et al, 1999](#)). Both profiles show similar absorption depth ( $\gtrsim 10$  per cent below the continuum level) and blue-edge velocity ( $\sim 2500 \text{ km s}^{-1}$ ). However, they are not seen in other transitions that are typically more prone to P-Cyg profiles (e.g. He I; see Sec. 3.1), nor in earlier spectroscopy of either object ([Bandyopadhyay et al, 1997](#)).

There are several reasons to treat these detections with caution. First, the P-Cyg profiles are only seen in  $\text{Br}\gamma$ , a line affected by telluric absorption on both the blue and red wings. At low spectral resolution, this is difficult to correct and may result in spurious absorption components. In fact, high-resolution studies of systems with strong NIR P-Cyg profiles have never found them in this transition, which instead often shows very broad emission profiles (see Fig. 3; [Sánchez-Sierras et al 2023b](#)). It is also striking how similar the observed P-Cyg profiles are in both sources, especially given the significant difference in inclination. In particular, most modern studies of Sco X-1 have failed to detect P-Cyg profiles in either  $\text{Br}\gamma$  ([Mata Sánchez et al, 2015](#)) or other NIR transitions ([Muñoz-Darias et al., in prep](#)). Thus, wind detections in these objects remain tentative.

- **GRO J1655–40 and 4U 1543–47:** Both BH transients have exhibited peculiar emission profiles that might be linked to wind activity. However, their classification remains ambiguous. In the case of 4U 1543–47, a low-inclination source, sensitive NIR spectroscopy during its ultraluminous state is reminiscent of that seen in other low-inclination systems (Sec. 3.2.3), although the signatures are significantly more subtle ([Sánchez-Sierras et al, 2023a](#)). GRO J1655–40 shows very complex optical line profiles ([Soria et al, 2000](#)). Given the high inclination of the system and the strong signatures of X-ray winds it has displayed (e.g. [Miller et al 2006](#)), these features may be linked to low-ionisation outflows. This system should be considered a prime candidate for low-ionisation wind searches in future outbursts.
- **A nebular phase in Aql X-1:** Detailed optical spectroscopy of the prototypical NS X-ray transient Aql X-1 revealed a highly ionised spectrum from the early phases of its 2016 outburst, with very weak hydrogen (Balmer) and He I lines ([Panizo-Espinar et al, 2021](#)). However, enhanced Balmer emission, especially in  $\text{H}\alpha$ , was observed at the end of this luminous event. The line profile, as well as other observables such as the Balmer decrement (i.e. the  $\text{H}\alpha$ -to- $\text{H}\beta$  ratio), are reminiscent of a nebular phase. This is, however, characterised by relatively low velocities (the lines meet the continuum at  $\sim 800 \text{ km s}^{-1}$ ), which does not rule out an alternative scenario in which the nebular-like line profiles are formed in the disc atmosphere.

### 3.3 Wind visibility across the states and ionisation effects

As described above, the picture that emerges from observational studies of low-ionisation winds is that they are preferentially detected during the hard state (i.e. when the radio jet is active). These detections have been made primarily in the optical regime, most notably in the  $\text{H}\alpha$  and He I  $\lambda 5876$  lines. In contrast, such optical wind features are typically absent during the soft state, with only occasional weak detections reported during soft-intermediate states in some sources. Observations in the NIR remain scarce, but conspicuous signatures have been found during the hard state and the hard-to-soft transition, similarly to what is observed in optical lines. However, growing evidence suggests that, in some cases (see below), these features persist—at least to some extent—during the soft state. (e.g. [Muñoz-Darias et al 2019](#); [Sánchez-Sierras and Muñoz-Darias 2020](#); [Panizo-Espinar et al 2022](#); [Ambrifi et al 2025](#)). This observational picture contrasts markedly with that of high-ionisation winds (Sec. 4), as discussed further in Sec. 6.

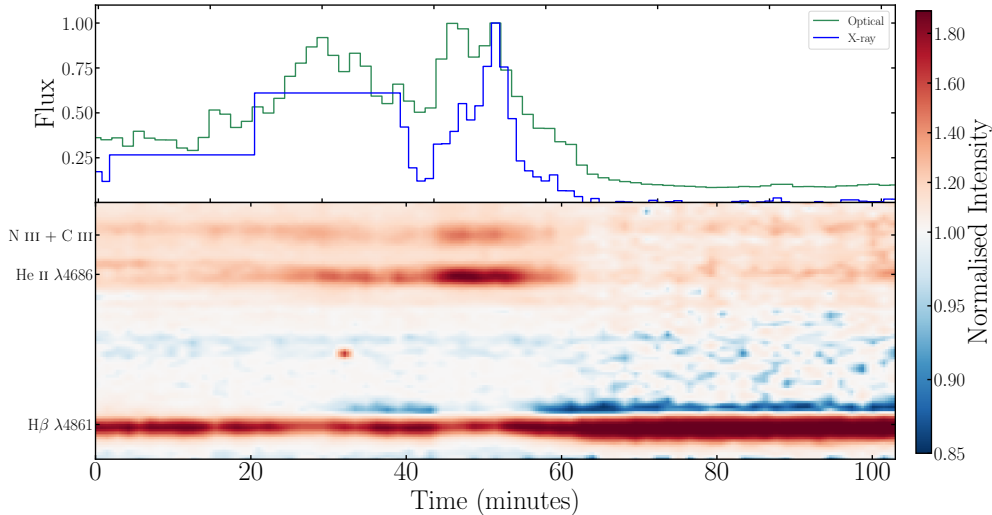


**Fig. 5** Minute time-scale evolution of wind features in V404 Cyg. Top panel: Optical and X-ray light curves (normalised to the peak) during a 103 min GTC spectroscopic window. Bottom panel: Trailed spectrum (from 75 individual spectra) showing the evolution of  $H\beta$  (bottom), as well as  $He\ II\ \lambda 4686$  and the Bowen blend (approximately  $N\ III + C\ III$  at  $\lambda \sim 4640\ \text{\AA}$ ). The  $H\beta$  blue-shifted absorption (blue horizontal band) disappears during the main flare, when the higher ionisation features (i.e.  $He\ II$ ,  $N\ III$  and  $C\ III$ ) become stronger. From data originally presented in [Muñoz-Darias et al 2016](#).

There is solid evidence indicating that ionisation effects significantly impact the visibility of the wind, which might help explaining the above picture. In V404 Cyg, the system with arguably the richest low-ionisation wind dataset, wind signatures are only observed at low  $He\ II/H\beta$  ratios ([Muñoz-Darias et al 2016](#)). Likewise, high-cadence spectroscopy reveals how the blueshifted  $He\ I$  components disappear as  $He\ II$  emission becomes stronger during flare events (see Fig. 5). Interestingly, this complex variability in wind-affected line profiles can, in turn, be used for deep searches of wind signatures, as it imprints characteristic shapes in the optical variability spectrum ([Vincentelli and Muñoz-Darias, 2025](#)). Similar results have been obtained in AGN using the same technique ([Igo et al, 2020](#)).

The optical spectra of BH transients during the soft state are characterised by strong high-excitation lines (e.g.  $He\ II$ ,  $C\ III$ ,  $N\ III$ ), consistent with the absence of wind signatures due to the ionisation effects described above (e.g. [Muñoz-Darias et al 2019](#)). In contrast, NIR observations during this state have revealed cold wind signatures, particularly in the  $Pa\beta$  line, but not in  $He\ I$  transitions (e.g.  $He\ I\ \lambda 10830$  and  $\lambda 20581$ ), which typically follow the behaviour of  $H\alpha$  and the optical  $He\ I$  lines. Although the available evidence is limited (see e.g. [Panizo-Espinar et al 2022](#)), the presence of  $Pa\beta$  absorption without a corresponding feature in  $He\ I$  or  $H\alpha$  allows us to speculate on the ionisation structure of the outflow.

As discussed in Sec. 3.1.1, the transition  $He\ I\ \lambda 10830$  is a powerful tracer of stellar and disc winds due to its large oscillator strength and the long-lived metastable  $2^3S$

lower level (see e.g. Erkal et al 2022 for applications in young stellar objects). However, its diagnostic power depends critically on the population of that level, which can be reduced, for instance, under intense irradiation. In such environments, helium is often significantly overionised (i.e. He II dominates), and He I  $\lambda 10830$  absorption may be absent. Although hydrogen is also typically ionised, its high abundance and fast recombination rate can sustain small reservoirs of neutral gas. In these regions, recombination cascades can populate the  $n = 3$  level, enabling Pa $\beta$  absorption ( $n = 3 \rightarrow 5$ ). This absorption component might be absent in H $\alpha$  if the significantly ionised gas makes the required  $n = 2$  population hard to sustain. In addition, the high H $\alpha$  optical depth results in strong emission that fills in any absorption. Thus, under these conditions, Pa $\beta$ , typically less optically thick, can retain a detectable blueshifted absorption component and act as a more sensitive wind tracer.

Br $\gamma$  ( $n = 7 \rightarrow 4$ ), another strong NIR line, shares a similar physical origin with Pa $\beta$ , but it is almost exclusively observed in emission and only rarely shows wind-related absorption features. This is likely due to its intrinsically lower opacity (transition involving  $n = 4$  instead of  $n = 3$ ), which makes it typically less sensitive to absorption. It is worth noting that in particularly strong winds, such as those observed in GRS 1915+105, absorption components can appear superimposed on both the Br $\gamma$  and Pa $\beta$  emission profiles. However, in these cases, strong P-Cyg profiles are detected in He I  $\lambda 10830$  and He I  $\lambda 20581$  (Fig. 3; Sánchez-Sierras et al 2023b).

## 4 High ionisation winds

We consider high-ionisation winds to be those detected in the X-ray domain, typically characterised by  $\log \xi \gtrsim 1.5$ . They have been primarily identified through absorption lines of Fe XXV and Fe XXVI, which trace plasma with ionisation parameters of  $\log \xi \sim 3$ –6. We refer to these as *hot winds*. However, as we will show, there are also detections of X-ray lines tracing lower-ionisation plasma, which we designate as *warm*. While the first detections of such lines were made by *ASCA* (Ueda et al, 1998; Kotani et al, 2000), determining significant line blueshifts ( $\gtrsim 200$ –2000 km s $^{-1}$ ) only became possible with the resolution of gratings aboard *Chandra* and *XMM-Newton*. Since 2024, *XRISM* has been pushing these boundaries down to just a few tens of km s $^{-1}$ .

Tables 2 and 3 list the BH and NS systems, respectively, with detections of highly ionised absorbers. Following Sect. 3, we have divided the detections into two groups: confident and tentative. Confident detections are those in which (i) at least one absorption line is detected at more than  $5\sigma$  in high-resolution spectra, (ii) multiple lines are identified with high significance in low-resolution data, or (iii) a single line is consistently detected in observations with different instruments.

We note that, even when the lines are confidently detected, their blueshift may not be reliable. This is often the case for observations performed at low resolution; when the Fe XXV and Fe XXVI transitions appear blended due to limited spectral quality; when spectra are modelled with a reflection component in addition to the absorber (introducing model degeneracy); or when two absorbing components are modelled but their lines are not spectrally resolved.

Given the resolution of the *Chandra* and *XMM-Newton* gratings, we conservatively quote only those shifts  $\gtrsim 200 \text{ km s}^{-1}$ , while those down to a few tens of  $\text{km s}^{-1}$  fall within the realm of *XRISM*. Overall, the majority of the BH systems and one third of the NSs show significant blueshifts (Table 2 and Table 3, respectively). In many of these sources, lines have been detected on multiple occasions, and for BHs in particular, changes in velocity between observations have been reported.

The majority of sources show the lines in absorption. P-Cyg profiles have rarely been detected, with all cases appearing at high luminosities ( $\gtrsim 0.5 L_{\text{Edd}}$ ; Brandt and Schulz 2000; King et al 2015). On the other hand, emission lines<sup>2</sup> are often observed in *Accretion Disc Corona* sources. This is a phenomenological class of LMXBs, seen at very high inclination ( $\gtrsim 80^\circ$ ), for which scattered emission from the extended wind or atmosphere becomes apparent as the direct emission from the central source is blocked by the disc rim. However, a more general condition for seeing emission lines is likely to obscure the central engine (due to inclination or by other means), so that the emission lines can stand out above the continuum. As we discuss below, emission lines are more often seen in optical and NIR spectra (see Sec. 6.1).

Finally, we note that in what follows we do not discuss absorption from plasmas during ‘dips’, particularly those associated with the impact of the accretion stream onto the disc and/or the presence of a thickened bulge at the disc rim during specific orbital phases (unless explicitly indicated).

#### 4.1 Main spectral lines for high ionisation winds

The main signatures of a high-ionisation plasma are Fe XXV and Fe XXVI. Detection of Fe XXVI typically implies  $\log \xi \gtrsim 3$ , and we will associate these signatures to hot winds. However, the Spectral Energy Distribution (SED) strongly affects the absolute value of  $\xi$ , and differences of up to one order of magnitude can arise for the same plasma when illuminated by different SEDs. In addition, the SED also influences whether plasma showing Fe XXV and Fe XXVI transitions may additionally exhibit lines down to O VIII or Ne X. For instance, the more than 60 lines detected in the spectrum of MXB 1659–298, spanning from Ne X to Fe XXVI, were satisfactorily modelled with a single plasma component of  $\log \xi \sim 3.8$  and a column density of  $10^{23.5} \text{ cm}^{-2}$  (Ponti et al, 2019). In contrast, Allen et al (2018) required at least two plasma layers to explain the presence of both Mg XII and Fe XXVI in GX 13+1.

We note that the number of detections associated with  $\log \xi \sim 2$ –3 and below may be underestimated as result of observational biases (see Sec. 4.5). Fe K transitions other than Fe XXV–Fe XXVI are blended at pre-*XRISM* resolutions (e.g. Kallman et al, 2004), while the strongest transitions for plasmas with  $\log \xi \sim 2$ –3 and  $\log \xi \sim 1$ –2 correspond to the Fe L and Fe M shells, located at  $\sim 1 \text{ keV}$  (e.g. Gu et al 2019) and  $\sim 0.7$ – $0.8 \text{ keV}$  (Behar et al, 2001), respectively. Detecting such transitions in LMXBs is challenging, as these systems are typically located in the Galactic plane, which is often heavily obscured by interstellar gas and dust along the line of sight. For example, among all LMXBs with confident line detections listed in Tables 2 and 3, about 40 percent have column densities above  $10^{22} \text{ cm}^{-2}$ , while only one source, EXO 0748–676,

---

<sup>2</sup>We list significant detections of narrow lines, up to widths of  $\sim 1000$ – $2000 \text{ km s}^{-1}$ , thus excluding relativistically broadened lines.

is observed through a column density below  $10^{21} \text{ cm}^{-2}$ . Overall, in Tables 2–3, only a few sources show detections spanning from O VIII and Ne X to Fe XXVI. We emphasise that modelling the full set of lines with a photoionised plasma and a broadband SED is required to robustly assign such features to one or more plasma components (see Sec. 4.4).

## 4.2 Black hole systems

Table 2 lists both confident and tentative detections of high ionisation winds in BH systems, together with the range of outflow velocities measured for each source. Most detections correspond to hot winds (i.e. Fe XXV and Fe XXVI lines), while observations of warm winds are restricted to a few cases, for which a selection of transitions associated with lower  $\xi$  is given.

### 4.2.1 Confident detections

The eight systems with confident detections indicate outflow velocities ranging from a few hundreds (i.e. pre-*XRISM* resolutions) to  $\sim 4000 \text{ km s}^{-1}$ . We do not report the outflow velocity for the absorbing plasma of IGR J17091-3624. In this source, Fe XXV and Fe XXVI absorption lines are detected at high significance in *NICER* data, although the limited resolution (i.e. not a grating) does not enable to constrain the velocity (Wang et al, 2024). Likewise, *Chandra* observations of the same source reveal an absorption feature that, if identified with Fe XXV, would correspond to a velocity of  $\sim 9 \times 10^3 \text{ km s}^{-1}$ . This may be accompanied by another absorption component, tentatively detected, indicating  $\sim 15 \times 10^3 \text{ km s}^{-1}$ . In addition to the possible uncertainty in line identification, the significance of these detections varies between 2 and  $6\sigma$ , depending on the assumed underlying continuum, thus falling into the category of tentative detections (King et al, 2012).

Confident detections have been found in high-inclination systems, supporting an equatorial geometry for these outflows (see Sec.6.2). Furthermore, they are much more frequently detected during the softest states, as discussed in Sec. 4.5 (see also Sec. 6.3).

### 4.2.2 Tentative detections

Table 2 also lists sources with tentative evidence for X-ray winds, a large fraction of which correspond to single-line detections in low-resolution spectra characterised by complex underlying continua. These tentative detections are generally associated with systems observed at low to intermediate inclinations, during or near the hard state.

- **EXO 1846–031 and MAXI J1631–479:** In these two sources, a single line was detected in low-resolution spectra after fitting complex broadband continua (see Wang et al 2021 and Xu et al 2020, respectively).
- **MAXI J1348–630:** The presence of absorption components around 7–7.3 keV has been reported in this source. The low-resolution spectra only allow the identification of either a single line (Chakraborty et al, 2021) or an absorption trough (Wu et al, 2023), once the complex broadband continua is fitted.
- **4U 1543–47:** Prabhakar et al (2023) report the detection of a broad, dynamic absorption feature in the 8–10 keV range, interpreted as originating from a highly relativistic

**Table 2** High-ionisation winds in BH systems: observational evidence.

Source	Signature <sup>a</sup>	Warm <sup>b</sup>	Hot <sup>c</sup>	Vel <sup>d</sup> (km s <sup>-1</sup> )	References
<b>Confident detections</b>					
4U 1630–47	Abs		✓	200–400	1–1m
GRO J1655–40	Abs	Mg xii, Fe xxiv(L), Si xiv	✓	200–1200	2–2p
GRS 1915+105	Abs		✓	200–1100	3–3m
	Emi		✓		3m
H 1743–322	Abs		✓	200–400	4–4j
V404 Cyg	P-Cyg, Emi	Mg xii, Si xiv, S xvi	✓	1500–4000	5, 5b
MAXI J1803–298	Abs		✓	few ×10 <sup>2</sup>	6
IGR J17451–3022 <sup>†</sup>	Abs		✓		7
IGR J17091–3624	Abs	Ne x, Mg xii, Si xiii	✓		8a–8c
<b>Tentative detections</b>					
GX 339–4	Emi [T]		✓		9
EXO 1846–031	Abs [SL, BC]		✓	18000	10
MAXI J1348–630	Abs [SL, BC]		✓	10000	11, 11b
MAXI J1631–479	Abs [SL, BC]		✓	20000	12
MAXI J1820+070	Abs [LR, BC]		✓	4000	13
4U 1543–47	Abs [SL, BC]		✓		14, 14b
MAXI J1810–222	Abs [SL, LR]		✓	15000–45000	15

**Notes.** (a) P-Cyg line profile (P-Cyg); Absorption (Abs); Emission (Emi). In cases of tentative detections, the reason is indicated in brackets: SL (single line), BC (broad continuum on reflection), LR (low-resolution spectra), and T (the features themselves are only tentative or there are alternative explanations). These are further explained in Sec. 4.2.2. (b) Detection of warm winds ( $\log \xi \sim 1.5 - 3$ ). (c) Detection of hot winds ( $\log \xi \gtrsim 3$ ; mainly Fe xxv and Fe xxvi). (d) Outflow velocity (blue-edge for P-Cyg). We only quote velocities above  $\sim 200$  km s<sup>-1</sup> for gratings (*XMM-Newton*/RGS, *Chandra*/HETGS or *Chandra*/LETGS) and above a few tens of km/s for *XRISM*/Resolve. (†) The nature of the compact object, either BH or NS, is unclear.

**References.** (1) Ponti et al (2012); (1b) King et al (2013); (1c) King et al (2014); (1d) Neilsen et al (2014); (1e) Diaz Trigo et al (2014); (1f) Miller et al (2015); (1g) Wang and Méndez (2016); (1h) Pahari et al (2018); (1i) Hori et al (2018); (1j) Gatuzz et al (2019); (1k) Zeegers et al (2019); (1l) Trueba et al (2019); (1m) Miller et al (2025); (2) Miller et al (2006); (2b) Diaz Trigo et al (2007); (2c) Sala et al (2007); (2d) Miller et al (2008); (2e) Kallman et al (2009); (2f) Reis et al (2009); (2g) Zhang et al (2012); (2h) Neilsen and Homan (2012); (2i) Luo and Fang (2014); (2j) Madej et al (2014); (2k) Miller et al (2015); (2l) Gatuzz et al (2016); (2m) Shidatsu et al (2016); (2n) Fukumura et al (2017); (2o) Higginbottom et al (2018); (2p) Tomaru et al (2023); (3) Ponti et al (2012); (3b) Neilsen and Homan (2012); (3c) King et al (2013); (3d) Madej et al (2014); (3e) Miller et al (2015); (3f) Lee et al (2002); (3g) Neilsen and Lee (2009); (3h) Ueda et al (2009); (3i) Miller et al (2016); (3j) Zoghbi et al (2016); (3k) Rogantini et al (2020); (3l) Ratheesh et al (2021); (3m) Miller et al (2020); (4) Miller et al (2006); (4b) Blum et al (2010); (4c) Miller et al (2012); (4d) Tetarenko et al (2018); (4e) Shidatsu and Done (2019); (4f) Tomaru et al (2020a); (4g) Ponti et al (2012); (4h) King et al (2013); (4i) Madej et al (2014); (4j) Miller et al (2015); (5) King et al (2015); (5b) Muñoz-Darias and Ponti (2022); (6) Zhang et al (2024); (7) Bozzo et al (2016); (8) King et al (2012); (8b) Gatuzz et al (2020); (8c) Wang et al (2024); (9) Miller et al (2015); (10) Wang et al (2021); (11) Wu et al (2023); (11b) Chakraborty et al (2021); (12) Xu et al (2020); (13) Fabian et al (2020) (14) Prabhakar et al (2023); (14b) Shidatsu et al (2013); (15) Del Santo et al (2023);

disc wind. However, the absorption trough is not resolved into individual lines, and is instead observed in a low-resolution spectrum with an underlying complex continuum.

- **MAXI J1820+070:** Fabian et al (2020) found that adding a hot, outflowing, photoionised absorber to their model significantly improved the fit to complex broadband, low-resolution spectra taken during the soft state.
- **MAXI J1810–222:** Del Santo et al (2023) report an absorption trough around 1 keV in the low-resolution *NICER* spectra, which is interpreted as evidence for an

ultrafast outflow. However, the limited energy resolution prevents the identification of individual absorption lines.

- **GX 339–4:** Miller et al (2015) detect tentative evidence for the presence of broad emission lines in third-order *Chandra* spectra, suggesting the presence of an equatorial high-ionisation wind seen at low inclination.

### 4.3 Neutron star systems

Table 3 lists the 13 NS LMXBs with confident detections of photoionised plasmas, together with nine systems showing tentative detections. Most correspond to hot components (i.e. Fe XXV and Fe XXVI lines), although a significant fraction also exhibit warm plasmas, for which a selection of transitions with lower  $\log \xi$  values are recorded. As discussed below (Sec. 4.5), the non-detection of soft X-ray lines is, in many cases, likely due to a combination of high interstellar absorption and/or relatively low flux at those energies.

#### 4.3.1 Confident detections

Among the 13 NS systems with confident detections, outflow velocities ranging from 200 to 2000  $\text{km s}^{-1}$  have been measured for six of them. For the remaining seven sources, no significant velocity (i.e.  $\gtrsim 200 \text{ km s}^{-1}$ ) was determined, and they are thus consistent with disc atmospheres (see discussion in Sec. 6.1).

Confident detections are classified as such based on the observation of at least two lines (typically Fe XXV and Fe XXVI), identified through grating observations (with 4U 1323–62 being the exception). These are often detected across multiple epochs, which frequently reveal variability in the physical conditions of the plasma. For example, 1A 1744–361 (Gavriil et al, 2012; Ng et al, 2024) shows detections of both Fe XXV and Fe XXVI, although sometimes only Fe XXVI is present. This mild variability is likely driven by small changes in the intrinsic luminosity or the spectral hardness of the irradiating SED. More abrupt variability – such as the presence versus absence of both Fe XXV and Fe XXVI – is observed in systems like AX J1745.6–2901 (Ponti et al, 2015) and MXB 1659–298 (Ponti et al, 2019), which appear to be correlated with the accretion state (see Sec. 4.5).

One source with detections labelled as confident, 4U 1254–69, shows only Fe XXVI. However, this line has been consistently observed across different epochs and with various instruments, which in some cases also reveal the presence of the Fe XXVI  $K\beta$  transition, reinforcing the line identification and indicating a plasma with  $\log \xi \gtrsim 4$  at rest (Boirin and Parmar 2003; Díaz Trigo et al 2009; see also Iaria et al 2007a for a tentative *Chandra* detection). This high ionisation parameter likely explains the absence of soft X-ray features despite the relatively low interstellar absorption ( $2.3 \times 10^{21} \text{ cm}^{-2}$ ) towards this source.

Winds have also been observed in Cir X-1 and GX 13+1, systems that belong to the class of  $Z$  sources, characterised by their particular phenomenology at high luminosity ( $>0.5 L_{\text{Edd}}$ ; e.g. Hasinger and van der Klis 1989; Kuulkers et al 1994; Homan et al 2010). In GX 13+1, winds are consistently observed, showing moderate variability (Ueda et al 2004; Allen et al 2018; XRISM collaboration et al 2025; Fig. 6).

**Table 3** Highly ionised winds in NS systems: observational evidence.

Source	Signature <sup>a</sup>	Warm <sup>b</sup>	Hot <sup>c</sup>	Vel <sup>d</sup>	References
<b>Confident Detections</b>					
4U 1916–054	Abs	Ne x, Mg xii	✓	atm	1–1g
1A 1744–361	Abs		✓	atm	2–2c
4U 1323–62	Abs		✓	atm	3–3c
EXO 0748–676	Abs, Emi	O vii, Ne ix, Ne x	✓	atm	4–4g
4U 1254–69	Abs		Fe xxvi	atm	5–5d
4U 1822–37	Emi	O vii, Ne ix, Ne x	✓	atm	6–6d
MXB 1659–298	Abs	O viii, Ne x, Fe xxiv(L)	✓	atm	7–7e
AX J1745.6–2901	Abs		✓	~ 200	8–8e
4U 1624–49	Abs		✓	~300	9–9e
Her X–1	Abs, Emi	N vi, N vii, O vii	✓	300–1000	10–10e
2S 0921–63	Emi	O vii, O viii, Ne x	✓	<1000	11–11c
Cir X–1	Abs, Emi, P-Cyg	Ne x, Mg xi, Mg xii	✓	300–2000	12–12g
GX 13+1	Abs, Emi	Mg xii, Si xiv, S xvi	✓	300–1000	13–13i
<b>Tentative Detections</b>					
4U 1820–30	Abs [T]	O iv, O v		1200	14
XTE J1710–281	Abs [SL, LR]		Fe xxv?	atm	15, 15b
Swift J1858.6–0814	Emi [T]	N vii, O vii		atm	16
IGR 17062–6143	Abs [T]	O viii?		2000–3500	17, 17b
1RXS J180408.9–342058	Abs [SL]		Fe xxvi?	~26000	18
IGR J17591–2342	Abs [BC]	Si xiii		~3000	19, 19b
IGR J17480–2446	Abs [SL]		Fe xxv?	~3000	20
GRO J1744–28	Abs [SL]		Fe xxv?	~8000	21, 21b
GX 340+1	Abs [SL]		Fe xxv?	~12000	22

**Notes.** (a) P-Cyg line profile (P-Cyg); Absorption (Abs); Emission (Emi). In cases of tentative detections, the reason is indicated in brackets: SL (single line), BC (broad continuum on reflection), LR (low-resolution spectra), and T (the features themselves are only tentative or there are alternative explanations). These are further explained in Sec. 4.3.2. (b) Detection of warm winds ( $\log \xi \sim 1.5-3$ ). Some of the transitions associated with the lowest  $\log \xi$  are given. (c) Detection of hot winds ( $\log \xi \gtrsim 3$ ; Fe xxv and Fe xxvi unless indicated otherwise). (d) Outflow velocity (blue-edge for P-Cyg). Low-velocities consistent with disc atmospheres are indicated marked as *atm*. We only quote velocities above  $\sim 200 \text{ km s}^{-1}$  for gratings (*XMM-Newton*/RGS, *Chandra*/HETGS or *Chandra*/LETGS) and above a few tens of km/s for *XRISM*/Resolve.

**References:** (1) Boirin et al (2004); (1b) Díaz Trigo et al (2006); (1c) Juett and Chakrabarty (2006); (1d) Iaria et al (2006); (1e) Zhang et al (2014); (1f) Gambino et al (2019); (1g) Trueba et al (2020); (2) Gavriil et al (2012); (2b) Mondal et al (2024); (2c) Ng et al (2024); (3) Boirin et al (2005); (3b) Church et al (2005); (3c) Bałucińska-Church et al (2009); (4) Cottam et al (2001); (4b) Jimenez-Garate et al (2003); (4c) Díaz Trigo et al (2006); (4d) van Peet et al (2009); (4e) Ponti et al (2014); (4f) Psaradaki et al (2018); (4g) Bhattacharya et al (2024); (5) Boirin and Parmar (2003); (5b) Díaz Trigo et al (2006); (5c) Iaria et al (2007a); (5d) Díaz Trigo et al (2009); (6) Cottam et al (2001); (6b) Ji et al (2011); (6c) Iaria et al (2013); (6d) Sasano et al (2014); (7) Sidoli et al (2001); (7b) Díaz Trigo et al (2006); (7c) Ponti et al (2018); (7d) Ponti et al (2019); (7e) Iaria et al (2019); (8) Hyodo et al (2009); (8) Ponti et al (2015); (8) Bianchi et al (2017); (8) Trueba et al (2022); (8) Tanaka et al. submitted to PASJ; (9) Parmar et al (2002); (9b) Díaz Trigo et al (2006); (9c) Iaria et al (2007b); (9d) Xiang et al (2009); (9e) Díaz Trigo et al. Submitted to A&A; (10) Jimenez-Garate et al (2002); (10b) Jimenez-Garate et al (2005); (10c) Ji et al (2009); (10d) Kosec et al (2020); (10e) Kosec et al (2023); (11) Kallman et al (2003); (11b) Yoneyama and Dotani (2023); (11c) Tomaru et al (2023); (12) Brandt and Schulz (2000); (12b) Schulz and Brandt (2002); (12c) D’Ai et al (2007); (12d) Iaria et al (2008); (12e) Schulz et al (2008); (12f) Schulz et al (2020); (12g) Tsujimoto et al (2025); (13) Ueda et al (2001); (13b) Sidoli et al (2002); (13c) Ueda et al (2004); (13d) Díaz Trigo et al (2012); (13e) Madej et al (2014); (13f) Allen et al (2018); (13g) Tomaru et al (2018); (13h) Rogantini et al (2025); (13i) XRISM collaboration et al (2025); (14) Costantini et al (2012) (15) Raman et al (2018); (15b) Trueba et al (2022); (16) Buisson et al (2020); (17) Degenaar et al (2017); (17b) van den Eijnden et al (2018); (18) Degenaar et al (2016); (19) Nowak et al (2019); (19b) Manca et al (2023); (20) Miller et al (2011); (21) Degenaar et al (2014); (21b) Younes et al (2015); (22) Miller et al (2016);

On the other hand, Cir X-1 exhibits strong, variable P-Cyg line profiles throughout its different  $Z$ -source phases (Brandt and Schulz, 2000; Schulz and Brandt, 2002; Tsujimoto et al, 2025). However, different ionisation absorbers were instead observed during fainter epochs, when P-Cyg profiles were not detected (Schulz et al, 2008). In addition to variability in the plasma conditions driven by intrinsic changes in the source, orbital variability has also been detected in Cir X-1 (Tominaga et al 2023; see also Xiang et al 2009 for the case of 4U 1624–49).

Finally, we note that complex variability in the wind-related components can also be associated with super-orbital evolution. In particular, thanks to our high-inclination line of sight to the precessing disc of Her X-1, strong super-orbital variability in the plasma properties is observed, which can be used to map the vertical structure of the disc wind (Kosec et al 2020, 2023; see Sec. 6.4).

### 4.3.2 Tentative detections

In addition to the sources showing confident detections, nine other NS LMXBs have displayed possible X-ray wind signatures, which we classify as tentative detections:

- **4U 1820–30:** Costantini et al (2012) reported two features at 6.8 and  $3.8\sigma$  significance, identified as O IV and O V if blueshifted by  $\sim 1200 \text{ km s}^{-1}$ . However, the authors note that the inferred column densities of O IV and O V would imply a C IV ultraviolet line at a level two orders of magnitude above the upper limits obtained from a *Hubble Space Telescope* observation taken 8 years earlier. Moreover, the lines can be equally well fitted with either a photoionised or a collisionally ionised plasma.
- **XTE J1710–281:** Raman et al (2018) reported the detection of two absorption lines at 6.60 and 7.01 keV with *Suzaku*, of which the first one – identified as a blend of Fe XXV to Fe XIX – is highly significant. However, the line is detected in an aggregated spectrum that includes emission occurring during absorption dips, while for the phase-resolved persistent spectrum only a fit with a photoionised absorber ( $\log \xi = 2.6$ ) is reported. No lines could be resolved in *Chandra* observations, likely due to the faintness of the source.
- **Swift J1858.6–0814:** Buisson et al (2020) report an emission line in a *XMM-Newton* spectrum detected at the 99.7% confidence level, which are identified as slightly redshifted N VII. A second line, consistent with O VII at rest, is also present at more than 95% confidence level.
- **IGR J17062–6143:** A handful of low-significance emission and absorption features at  $\sim 0.5$ – $1.5$  keV were reported after modelling the continuum and reflection components. These features were tentatively identified as signatures of a potential outflow (Degenaar et al, 2017). However, a subsequent analysis modelled the features as collisionally ionised absorption from circumbinary material, effectively ruling out the disc outflow interpretation (van den Eijnden et al, 2018).
- **1RXS J180408.9–342058:** An absorption feature at  $\sim 7.64$  keV was reported with a significance of  $4.8\sigma$  in this low-inclination system (Degenaar et al, 2016). Identifying the line with Fe XXVI would imply an outflow velocity of  $\sim 26\,000 \text{ km s}^{-1}$ . In addition to the uncertainty in associating a single line with a specific transition, the unusually

high velocity compared with other LMXB outflows and the low inclination of the system were also raised as concerns by the authors.

- **IGR J17591–2342**: An absorption feature is found at the Si edge in the combined *Chandra* spectrum of this pulsar (Nowak et al, 2019). When identified with Si XIII, it indicates an outflow at  $\sim 3000 \text{ km s}^{-1}$ . However, the significance of the line only reaches  $5\sigma$  for one of the possible models and decreases to  $\sim 3\sigma$  for alternative models with similar goodness of fit. A modelling with a photoionised absorber is not performed. However, we note the rarity of detecting a transition from Si without corresponding transitions from other key elements. The line is not reported in low-resolution spectra (Manca et al, 2023), where potential O VIII and Ne IX features are instead mentioned.
- **IGR J17480–2446**: two absorption features at 6.77 and 6.98 keV were reported by Miller et al (2011) and identified with Fe XXV and Fe XXVI. However, this identification would imply different blueshifts for the lines of  $\sim 3000$  and  $1000 \text{ km s}^{-1}$ , respectively. Thus, modelling with photoionised absorption is challenging due to the different blueshifts implied by the two lines, while including a relativistic disc line to account for the broad superposed Fe emission line results in model degeneracy. These facts, together with the  $3\sigma$  significance of the feature at 6.98 keV and the low inclination of the system justify our classification as tentative.
- **GRO J1744–28**: an absorption feature at 6.85 keV was reported after modelling the X-ray spectrum of this pulsar with continuum and disc reflection components (Degenaar et al, 2014). If identified with Fe XXV, this would imply an outflow at  $\sim 8000 \text{ km s}^{-1}$ . However, modelling the broad Fe emission with a relativistic disc line, instead of a broad Gaussian, reduces the significance of the line from  $\sim 5\sigma$  to  $\sim 3\sigma$ . Moreover, the absorption feature is not reported by Younes et al (2015), who model the emission excess as a blend of neutral Fe, Fe XXV and Fe XXVI at rest, making the detection of the absorption line highly dependent on the modelling of the emission.
- **GX 340+1**: an absorption line at 6.94 keV is reported at a  $5\sigma$  significance level and identified with Fe XXV, implying an outflow of  $\sim 12000 \text{ km s}^{-1}$  (Miller et al, 2016). However, this feature has only been observed in a relatively short ( $\sim 6 \text{ ks}$ ) exposure and not in the numerous, longer observations of the source obtained with the same instrument. While variability is not unexpected, the other two *Z* sources listed in Table 3 display quasi-persistent outflows with multiple transitions. This leads us to consider the detection as tentative.

#### 4.4 Multiple high-ionisation components

In the past two decades, the presence of multiple high-ionisation plasma components has been claimed in a handful of cases (e.g. Iaria et al, 2006; Schulz et al, 2008; Kallman et al, 2009; Allen et al, 2018; Tomaru et al, 2023).

These detections have mostly been reported in studies based on spectra with high spectral resolution and very good statistics, allowing the identification of multiple lines over a broad range of ionisation conditions. However, we note that, in general, the different components have not been resolved in velocity space and, in some cases, their presence strongly relies on the SED used to model the spectra and on whether it can produce a wide range of lines for a single ionisation parameter.

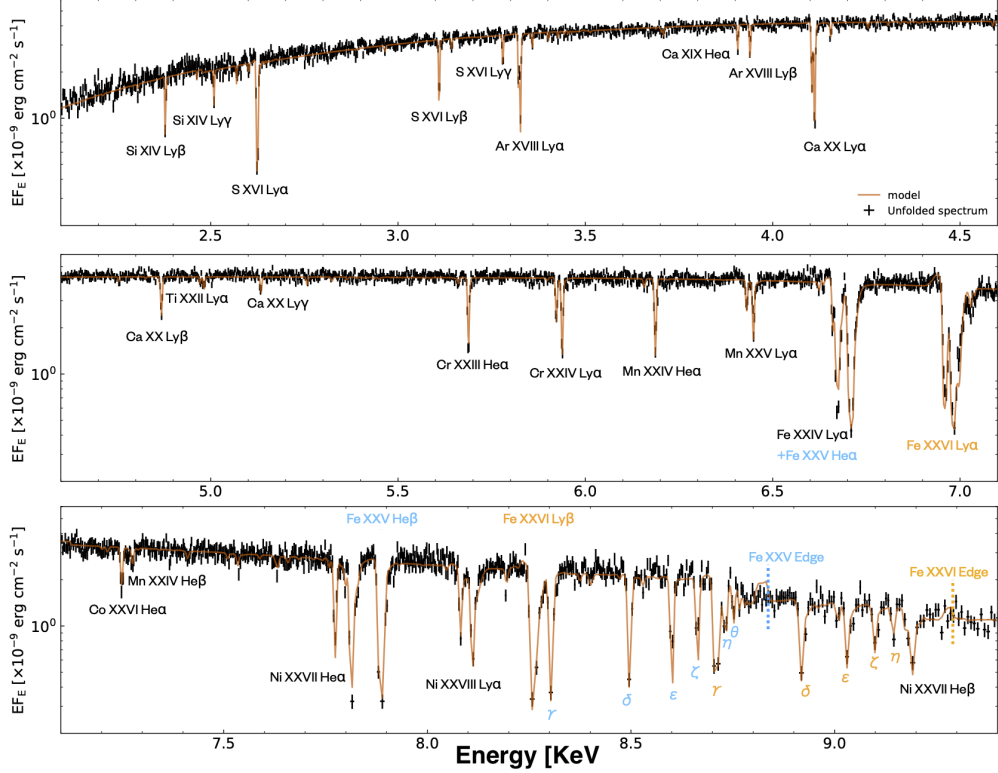


**Fig. 6** XRISM spectrum (black) of GX 13+1 together with the fitted model (orange). The main transitions are labelled, with the Fe xxv and Fe xxvi lines indicated in cyan and orange, respectively. The data were taken during a luminous, likely super-Eddington, epoch. A slower, wind component ( $\sim 300 \text{ km s}^{-1}$ ) and a faster ( $\sim 700 \text{ km s}^{-1}$ ), highly ionised one are detected. Adapted from [XRISM collaboration et al \(2025\)](#).

This picture is quickly changing with the arrival of *XRISM*. The few studies published at the time of writing this review indicate the need for more than one plasma component in several cases (e.g. [Miller et al, 2025](#); [Tsujimoto et al, 2025](#); [XRISM collaboration et al, 2025](#)). However, how these components or plasma phases are structured within the wind has not yet been established. For example, the two wind components resolved in GX 13+1 point to wind stratification (see Fig. 6; [XRISM collaboration et al 2025](#)). Conversely, the two plasma phases seen during a portion of a 4U 1630–47 observation, taken in a low-luminosity soft state, appear to indicate locally coexisting conditions, potentially related to temporary obscuration, such as that caused by a clumped medium. Wind stratification or multi-phase (i.e. spatially coexisting) components are expected in different wind scenarios. Therefore, resolving and characterising the different X-ray components is an important step towards understanding wind structure and launching mechanisms, not only in the context of high-ionisation winds but also in relation to the connection between low and high ionisation wind phases (see Secs. 5 and 6).

## 4.5 High ionisation wind detection across accretion states

In contrast to low-ionisation winds (see Sec. 3.3), the presence of X-ray wind signatures is prevalent during soft states and practically absent in hard states.

### 4.5.1 The observational picture

The current picture of how wind signatures evolve with accretion state is mostly based on monitoring programmes of BH LMXBs across their outbursts. These studies reveal the presence of wind signatures during the softer states of high-inclination sources (see also Sec. 6.2), while such features are typically absent during the hard state (e.g. Neilsen and Lee, 2009; Ponti et al, 2012; Parra et al, 2024).

Overall, NSs offer a consistent, albeit more complex, view than that inferred from BHs. Most of the NS LMXBs listed in Table 3 are persistent sources, and broadband SEDs, as well as timing and multiwavelength data, are not always simultaneously available to allow for meaningful state classification. In fact, our current knowledge relies primarily on three sources that sample hard and soft states in a way comparable to BH outbursts – the *atoll* sources EXO 0748–676, AX J1745.6–2901, and MXB 1659–29 (Ponti et al, 2014, 2015, 2019) – as well as the aforementioned luminous *Z* sources (i.e. Cir X–1 and GX 13+1; see also van der Klis 2006 and Muñoz-Darias et al 2014 for NS accretion states and their comparison to those of BHs).

In order to explain the current observational picture, particularly the prevalence of high ionisation wind detections in the soft state, significant efforts have been made over the past decade. These have focused on determining whether radiative effects—either associated with an overall increase in luminosity or with changes in the SED—and/or a reconfiguration of the magnetic field resulting from accretion state transitions can account for the observations (e.g. Neilsen and Lee, 2009; Díaz Trigo et al, 2014; Gattuzz et al, 2019; Tomaru et al, 2019).

### 4.5.2 Winds, ionisation, and the hard state

The importance of characterising the broadband SED to understand the evolution of plasma conditions cannot be overstated. For instance, NSs exhibit an additional soft, thermal component from the boundary layer, which is absent in BHs. Among NSs themselves, the luminous *Z* sources are generally significantly softer than the fainter *atolls*. Moreover, variability in the physical conditions of the plasma may result from spectral changes not captured by observations limited to a narrow energy band, such as variations in the hard flux above the typical range of X-ray monitoring programmes.

X-ray spectral lines are strongly affected by both the amount (i.e. normalisation) and the shape of the broadband SED illuminating the plasma. Gradual changes in the ionisation state and column density have been observed in several cases (e.g. Miller et al, 2006; Kubota et al, 2007; Díaz Trigo et al, 2014). In particular, plasmas dominated by Fe XXVI can become over-ionised and thus undetectable through line absorption. For instance, the disappearance of the wind when transitioning from a regular soft state to a very luminous one (sometimes referred to as a *very high state*) might be explained by such ionisation effects (Díaz Trigo et al 2014; but see Tomaru et al 2019 for a counterexample).



Finally, we note that while the BH picture seems significantly better established than for NSs, new evidence suggests that more sensitive observations with well-sampled SEDs across the different states are needed. For instance, in the case of 4U 1630–47, *XRISM* has recently detected absorption from Fe XXV and Fe XXVI at rest during a very dim ( $0.05L_{\text{Edd}}$ ) soft state. This was observed shortly before the transition to the hard state during the decay of the outburst (Miller et al, 2025). This contrasts with the absence of lines in a brighter but slightly harder observation during a similar (soft-to-hard) transition previously obtained with *Chandra* (Gatuzz et al, 2019). In another system, IGR J17091–3624, a low ionisation absorber at rest ( $\log \xi \sim 2$ ) has been reported prior to the hard-to-soft transition, simultaneously with the presence of jets (Gatuzz et al, 2020). This was interpreted as a potential precursor to the high ionisation winds observed in the soft state. If such low ionisation X-ray plasmas are indeed present during bright hard states, *XRISM* should be able to detect them in the Fe K band (see Fig. 7), overcoming the limitations associated with detecting them in the soft X-ray band. This highlights the exciting potential of combining *XRISM* observations with optical/NIR spectroscopy during hard states, when low-ionisation winds are best traced (see Sec. 6.3).

## 5 Theoretical wind models and numerical simulations

Launching a wind requires a force which can overcome gravity. There are only three types of pressure forces which can do this, from radiation pressure, hydrodynamic pressure or magnetic pressure. Whatever the driving force, the resulting wind velocity is typically of the order of the escape velocity at the launch radius, so the observed wind velocity can be used as a tracer of this radius via  $v/c \sim (R_g/R)^{1/2}$ .

There is a broader context to understanding winds in X-ray binaries, which is that these may give us a higher signal to noise view of the winds in the supermassive black holes, where they link to AGN feedback. Some of the wind mechanisms described here connect quite naturally across the mass scale. For example, super-Eddington winds driven by radiation pressure on electrons should be similar for objects of different masses. Likewise, self-similar magnetic wind models are expected to scale with mass (e.g. Fukumura et al 2017). Conversely, if the winds differ across systems of different masses, this would point to mechanisms that depend on the specific temperature of the radiation spectrum. In AGN, the accretion disc peaks in the ultraviolet, perhaps enhancing line driving winds, whereas in stellar-mass systems the disc peaks at X-ray temperatures, favouring the production of thermal winds. Thus, understanding winds in LMXBs can also provide valuable clues for interpreting the winds in AGN. These are responsible for AGN feedback, controlling galaxy formation across cosmic time.

There are several types of winds seen in AGN, but typically the fastest ones carry the most kinetic power. Ultra-fast outflows (UFOs) with  $v \sim 0.1\text{--}0.3c$ , detected as X-ray winds in some AGN (e.g. PDS 456; Reeves et al 2009, recently confirmed by *XRISM*; *XRISM collaboration 2025*), are considered the most likely drivers of AGN feedback (e.g. King and Pounds 2015).

While UFOs have not yet been firmly observed in X-ray binaries (although tentative detections exist; see Sec. 4), this does not imply that they are absent. They may

simply be more highly ionised than in AGN, making them difficult to detect. Therefore, we use the observed, much slower X-ray winds in binaries to investigate the underlying wind mechanisms, and then examine what these mechanisms predict for faster material originating at smaller radii. We will focus on the high-ionisation (X-ray) winds, but we will also briefly discuss mechanisms for the low-ionisation (optical/NIR) winds at the end.

## 5.1 Radiatively driven wind

### 5.1.1 Eddington winds

Bright accretion flows very naturally power winds. This was realised even in the earliest paper outlining the disc structure (Shakura and Sunyaev, 1973). Radiation carries momentum, and the momentum is transferred to the gas in the photosphere as the radiation produced within the disc diffuses outwards towards the surface. For completely ionised material, the cross-section for momentum transfer is the electron cross-section,  $\sigma_T$ . This can launch a wind from  $\sim 20R_g$  for  $\dot{m} = L/L_{\text{Edd}} = 2.4$  (higher than Eddington as it requires the local disc flux to be at Eddington, not just the total flux integrated over the entire disc, see e.g. Kubota and Done 2019). This radius increases approximately linearly with higher  $\dot{m}$ , so any moderately super-Eddington flow should launch a wind from 20–50  $R_g$ , where the typical velocity is very fast (0.15–0.2  $c$ ; Shakura and Sunyaev 1973; Poutanen et al 2007).

The first pioneering radiation hydrodynamic (RHD) simulation was by Eggum et al (1988). Multiple others have followed, with increasing resolution driven by the exponential growth of computational power (Ohsuga et al, 2005; Sadowski et al, 2014; Jiang et al, 2014; Zhang et al, 2025). These consistently demonstrate the emergence of outflows with velocities  $\sim 0.1$ – $0.2 c$ . Those are similar to the velocities observed in UFOs in AGNs (see e.g. XRISM collaboration 2025), so superEddington winds are a prime candidate for AGN feedback (e.g. King and Pounds, 2015).

### 5.1.2 Ultraviolet line driven winds

Radiatively driven winds can occur even at luminosities below the Eddington limit if the gas has other processes which provide additional cross-section  $\sigma$  beyond just electron scattering ( $\sigma_T$ ). This reduces the effective Eddington limit where radiation pressure can launch a wind to  $L_{\text{Eff,Edd}} = L_{\text{Edd}}/(1 + \sigma/\sigma_T)$  so winds can be launched for  $(1 + \mathcal{M})L/L_{\text{Edd}} > 1$ , where  $\mathcal{M} = \sigma/\sigma_T$  is known as the force multiplier.

Bound-bound (line) transitions introduce very large but narrowly peaked cross sections that, in static gas, quickly saturates at the line centre and therefore imparts little net acceleration. However, in an accelerating flow, the Doppler shift may move the line centres sufficiently to shift them out of their own absorption cores and into unattenuated continuum<sup>3</sup>. As a result, the line continues to absorb photons and impart momentum, yielding the well-known ultraviolet line-driving mechanism. This process is effective in gases with low ionisation, where a multitude of bound-bound transitions remain available. It is intrinsically non-linear since the local radiative acceleration

---

<sup>3</sup>Formally, the condition is given in terms of the Sobolev length  $l_{\text{Sob}} \equiv v_{\text{th}}/(dv/dl)$ , where  $v_{\text{th}}$  is the thermal speed, and  $l$  is the path length along the radiation direction

depends on the velocity gradient via the Sobolev optical depth<sup>4</sup>. That gradient is, in turn, determined by the radiative force, and the force itself depends on the opacity distribution (Castor et al, 1975), but at its peak it can result in  $\mathcal{M} \sim 4000$ .

The above means that ultraviolet line-driven disc winds can be produced in objects that are inherently less luminous, those with  $L/L_{\text{Edd}} > 10^{-3}$ , if the disk peaks in the UV. This is why the first two-dimensional RHD accretion-disc wind simulations were performed for white dwarfs. (Proga et al, 1998). Any disc luminosity is set by the mass-transfer rate from the companion, giving  $L \sim GMM/(2R_{\text{in}})$ , but  $R_{\text{in}}$  is about  $2000\times$  larger for a white dwarf than for a NS. Thus, the same mass-transfer rate that yields  $L_{\text{Edd}}$  from a NS produces only  $\sim 10^{-3}L_{\text{Edd}}$  in a white dwarf. Hence, the observed winds cannot be powered by radiation pressure alone. However, the white-dwarf disc luminosity peaks in the ultraviolet, with an additional, hotter (ultraviolet/extreme-ultraviolet) boundary layer where the disc impacts the stellar surface. These first RHD simulations showed that ultraviolet line-driven winds could indeed be produced from disc-accreting white dwarfs.

However, the above simulations necessarily made some approximations in order to treat the complex non-linear dependencies of the matter and radiation coupling. In particular, the wind itself filters the radiation field which illuminates any point in the flow. But this radiation field sets the ionisation of the material, which determines how many ultraviolet line transitions can contribute to the force multiplier, which sets the dynamics of the wind, which sets its density, affecting the radiation field. These first RHD simulations of accreting white dwarfs assumed an isothermal outflow with fixed ionisation state to make the calculations tractable. More recent and complete calculations which couple the RHD with Monte Carlo radiation transfer find much weaker winds from accreting white dwarfs (Fig. 8). The issue appears quite fundamental: discs which are sufficiently ultraviolet luminous to produce a line-driven wind are also hot enough to overionise the wind, potentially suppressing it entirely (Higginbottom et al, 2024).

AGN similarly have discs which peak in the UV, but are intrinsically much more luminous, with  $L/L_{\text{Edd}} \sim 0.1 - 1$ . Thus these are systems where the requirement is only  $\mathcal{M} > \infty - \infty$ . However, AGN ubiquitously have an X-ray corona in addition to the UVU emitting disk, and X-rays are very effective at overionising the wind material. Nonetheless, the first simulations showed that the ultraviolet-luminous disc in bright AGN can launch a funnel-shaped wind due to self-shielding (Proga et al, 2000). Ultraviolet line driving lifts material off the disc photosphere, where it is illuminated by X-ray emission from the central source. This overionises it almost immediately, causing the material to fall back down. However, this produces a slightly vertically extended region that casts a shadow, allowing the ultraviolet line-driven wind from further out to be accelerated until it rises above this shadow, reaching higher speeds before it becomes overionised. This, in turn, increases the height of the shadow, and a wind can form if low-ionisation gas is accelerated by ultraviolet line driving within the shadowed region, reaching escape velocity before being exposed to ionising X-rays (Proga et al, 2000).

---

<sup>4</sup>The Sobolev optical depth is the line optical depth across  $l_{\text{Sob}}$

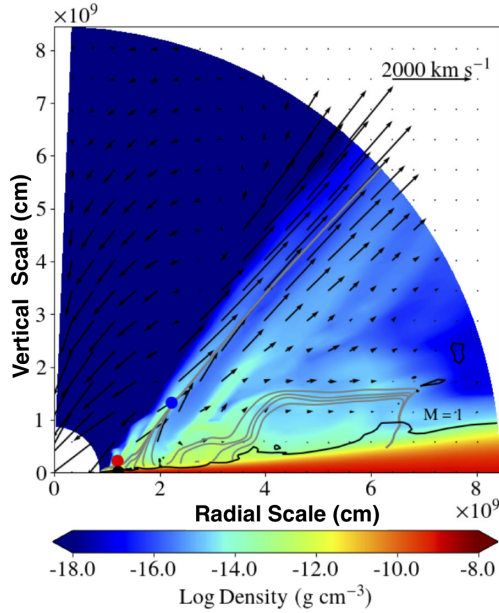


**Fig. 8** The density distribution of ultraviolet-line driven wind for an accreting white dwarf taken by state-of-the-art rad HD simulation (adapted from [Higginbottom et al 2024](#)).

The above provides an alternative mechanism to super-Eddington winds for driving the UFOs discussed earlier ([Nomura et al, 2016](#); [Mizumoto et al, 2021](#)). UFOs are highly ionised, far beyond the range where ultraviolet line driving is effective. Yet, in a two-dimensional disc-wind geometry, ultraviolet line driving can accelerate much less ionised gas within the shadowed region. This gas becomes overionised only after reaching escape velocity, so it is no longer accelerated but follows a ballistic trajectory, producing a highly ionised, high-velocity wind.

These simulation results, though, again rely on approximate radiation transfer to estimate the ionisation structure of the wind. In particular, shadows are crucial for accelerating the outflow, and scattering within the wind can enhance illumination, suppressing the wind ([Higginbottom et al, 2014](#)), and better treatment of ionisation within the wind also reduces the predicted outflow rates ([Higginbottom et al, 2024](#)). However, even the best radiative transfer codes remain seriously incomplete. Firstly, they do not yet incorporate the full clumpy structure known to arise in ultraviolet line-driven winds in massive stars. All radiation-driven winds become clumpy once they turn optically thick, as they cast shadows on gas further out, preventing efficient acceleration. Faster material from inner regions collides with slower, shadowed gas, producing a clumpy outflow. In the case of ultraviolet line driving, the shadows occur in velocity space as well (line deshadowing instability), so these winds are inherently highly clumped (see e.g. [El Mellah et al 2018](#)).

Modelling this is challenging even in the spherically symmetric O-star simulations, and no accretion-disc wind codes can yet handle this level of complexity. Secondly, the inner disc may puff up, especially at accretion rates close to Eddington. This would cast

a shadow over the disc, shielding the critical acceleration region from the X-ray flux and enabling the wind to form. A better understanding of AGN disc physics is therefore required to place ultraviolet line-driving simulations—and hence our understanding of the origin of UFOs and AGN feedback—on a more secure footing.

In the above, line-driven winds have been discussed in the context of accreting white dwarfs and AGN, since they have cooler discs than those of LMXBs, which peak in the X-ray domain. This makes the overionisation issues even more challenging than in the case of AGN (see e.g. [Proga and Kallman 2002](#)). Thus, other mechanisms, such as the thermal and magnetic winds (see below), are likely better suited to explain (sub-Eddington) winds in LMXBs, unless stronger-than-anticipated shielding and/or clumps are present.

## 5.2 Thermally driven winds (Thermal winds)

The second type of wind is where the thermal energy of the gas powers the outflow via a force from the pressure gradient. The bright inner disc heats the photosphere at larger radii by illumination, producing a hot skin as was clearly recognised in [Shakura and Sunyaev \(1973\)](#). The electrons in the outer disc photosphere are illuminated by the spectrum from the central regions, and are heated by scattering high energy photons, and cooled by scattering low energy photons. This gives an equilibrium Compton temperature as a weighted sum over the spectral energy distribution  $F(E)$  as:

$$T_{\text{IC}} = 0.25 \frac{\int E F(E) dE}{\int F(E) dE}$$

Typically  $T_{\text{IC}} \sim 10^7 - 10^8$  K in X-ray binaries. Thus X-ray irradiation of the outer disc forms an X-ray heated atmosphere whose temperature depends only on the spectrum of the radiation. This stays constant with radius, but the local gravity decreases with it. Hence, the scale height of the atmosphere increases with radius until it reaches  $H \sim R$  and can escape as a wind. This occurs at radii where the temperature implies a sound speed greater than the escape velocity; that is,  $kT_{\text{IC}} \geq GM/R_{\text{IC}}$ , defining the Compton radius as:

$$R_{\text{IC}} \sim 6.4 \times 10^4 / T_{\text{IC},8} R_{\text{g}}$$

where  $R_{\text{g}} = GM/c^2$  and  $T_{\text{IC},8} = T_{\text{IC}}/10^8$  ([Begelman et al, 1983](#); [Done et al, 2018](#)]. More accurate estimates (see below) show that the wind can be launched at  $\sim 0.2R_{\text{IC}}$ , but this is still a large radius, so the wind is slow.

The behaviour and mass loss rate of thermal winds is strongly related the thermal instability of photoionised plasma produce by X-ray illumination. [Fig. 9](#) illustrates the incident SEDs for typical hard (blue,  $T_{\text{IC}} \sim 10^8$  K) and soft (black,  $T_{\text{IC}} \sim 10^7$  K) state BH LMXBs, with its corresponding thermal equilibrium (heating=cooling) curve to determine the resulting gas temperature for different illuminating X-ray flux  $F_x = L/4\pi R^2$  (right). This is calculated using photoionised plasma codes, such as CLOUDY ([Gunasekera et al, 2023](#); [Ferland et al, 2017](#)) and XSTAR ([Kallman and Bautista, 2001](#)), as the cooling processes include atomic processes such as lines and recombination radiation as well as bremsstrahlung and Compton scattering. Thus, cooling is dependent on metallicity and density, so here we assume solar abundances

and that the gas is at constant pressure,  $P_{\text{gas}}$ . The most physically revealing way to show the behaviour is to plot the gas temperature,  $T$ , not simply versus flux, but rather versus the pressure ionisation parameter  $\Xi = P_{\text{rad}}/P_{\text{gas}}$ . Radiation pressure is simply  $F_x/c = L_x/(4\pi R^2 c)$  while gas pressure is  $nkT$ . Hence, in c.g.s. units:

$$\Xi = L_x/(nR^2T) \times 1/(4\pi kc) = 10^{4.3}\xi/T$$

where  $\xi(= L_x/nR^2$ ; Eq. 1) is the more usual density version of the photoionisation parameter.

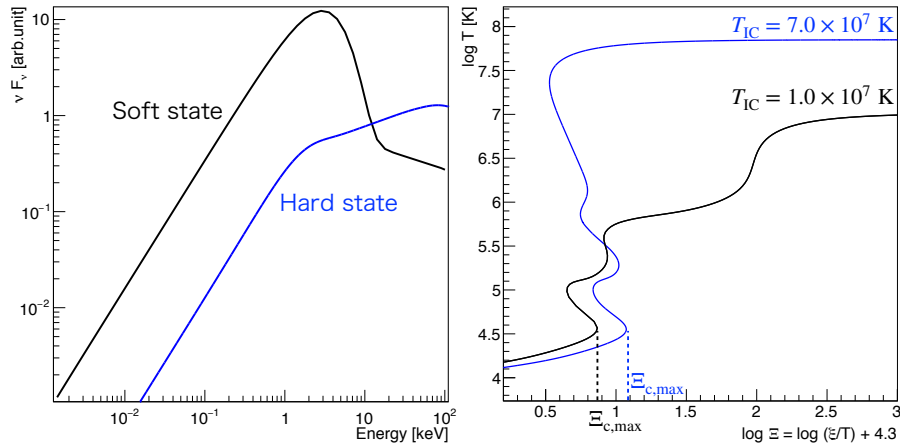


**Fig. 9** The typical SEDs of soft and hard states in BHLMBs to ionised plasma (left) and their corresponding thermal equilibrium curve (right). Adapted from Tomaru et al (2019)

### 5.2.1 Hard spectra mass loss rates

The physics of the heating/cooling process is simpler for a hard illuminating spectrum, as here the gas is completely ionised when there is strong illumination of low-density material (i.e. high  $\Xi$ , the blue lines in Fig. 9). The temperature is set by the balance of Compton heating and cooling, so it reaches  $T_{\text{IC}}$ . As the gas becomes denser ( $\Xi$  decreases), thermal bremsstrahlung (free-free) cooling becomes larger than the Compton process at certain  $\Xi$ , and the temperature drops below  $T_{\text{IC}}$ . Once the gas cools, the electrons can recombine with atoms, and line emission becomes more significant, further enhancing the cooling process. This leads to a very rapid transition from the high-ionisation state at the Compton temperature to the much lower gas temperatures of  $\sim 10^4$  K typical of atomic cooling by hydrogen and helium radiative recombination.

This rapid transition is seen in Fig. 9 (right panel), where the slope of the equilibrium curves changes sign. Those curves indicate heating = cooling, and divide the  $\Xi$ – $T$  plane into regions above/left of the curve where cooling dominates, and below/right where heating dominates. A small perturbation in temperature with constant  $\Xi$  (the gas is isobaric) shifts the gas parcel vertically on the plot. The system is stable if an increase(decrease) in temperature pushes the gas into a cooling(heating) dominated

region, as it will return to the equilibrium curve. This happens if the equilibrium curve has a positive gradient. Conversely, in the regions with a negative slope, a small temperature increase drives the system into a heating-dominated regime, causing further heating until the gas reaches the high Compton temperature (or a smaller intermediate stable branch).

This rapid transition of the thermal instability enables analytic estimation of the mass loss rate from the disc. Material on the disc surface is at low  $\Xi$  as it has high density, so it is at typical atomic temperatures of  $10^4$  K (or the disc surface temperature). If the hard X-ray illumination is bigger than  $\Xi_{c,\max}$  (Fig. 9; right panel) then this triggers the thermal instability and the material moves vertically up to the upper branch at this  $\Xi$ , increasing in temperature by a factor of 1000, producing a hot disc atmosphere. The maximum ionization parameter  $\Xi_{c,\max}$  ( $\approx 12$  for the hard state SED in Fig. 9a) determines the density  $n_c$  at the base of the hot atmosphere/wind at radius  $R$  via the pressure ionisation parameter:

$$\Xi_{c,\max} = L/(4\pi n_c c k_B T_{\text{IC}} R^2)$$

This material becomes unbound and escapes as a wind for  $R > R_{\text{in}} = 0.2R_{\text{IC}}$ , whereas it remains bound as an atmosphere for  $R < R_{\text{in}}$ . In the wind region near the disc, the gas outflow is predominantly vertical with velocity given by the isothermal sound speed:

$$c_{\text{IC}} = \sqrt{k_B T_{\text{IC}} / (\mu m_p)}$$

This velocity is reached as the temperature approaches  $T_{\text{IC}}$  due to rapid heating. The mass loss rate per unit area is given by

$$\dot{m} = 1/2 \mu m_p n_c c_{\text{IC}}$$

with the the total mass loss rate:

$$\dot{M} = 2 \times 2\pi \int_{R_{\text{out}}}^{R_{\text{in}}} \dot{m} R dR = \frac{L}{(2c c_{\text{IC}} \Xi_{c,\max})} \ln(R_{\text{out}}/R_{\text{in}})$$

Here,  $R_{\text{out}}$  is the outer disc radius, which can be constrained from the orbital period of the system, while  $R_{\text{in}}$  is the inner wind radius. This can be simply estimated as  $R_{\text{IC}}$ , or calculated more precisely from the energy equation for a Keplerian rotating hot atmosphere at  $T = T_{\text{IC}}$ :

$$\epsilon = 1/2 v_{\text{K}}^2 + \frac{p}{(\gamma - 1)\rho} + p/\rho - GM/R$$

This gives  $R_{\text{in}} = (\gamma - 1)/(2\gamma)R_{\text{IC}} = 0.2R_{\text{IC}}$ , where  $\gamma = 5/3$  (see Woods et al 1996 for further details). Therefore, the total mass loss rate is then larger for larger luminosities and large disc radii.

On the other hand, the hardness of the spectrum has a complex impact, as harder spectra increase  $T_{\text{IC}}$ , which means the material flows away faster, decreasing the density ( $\propto T_{\text{IC}}^{-1}$ ), and the total mass loss rate ( $\propto T_{\text{IC}}^{-1/2}$ ). However, this is partly compensated by the increase in the range of disc radii over which the wind can be produced (Begelman et al, 1983; Woods et al, 1996; Done et al, 2018).

### 5.2.2 Soft spectra mass loss rates

In cases where the irradiated SED is softer, e.g. in the soft state of BHs (black in Fig. 9), the simple arguments outlined above change slightly since not all elements are completely stripped for  $\Xi > \Xi_{c,max}$  and optical depth effects become important in illuminating the disc. Fig 9 (right panel) is calculated assuming that the X-ray illuminated material is optically thin. However, this is not the case for a soft state SED.

Fig. 9b shows the thermal equilibrium curve for illumination by the soft-state SED. This is no longer a simple S-shaped profile, where the gas jumps from atomic temperatures to  $T_{IC}$ ; instead, there is an intermediate stable branch at  $T \sim 10^6$  K for  $\Xi \sim 10 - 100$ . In this regime, heating resulting from Compton scattering and photoelectric absorption by oxygen and iron ions is balanced by cooling via bremsstrahlung and re-emission from these elements, leading to a plateau. This gas typically has  $\log \xi \sim 2$ , and has considerable absorption opacity, so this gas shields the disc below from illumination. Hence the wind emerges not from  $\Xi_{c,max} \sim 10$  from the disc surface itself, but at the transition between the hot and intermediate branch, at  $\Xi_{h,min} \sim 100$  (Tomaru et al, 2019). Material in the intermediate branch forms a partially ionised atmosphere, transitioning to a very slow wind at larger radii where material at the lower temperature of  $T \sim 10^6$  K can escape.

Simulations, which include only radiative heating and cooling, do indeed show that the slow, outer wind from material in this plateau at  $\sim 10^6$  K can dominate in some soft states (Higginbottom et al, 2017; Tomaru et al, 2019). However, because the gas is not completely ionised in this regime, it can also experience radiative forces due to line absorption and photoionisation. These forces are approximately ten times stronger than those from electron scattering for gas at the plateau ionisation state (standard  $\xi \sim 100$ ), and RHD simulations show that this is important in giving the material an extra push at luminosities  $\gtrsim 0.1L_{Edd}$  (Tomaru et al, 2019). Thus, in soft states, thermal winds are really thermal-radiative winds, where the radiation pressure is due to atomic absorption as well as electron scattering. Although there are some differences in the wind properties between soft states and hard states, especially the ionisation parameter, the mass loss rate of winds is still basically proportional to the luminosity of the central source (Tomaru et al, 2019; Higginbottom et al, 2020).

### 5.2.3 Predicting observables

The analytic thermal wind models predict that the wind material should expand at approximately constant speed,  $c_{IC}$ , so the wind lines should be blueshifted by this factor, and be quite narrow as there is little velocity spread. Both mean outflow velocity and velocity dispersion are directly observable from the line profile, so these can be directly tested.

However, the mass loss rate,  $\dot{M}$ , is not directly observable. Instead, we observe column density and ionisation state along a single sight-line, so this depends on how the mass loss makes a 2D structure. Assuming the wind is radial and at constant velocity gives (Hori et al, 2018):  $N_H \propto \dot{M}/(R_{in}c_{IC}) \propto L \ln(R_{out}/R_{in})$  and  $\xi \propto T_{IC} \propto c_{IC}^2$  (constant with radius as the wind density is approximately  $\propto R^{-2}$ ).

This dependence of  $\xi$  on  $T_{\text{IC}}$  means that the wind features are almost completely ionised in hard states, but not in the soft states. This naturally predicts that absorption lines of H- and He-like Fe are only seen in soft states. The wind may be present in the hard state, with a similar mass loss rate and  $N_{\text{H}}$  to the soft states at similar luminosities, but it can be invisible in terms of atomic features. Alternatively, the hard state wind may be suppressed by shadowing from an inner disc atmosphere (Begelman and McKee, 1983; Tomaru et al, 2019).

These analytic approximations can be used to track the wind in a given source as the spectral shape and luminosity change, where they are quite successful in quantitatively matching the observed trends (Done et al, 2018; Hori et al, 2018; Shidatsu and Done, 2019).

#### 5.2.4 Numerical simulations and match to observations of hot winds

The analytic approximations above only treat the region where the source luminosity is sufficient to heat the base of the wind to the Compton temperature. There are multiple other regions that can be treated analytically (Begelman et al, 1983; Begelman and McKee, 1983; Done et al, 2018). However, these approaches can only take us so far until the neglect of the full 2D wind structure becomes important. Instead, the thermal (and thermal-radiative) winds can be numerically simulated in RHD codes, giving the full 2D behaviour at all luminosities (Tomaru et al, 2019, 2020a; Shidatsu and Done, 2019; Higginbottom et al, 2020). Coupling these with radiation transfer allows detailed calculations of the line profiles for direct comparison with observables.

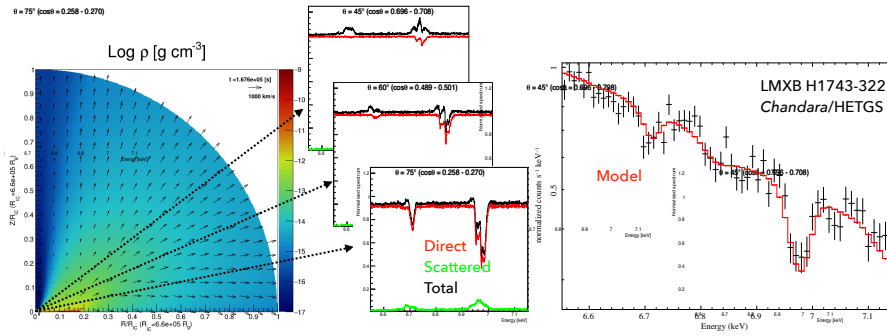


**Fig. 10** The thermal-radiative winds model, which can explain the observed X-ray spectrum. The density distribution of the radiation hydrodynamics simulation included radiative heating and acceleration (left), the line profiles via Monte Carlo radiation transfer in different inclination angles (middle), and the comparison with observation (right). Adapted from Tomaru et al (2019)

These results show explicitly that the SED dependence of thermal (and thermal-radiative) winds can explain the observational absorption line in the soft states and disappearance in the hard states in H1743-322 (Fig. 10), and the observed X-ray absorption line features in GX 13+1 (Tomaru et al, 2020b) by changing the incident SED and outer disc size. Even the unusual high column, low ionisation absorption line features in a dim ( $L \sim 0.05L_{\text{Edd}}$ ) soft state of GRO J1655-40 can be explained by

these models (Tomaru et al, 2023). This is an important test case as the data include a density diagnostic metastable line which requires  $n \sim 10^{14} \text{ cm}^{-2}$  for collisions to populate the level. Combining this with the observed ionisation parameter requires a launching radius  $\ll 0.2R_{\text{IC}}$ , apparently ruling out thermal winds (Miller et al, 2006). However, for soft state spectra the metastable level is instead populated mostly from radiative recombinations, and the data can be reproduced if the source is much more luminous, with  $L \sim L_{\text{Edd}}$ , resulting in more wind, which has gone optically thick, reducing the observed luminosity (Tomaru et al 2023; see also Shidatsu et al 2016).

These radiation transport codes enable the direct study of both wind emission and absorption. The wind scatters some fraction of the illuminating flux, but the hot, photoionised gas also directly emits radiation as free-free and bound-free recombination continua and lines. Usually, those lines can not be observed since the direct source emission is much stronger than those lines. However, when the object is very highly inclined, so that the vertical extent of the disc and/or its atmosphere blocks the direct emission, then the observed flux is dominated by the wind. This is the case in *Accretion Disc Corona* sources, and the previous model can well describe the emission line in the 2S 0921-630 (Tomaru et al, 2023).

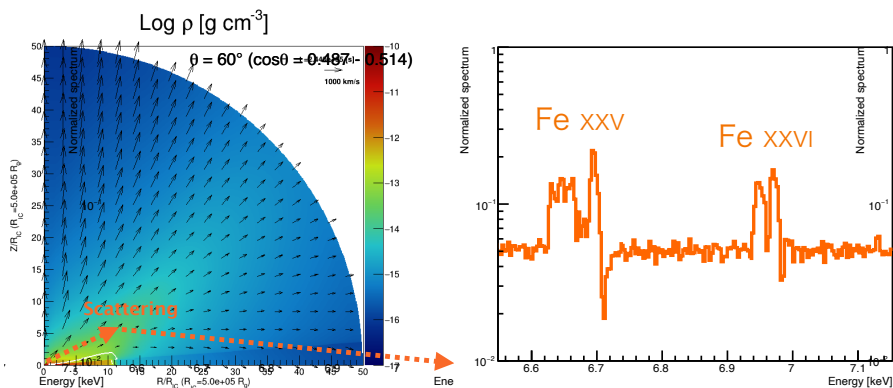


**Fig. 11** The schematic view of the accretion disk coronal source. The density/velocity distribution taken by the RHD simulation (adapted from Tomaru et al, 2020b) and the line profiles obtained by the MCRT simulation (adapted from Tomaru et al, 2023).

### 5.2.5 Numerical simulations and match to observations of cold winds

Despite the success of thermal wind models in reproducing the X-ray line features observed in soft states (i.e. hot winds), they currently cannot easily account for the optical/NIR absorption and emission lines associated with the low-ionised winds predominantly detected during hard states (see Sec. 3.1).

Focussing first on the optical absorption lines, the observed blueshifts require that this low ionisation gas is outflowing at  $\sim 1000 - 2000 \text{ km s}^{-1}$ . These optical absorption lines require low ionisation gas, so might be expected to be at low  $\Xi$ ,

below the thermal instability. But gas here has very low velocity, with sound speed  $c_s = \sqrt{k_B 10^4 \text{ K} / (\mu m_p)} = 10 \text{ km s}^{-1}$ .

Instead, the observed velocity of the optical winds is quite close to the higher velocity ( $\sim 1000 \text{ km s}^{-1}$ ) of material at the high Compton temperature of the hard state ( $\sim 10^8 \text{ K}$ ). However, here the material is far too highly ionised to make the optical transitions.

If these hard state optical winds are indeed thermal winds, then they could be produced if there is some clumping instability which operates after the wind is launched, such that the material returns below  $\Xi_{c,\text{max}}$  and triggers the thermal instability in reverse. Adiabatic expansion alone cannot do this as  $\Xi$  *increases* in the expanding wind as the density drops as  $R^{-2}$ , far faster than the temperature. Instead, it requires some other mechanism to compress the gas to trigger the thermal instability, perhaps via interaction with higher inclination, slower material forming the disc photosphere. However, detailed models of this show that clumps would grow only at very large radii ( $\sim 100 - 1000 R_{\text{IC}}$ , resulting in velocities much smaller ( $\leq 100 \text{ km s}^{-1}$ ) than those observed in winds (e.g. [Waters et al 2021](#)). Perhaps a more likely mechanism is that the hot, overionised wind expands out and sweeps up mass from previously ejected wind material, and that the subsequent shock gives rise to clumping, but no detailed simulations of this scenario exist as yet.

The emission lines are perhaps easier to explain, as these could be produced at the base of the wind, where the X-ray irradiation quickly heats the material from atomic cooling to the hot branch (see [Fig 9](#)). There are simulations by [Koljonen et al \(2023\)](#) which show that this can give a good match to all the emission lines seen in the soft state of the black hole MAXI J1820+070. However, none of these lines have the obvious wind signatures of absorption, and/or broader wings on the emission lines. Also, this was a soft state observation, where the optical winds are not so often detected. Nonetheless, these simulations clearly show the potential to explain the standard optical emission lines seen from the irradiated disc at the base of the wind.

### 5.3 Magnetically driven winds (MHD winds)

Radiative and thermal (and thermal-radiative) winds can be calculated (with varying degrees of difficulty, see above) from the given conditions, but the MHD winds are currently completely undefined as the baseline magnetic field configuration in the accretion disc is not known. Magnetic fields are almost certainly present, as again recognised by [Shakura and Sunyaev \(1973\)](#), as the viscosity required to transport angular momentum outwards so material in the disc can accrete inwards is most likely magnetic. However, there is still debate about whether this is caused solely by a small-scale magnetic dynamo driven by the magneto-rotational instability (MRI) ([Chandrasekhar, 1961](#); [Balbus and Hawley, 1991](#)).

Decades of simulations have uncovered some of the properties of this process, and it is now clear that the initial conditions in terms of net magnetic flux imposed are very important in determining the non-linear outcome of the process. Initialising with no net flux gives rise to SANE (standard and normal evolution) flows, where the small-scale dynamo gives an effective viscosity parameter  $\alpha \sim 0.01$ . These flows launch jets, but the jet power is low. By contrast, with some initial net flux, the flow is magnetically

arrested close to the innermost stable circular orbit (MAD: magnetically arrested disc; Narayan et al 2003), and the effective  $\alpha$  and jet powers are both much higher.

Thus, even for the known magnetic dynamo process, the properties of the resulting flow are not yet clear. However, this need not be the dominant magnetic configuration. Before the MRI was discovered, other ways of transporting angular momentum via large-scale, coherent fields threading the disc were explored. The earliest were the Blandford-Payne self-similar models, where the magnetic field connects into the disc at all radii and torques it by accelerating some small amount of material up the field lines, converting azimuthal motion to radial outflow (Blandford and Payne, 1982). After this pioneering work, different solutions with similar large-scale magnetic fields but different assumptions were studied (Contopoulos and Lovelace 1994; Ferreira and Pelletier 1995; Ferreira 1997). This mechanism was also explored for the case of young stellar objects (Pudritz and Norman, 1986).

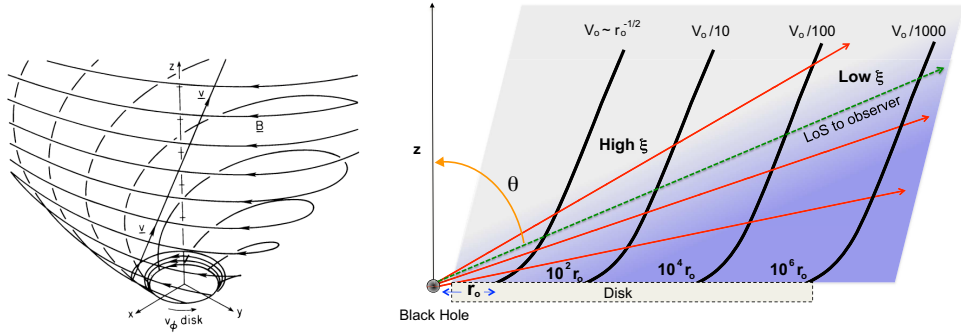


**Fig. 12** Schematic diagram of the MHD wind model, with 3D streamlines on the left. The right shows their projection onto 2D, where the solid black lines show the magnetic field lines and streamlines of the wind. Composite figure from Lovelace et al 1991 and Fukumura et al 2017, respectively

The current MHD wind model for observational spectra developed by Fukumura et al (2010, 2015, 2017) is based on the formalism of Contopoulos and Lovelace (1994), which itself generalises the pioneering centrifugally driven wind mechanism of Blandford and Payne (1982). In these formulations, self-similar global magnetic fields thread the entire accretion disc, naturally driving an outflow across all radii. By adjusting the field configuration, one may impose a radial density law of the form as  $n(R) = n_0(R/R_{\text{in}})^{-\alpha}$ , where  $n_0$  is the density at the inner radius of the wind,  $R_{\text{in}}$ , and  $\alpha$  ( $0 < \alpha < 2$ ) is a free parameter. At each radius, the wind speed have similar velocity as the Keplerian velocity,  $v(R) \sim v_K(R)$ . Using those parameters, one can calculate the line profile by a photoionisation code such as XSTAR (Kallman and Bautista, 2001) or CLOUDY (Ferland et al, 2017; Gunasekera et al, 2023). The typical feature of this model is that the wind density, ionisation parameter  $\xi = L/(nR^2) \propto R^{\alpha-2}$ , and velocity  $v \propto v_\phi(R) \propto R^{-1/2}$  decrease with radius. This causes the highly ionised ions to be faster than those at lower ionisation, producing asymmetric lines with a strong blue wing (Fig. 13). A different MHD formalism by Ferreira and Pelletier (1995), applied

in models by [Chakravorty et al \(2016, 2023\)](#), yields similar results, as also shown by [Datta et al \(2024\)](#).

MHD winds are then capable of explaining the wide range of outflow velocities observed – from the highly relativistic velocities associated UFOs in AGN ([Fukumura et al, 2015](#)) to the slower X-ray absorption lines seen in X-ray binaries, where the inner disc wind may be so highly ionised as to escape detection ([Fukumura et al, 2017](#)).

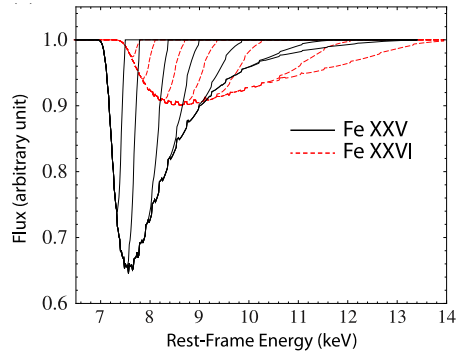


**Fig. 13** The typical line profiles of the MHD wind model adapted from [Fukumura et al \(2015\)](#). The highly ionised Fe xxvi is faster than the lower ionized Fe xxv. Both have strong blue wing components.

However, a critical issue for these models is that they invoke a self-similar ordered magnetic field structure which is not yet well physically justified. Although magnetic fields are a plausible driver for angular momentum transport via the small scale magnetorotational instability, the inherently turbulent nature of these fields casts doubt on the likelihood of establishing and sustaining the globally organised magnetic structures assumed in these models. This fundamental uncertainty regarding the formation and maintenance of such large-scale magnetic fields remains an important topic for future research.

## 6 Discussion

In this review, we attempt to compile, discuss, and place within the context of theoretical work the current observational evidence for the presence of accretion disc winds in accreting BHs and NSs. We do so using a multiwavelength approach, arguably for the first time, given the growing number of detections at wavelengths other than X-rays in recent years. This allows us to study winds with significantly different physical conditions, such as ionisation and presumably densities.

Since the focus is on accreting NSs and BHs with disc-fed accretion, this review is naturally centred on LMXBs. Nonetheless, we have included some systems with somewhat more massive donors, such as Her X-1 and V4641 Sgr, which can be considered intermediate-mass X-ray binaries. However, we do not include other markedly different compact binary populations that also display disc winds, such as accreting white dwarfs (cataclysmic variables; e.g. [Drew and Verbunt 1988](#); [Kafka and Honeycutt 2004](#); [Cúneo et al 2023](#)) and ultraluminous X-ray sources. The latter are thought to accrete in a supercritical regime where such winds are naturally produced and strongly influence their observational properties. For example, SS 433, the most promising Galactic candidate for this type of system, is known to display optical P-Cyg line profiles in addition to other features associated with its precessing jet (e.g. [Fabrika 2004](#); [Blundell et al 2011](#)).

Table 4 includes the 30 systems in which, to the best of our knowledge and based on the criteria discussed above, signatures of disc outflows have been confidently detected in at least one spectral range. Systems with only tentative detections are excluded from this discussion, although an extensive list of such cases is provided in Tables 1, 2, and 3. The general discussion that follows focuses on the global properties of winds, from cold to hot outflows, as more specific issues related to low- and high-ionisation cases, as well as modelling, have already been addressed in their respective sections.

### 6.1 Atmospheres, winds and failed winds

Since LMXBs were first studied at low energies, optical and NIR spectroscopy has revealed the presence of emission lines. These features originate in the disc atmosphere, a vertically extended layer of gas surrounding the disc, and are often characterised by double-peaked profiles produced by the Doppler shifts from opposite sides of the outer accretion disc. However, such double-peaked profiles can persist even if the atmosphere is outflowing, as long as the opacity is such that the lines trace material close to the disc, where the velocity field is still dominated by rotation (e.g. [Koljonen et al 2023](#)). Single-peaked profiles are also observed, particularly during outbursts<sup>5</sup> and are often interpreted as arising in an outflow or high up in the disc atmosphere (e.g. [Matthews et al 2015](#)).

In addition, although less frequent, broad absorption components with no significant shifts (typically  $\lesssim 100 \text{ km s}^{-1}$ ) are present in the optical and NIR spectra of

---

<sup>5</sup>Note, however, that at low velocity resolution, the double-peak cannot always be resolved during outburst, as the (cooler) optical emitting regions move further out to lower velocity zones, naturally forming narrower profiles (e.g. [Casares 2015](#)). This is particularly challenging for low inclination systems given their lower projected disc's velocities.

LMXBs and are also common in accreting white dwarfs. The origin of these components is unknown but might be associated with the disc photosphere under certain physical conditions (see e.g. [Dubus et al 2001](#)). Interestingly, these absorptions are often superimposed on emission lines (e.g. [Miceli et al 2024](#)) and could signal the presence of outflows, as observed in Swift J1727.8–1624 ([Mata Sánchez et al 2024](#)) and possibly GRO J1655–40 ([Soria et al 2000](#)).

Most LMXBs accessible in the optical and NIR exhibit some form of emission and/or absorption features in their spectra. As such, in this review we have restricted ourselves to discussing only those that can be confidently (or at least tentatively) associated with winds (see [Sec. 2](#) and [Sec. 3](#)).

### 6.1.1 Static X-ray lines

Relativistically broadened emission components aside (e.g. [Miller 2007](#)), the presence of emission and/or absorption lines in X-ray spectra is relatively rare. Out of the 30 systems included in [Table 4](#), nine have shown confident detections of X-ray lines with no significant velocity shift, and are thus consistent with an origin in the disc atmosphere. Despite the lack of measured blueshifts, these features are in most cases similar to those associated with X-ray outflows. This supports a connection between disc winds and atmospheres, suggesting that the former may be understood as an outflowing version of the latter (see [Sec 6.2.3](#)). For this reason, in this review we consider both static and shifted X-ray components. Furthermore, until the recent launch of *XRISM*, instrumental capabilities for studying X-ray lines at high velocity resolution were limited. Future observations with this facility may therefore uncover low-velocity outflows in some of these systems

### 6.1.2 Inflows and failed winds

Redshifted absorption features that might trace the presence of infalling gas out of the disc plane have been observed in some LMXBs. These can be produced by material lifted from the disc (e.g. by one of the mechanisms described in [Sec. 5](#)) but failing to accelerate beyond the escape velocity (i.e. failed winds).

This is a common phenomenology in other accreting objects. For instance, inverted P-Cyg profiles (i.e. blueshifted emission accompanied by redshifted absorption) are common in the NIR lines (e.g.  $\text{Pa}\beta$  and  $\text{Br}\gamma$ ) of protostars (e.g. T Tauri stars; [Folha and Emerson 2001](#)). These are interpreted as signatures of infalling gas. However, the precise physical origin of the emission and absorption features remains uncertain, with magnetically driven accretion typically invoked.

In LMXBs, examples of this phenomenology exist, particularly for lines tracing low-ionised gas. These components can be narrow, pronounced, and transient on timescales significantly shorter than the orbital period ([Cúneo et al 2020](#); see also [Miceli et al 2024](#)), or rather persistent across large phases of the outburst ([Mata Sánchez et al, 2024](#)). Arguably, the main difficulty lies in ruling out a disc atmosphere origin or the possibility that the profile results from a combination of disc atmosphere and outflow features. Similar claims for high-ionisation gas exist (e.g. [Miller et al 2014](#); see also [Shidatsu et al 2013](#)), although the limited velocity resolution makes it difficult to distinguish these features from static disc-atmosphere lines. Even in the *XRISM* era,

the presence of multiple absorption components makes this distinction challenging (Róžańska et al, 2014; Miller et al, 2025).

The combination of *XRISM* with optical and NIR spectroscopy at similarly high velocity resolution should lead to major improvements in our understanding of these components. In particular, a key question to address is whether winds, atmospheres, and failed winds represent different stages of the physical phenomenon, with winds being the material that escapes, and atmospheres or failed winds forming part of a cycle where material is lifted, forms an atmosphere, and eventually falls back.

## 6.2 Disc winds: observational properties

It follows a summary of the most relevant observational properties that can be directly derived from Table 4.

### 6.2.1 Black holes versus neutron stars

Outflow velocities are available for 21 X-ray binaries (sources in boldface in Table 4). These include most BH transients (top panel) and about half of the NS systems (lower panel). In the former, the majority of the detections come from the optical domain, specifically cold winds, while high ionisation winds vastly dominates in the case of NS. This might be the result of several combined factors:

- BH systems are mostly transient sources, and therefore observations rely on dedicated programmes such as *Target-of-Opportunity* campaigns, which are more difficult to implement with high spectral resolution facilities.<sup>6</sup> In the last decade, the advent of new large ground-based telescopes such as the *GTC* and *SALT*, in addition to existing facilities like the *VLT*, has mitigated this limitation in the optical band. However, outburst observations with high-resolution X-ray instruments such as *Chandra* and *XMM-Newton* remain relatively scarce.
- NS systems are mostly persistent sources, which makes it easier to schedule X-ray observations. However, many of them are faint or simply inaccessible in the optical, as they are located in the Galactic plane, where extinction is high. They also tend to exhibit hotter optical spectra (e.g. Panizo-Espinar et al 2021), often dominated by strong He II lines – a property that in BHs has been shown to be crucial for the detection of cold winds (see e.g. Fig. 5). This behaviour may stem from a combination of factors, including the smaller disc size in NS systems, the fact that luminous persistent sources typically remain in soft states, and the faster hard-to-soft transitions observed in NS transients (which prevents their observation in the former state; see e.g. Muñoz-Darias et al 2014).

Nonetheless, several characteristics – such as the range of observed wind velocities and the strong preference for detecting winds in high-inclination systems – are common to both BHs and NSs. Hereafter, we discuss the wind properties of BH and NS LMXBs globally.

---

<sup>6</sup>However, this is not the case for lower-resolution instruments such as *NICER*, which has provided some tentative detections (see Table 2).

**Table 4** Systems with confident detections of either low-ionisation (cold-cool) winds or high-ionisation (warm-hot) atmosphere/wind.

Source	$P_{\text{ORB}}^a$ (h)	Inclination <sup>b</sup>	$v_{\text{max}}^c$ (km s <sup>-1</sup> )	Cold <sup>d</sup>	Cool <sup>e</sup>	Warm <sup>f</sup>	Hot <sup>g</sup>
<b>Black Hole Systems [15]</b>							
IGR J17451–3022	?		–				✓ (no vel.)
IGR J17091–3624	?		–				✓ (no vel.)
<b>4U 1630–47</b>	?	High [Dips]	400				✓
<b>H 1743–322</b>	?	High [Dips]	400				✓
<b>GX 339–4</b>	42.1	Mid	1000 (b-e)	✓			✓?
<b>Swift J1727.8–162</b>	10.8	Mid	1150 (b-e)	✓	✓?		
<b>GRO J1655–40</b>	62.9	High [Dips]	1200	✓?		✓	✓
<b>MAXI J1803–298</b>	7.0	High [Dips]	1250 (b-e)	✓			✓
<b>MAXI J1348–630</b>	?	Mid-to-low	1700 (b-e)	✓			✓?
<b>MAXI J1820+070</b>	16.5	High [67–81°]	1800 (b-e)	✓			
<b>GRS 1716–249</b>	6.7	Mid	2000 (b-e)	✓	✓?		
<b>V4641 Sgr</b>	67.6	High [60–70°]	3000 (b-e)	✓			
<b>GRS 1915+105</b>	812	High [60–70°]	3000 (b-e)	✓			✓
<b>V404 Cyg</b>	155	High [60–70°]	4000 (b-e)	✓		✓	✓
<b>Swift J1357.2–0933</b>	2.8	High [≥80°]	4000 (b-e)	✓	✓		
<b>Neutron Star Systems [15]</b>							
4U 1916–054	0.8	High [Dips]	–			✓-atm	✓-atm
1A 1744–361	1.62	High [Dips]	–				✓-atm
4U 1323–62	2.94	High [Dips]	–				✓ (no vel.)
EXO 0748–676	3.82	High [Eclipses]	–			✓-atm	✓-atm
4U 1254–69	3.93	High [Dips]	–				✓-atm
4U 1822–37	5.57	High [Eclipses]	–			✓-atm	✓-atm
MXB 1659–298	7.11	High [Eclipses]	–			✓-atm	✓-atm
<b>AX J1745.6–2901</b>	8.35	High [Eclipses]	200				✓
<b>4U 1624–49</b>	20.89	High [Dips]	350				✓
<b>2S 0921–63</b>	216.2	High [Eclipses]	<1000			✓	✓
<b>Her X–1</b>	40.8	High [Eclipses]	1000			✓	✓
<b>GX 13+1</b>	577.6	High [Dips]	1000	✓?		✓	✓
<b>UW CrB</b>	1.8	High [Eclipses]	1500 (b-e)	✓?	✓		
<b>Cir X–1</b>	398.4	High [Eclipses]	2000 (b-e)			✓	✓
<b>Swift J1858.6–0814</b>	21.3	High [Eclipses]	2400 (b-e)	✓	✓	✓?	

**Notes.** Sources with confident wind detections (i.e. a blueshift) are highlighted in boldface. **(a)** Orbital period of the system. **(b)** Estimated inclination of the system. Values in brackets indicate either the approximate inclination angle in degrees or observational constraints (e.g. eclipses or dips). A low inclination refers to  $\lesssim 30^\circ$ , mid to  $30\text{--}60^\circ$ , and high to  $\gtrsim 60^\circ$  (see catalogues by [Corral-Santana et al 2016](#) and [Avakyan et al 2023](#) for details on the fundamental parameters). **(c)** Maximum outflow velocity measured across all spectral ranges. Values derived from the blue edge of P-Cygni line profiles or broad emission components are indicated with **(b-e)**. Confident detections with a measured outflow velocity are indicated by ✓. Detections consistent with a disc atmosphere (i.e. velocity consistent with zero) are marked as ✓-atm, while those with no solid velocity constraints are labelled ✓ (no-vel). Tentative detections are indicated by ✓?. **(d)** Low-ionisation wind detected in optical and NIR transitions of mainly H and He I ( $\log \xi \lesssim 1$ ). **(e)** Low-ionisation winds detected in He II and UV transitions (mainly C IV, N V) reaching up to  $\log \xi \sim 1.5$ . **(f)** High-ionisation (X-ray) winds with  $1.5 \lesssim \log \xi \lesssim 3$ . **(g)** High-ionisation winds detected mainly via Fe XXV and Fe XXVI, indicating  $\log \xi \gtrsim 3$ .

### 6.2.2 The orbital inclination and the wind geometry

As is evident from Table 4, inclination is a major factor in driving the detectability of winds. In fact, X-ray winds have so far only been confidently detected in high-inclination systems, which we define as those with inclinations greater than  $\sim 60^\circ$ . This behaviour has traditionally been interpreted as evidence for an equatorial wind geometry (e.g. Ponti et al 2012), where detection is naturally favoured when the line of sight lies close to the disc plane. While this remains the prevailing view, modelling studies (see e.g. Higginbottom and Proga 2015; Díaz Trigo and Boirin 2016) suggest that even for more isotropic wind geometries, absorption will still appear stronger at high inclinations due to the increased line-of-sight opacity. In this context, observations taken at different phases of the precessing disc period of Her X-1 offered a unique insight into the wind geometry, as the strongest and least clumpy outflow was detected when looking closer to the orbital plane (Kosec et al, 2023), supporting an equatorial geometry.

Although the situation is broadly similar in the optical and NIR domains, several low-ionised wind detections have been reported in lower-inclination systems. A key difference lies in the nature of the signatures. X-ray wind detections are associated with blueshifted absorption lines, as are optical-NIR P-Cygni line profiles (which are also always seen at high inclinations). However, detections at lower inclinations often arise from emission components (see Sec. 2). A unique case is that of MAXI J1348–630 (Panizo-Espinar et al, 2022). In this system, broad emission components were observed alongside an absorption trough detected in multiple high signal-to-noise optical and NIR spectra across several epochs. Interestingly, the system has a low-to-moderate orbital inclination (e.g. Carotenuto et al 2021), and the centroid of the absorption trough indicates a velocity of  $500 \text{ km s}^{-1}$  (with a blue-edge at  $\sim 900 \text{ km s}^{-1}$ ), significantly lower than the velocities inferred in other systems (see below) and those of the emission components detected simultaneously in the same object (up to  $1700 \text{ km s}^{-1}$ ). Since the latter are formed via scattering by material out of the line of sight (see Fig. 1), their velocities should be less dependent on the inclination. The lower velocity of the absorption trough, on the other hand, could be naturally explained as a projection effect in an equatorial wind geometry. Additional detections in low-inclination systems are required to establish more robust conclusions based on these arguments. In summary, while more observations and detailed modelling are needed, the current observables from both low- and high-ionisation winds largely support a prevailing equatorial wind geometry.

### 6.2.3 The wind velocity

The observed velocity is one of the most relevant wind properties to discuss. It can be directly derived from observations, with little to no modelling involved. However, distinguishing the specific wind signatures from which velocities are derived is fundamental for a meaningful comparison. In Table 4, we have sorted both NS and BH systems by the maximum velocity reported for each source, regardless of whether it

is derived from lines tracing low- or high-ionisation material. We also list the orbital period ( $P_{\text{ORB}}$ ), which serves as a proxy for accretion disc size.<sup>7</sup>

In the NS sample (lower panel in Table 4), which is dominated by X-ray detections, there is a clear trend: atmospheres or very low-velocity winds are preferentially found at short orbital periods. This was already noted by [Díaz Trigo and Boirin \(2016\)](#) and can be interpreted in the context of thermal winds. As discussed in Sec. 5, these require a minimum disc size to launch an outflow ( $\gtrsim 0.2R_{\text{IC}}$ ). Therefore, short-period systems – particularly those hosting NSs – might not reach the necessary outer disc radius. In these cases, the gas can still be lifted by the same mechanism but remains gravitationally bound to the system, forming a disc atmosphere.

In general, the observed wind velocities range from  $\lesssim 200 \text{ km s}^{-1}$  (which we associate with X-ray atmospheres) to  $\sim 4000 \text{ km s}^{-1}$ . While the overall distributions for BHs and NSs are similar, the highest velocities are found in BH systems. The four targets with the largest values (above  $3000 \text{ km s}^{-1}$ ) all harbour BHs. These also tend to be long-period systems, although exceptions exist. For instance, Swift J1357.2–0933 exhibits very large velocities despite its short orbital period. However, this may be related to its extremely high inclination and possibly to its peculiar phenomenology (and perhaps outflow nature), since low ionisation winds are only detected during the peculiar optical dips displayed by the system (see e.g. [Charles et al 2019](#); [Jiménez-Ibarra et al 2019](#); [Corral-Santana et al 2013](#); [Panizo-Espinar et al 2024](#)).

By comparing the detections listed in Table 1 with those in Tables 2 and 3, one might conclude that X-ray winds generally show smaller velocities than cold winds. However, it is crucial to note that measurements in these regimes are typically obtained using different methods. In the optical and NIR (i.e. low-ionised winds), the absorption components are often well resolved, allowing for velocity measurements based on the blue-edge of the P-Cyg profile. In contrast, X-ray velocities are usually derived from the centroid of the absorption line. In Table 4, we indicate which measurements were obtained using the blue-edge (labelled **b-e**), and it is clear (and expected) that the highest velocities are found with this technique. Although rare, this also includes a few X-ray detections. Interestingly, when X-ray winds are measured using the blue-edge (e.g. V404 Cyg and Cir X–1), the inferred velocities are as high as those derived from low-ionised winds. In fact, if we assume that the blue-edge velocity is typically about twice the velocity of the absorption centroid, then the characteristic velocities of low- and high-ionised winds become consistent. The arrival of *XRISM*, combined with observations at lower energies, should shed light on this topic – a key factor for understanding the nature of both low- and high-ionised winds. So far, the only simultaneous high-resolution study is that of V404 Cyg, which shows consistent kinematical properties across the different low- and high-ionisation components ([Muñoz-Darias and Ponti 2022](#)).

Finally, it is worth noting the significant number tentative X-ray wind detections reporting velocities an order of magnitude higher than those discussed here (see Tables 2 and 3). The presence of these components – approaching the UFOs regime

---

<sup>7</sup>Note, however, that this also depends on the compact object mass. A typical BH mass implies a disc 2–3 times larger than that of a NS at the same  $P_{\text{ORB}}$ ; see e.g. [Frank et al \(1992\)](#).

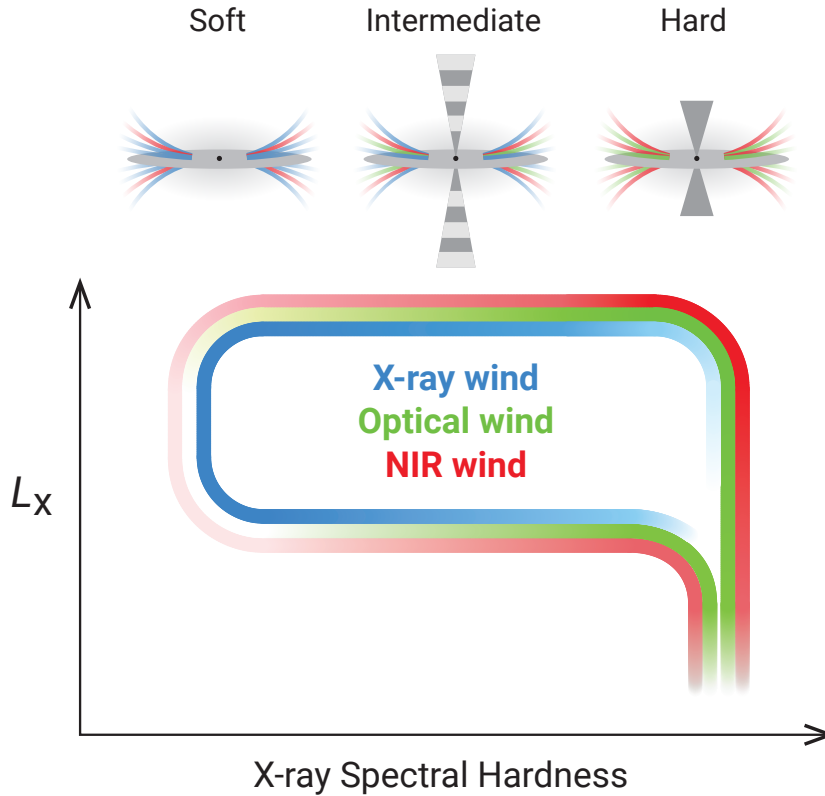


**Fig. 14** Sketch summarising the current observational evidence for both high (X-ray) and low (optical and NIR) ionisation winds across the BH accretion states. The coloured tracks illustrate wind detectability for the different spectral domains, where colour intensity follows the typical absorption strength for a high-inclination source. The tracks follow the standard outburst evolution of BHs in the X-ray luminosity versus spectral hardness plane (commonly plotted as the hardness–intensity diagram; e.g. [Homan et al 2001](#); [Dunn et al 2010](#)). The amount of fast X-ray variability can also be used as an alternative to X-ray hardness ([Muñoz-Darias et al, 2011, 2014](#)). This approach is particularly useful for NS systems, for which limited observations suggest that they follow a similar pattern (see Sec. 6.3). The full disc–outflow configuration, following the same colour scheme and showing the jet behaviour (e.g. [Fender et al 2004](#)), is also depicted in the top panel.

observed in AGN – is typically inferred from single lines, often detected using low-resolution instruments. This may reflect the intrinsic rarity of such features, as well as the need for high-cadence observations to capture them. While the existence of such high-velocity winds in LMXBs is intriguing and would have strong implications for constraining wind-launching mechanisms, conclusive detections are still lacking. Ideally, this would require several lines simultaneously displaying extreme blueshifts. Once again, the arrival of *XRISM* may play a key role in resolving this matter. We also note that, so far, there is no evidence for such high-velocity components in low-ionisation winds.

### 6.3 Accretion states and winds

In addition to winds, the other type of outflow present in LMXBs are collimated jets, best observed at radio wavelengths. A close connection between the accretion regime and the presence and observational properties of the jet is well established, to the extent that jets can be considered a defining element of the accretion state (e.g. [Fender and Belloni 2012](#)). The discovery of X-ray winds, preferentially detected during the soft state (see [Sec. 4.5](#)), added further complexity to this picture since, in most cases, high-ionisation winds and jets appear to be mutually exclusive phenomena (e.g. [Neilsen and Lee 2009](#); [Ponti et al 2012](#)).

The extensive optical and, to some extent, NIR and ultraviolet spectroscopic campaigns conducted over the last decade have shown that low-ionisation winds are as common as X-ray winds. However, they are typically observed during the hard state (see [Sec. 3.3](#)), that is, simultaneously with radio jets. As discussed above, both types of winds share key observational properties, such as similar velocities and a preference for being detected in high-inclination systems. The current observational evidence is sketched in [Fig. 14](#), where the visibility of winds as a function of the accretion state (as traced by the commonly used hardness–intensity diagram; e.g. [Homan et al 2001](#); [Fender et al 2004](#)), together with the jet properties, is depicted. It leads to some general conclusions, which can be summarised as follows:

- Winds, as a physical phenomenon, are present in all states, but their phenomenology changes dramatically from the soft to the hard state, with high-ionisation (X-ray) winds observed primarily in the soft state and low-ionisation (optical/NIR) winds in the hard state. This conclusion is primarily based on the hot and cold wind types, while the situation is less clear for the warm and cool winds owing to the smaller number of detections.
- Low- and high-ionisation winds are typically not observed simultaneously. However, this observational picture is not absolute and should not be interpreted in a deterministic way. X-ray winds can also be observed simultaneously with the jet (i.e. during the hard and intermediate states), and thus may coexist with low-ionisation winds. Signatures of low-ionisation winds (both in the optical and NIR lines), although weaker than those found in the hard state, have also been found during the hard-to-soft transition, and even in the soft-intermediate state (see e.g. [Panizo-Espinar et al 2022](#); [Mata Sánchez et al 2024](#)). In the NIR, these are also present during the soft state, supporting the presence of cold winds at this stage (see [Sec. 3.3](#)). Therefore, the variability of wind signatures across the spectral range and accretion states may simply reflect how the physical conditions in the soft and hard states influence the detectability of high- and low-ionisation winds, respectively.
- The current observational picture suggests that the relation between jets and winds is not direct. In addition, if jets and winds are linked by a common, albeit complex, mechanism, this would likely require them to originate from the same region of the system. For jets, this is generally thought to be the innermost few gravitational radii. However, most modelling of winds, as well as their kinematic properties, suggests that they are launched from the outer disc (see also [Sec. 5](#)).

It is important to bear in mind that the observational view sketched in [Fig. 14](#) provides a simplified representation of the situation at the time of writing this review.

For instance, not all regions of the hardness–intensity diagram have been equally sampled by observations, with the soft-to-hard transition being much less studied—at all wavelengths—than the more luminous hard-to-soft one. In the diagram, both are depicted in a similar way, but new observations may uncover significant differences. Also, as discussed in Sec. 4.5, future X-ray observations might reveal lower-ionisation (i.e. warm) X-ray winds during the harder states, while additional NIR studies are needed to establish the prevalence and properties of cold outflows in the softer states.

The above picture has been drawn mainly from BH transients. However, it seems to be broadly applicable to NS systems as well. Winds in these objects are primarily detected in persistent sources in the X-ray regime and show observational properties consistent with those seen in BHs (see Sec. 4.5). Considering both, high- and low-ionisation winds in NS LMXBs, the most complete comparison can be made against the NS transient Swift J1858.6–0814. During its long and rather extreme 2020 outburst (see e.g. Vincentelli et al 2023), it displayed strong optical and ultraviolet P-Cyg line profiles (i.e. cold and cool winds), contemporaneously with jet emission (van den Eijnden et al 2020; i.e. during the hard state). In particular, the optical features are remarkably similar to those seen in BH transients (Muñoz-Darias et al, 2020). Unfortunately, no high-resolution optical or X-ray spectroscopy is available during its soft state. However, there are hints of static X-ray emission lines during the hard state (Buisson et al, 2020). Likewise, ultraviolet observations taken during the soft state do not show the P-Cyg profiles (i.e. cool winds) present during the bright hard-state epochs (Castro Segura et al, 2022, 2024), suggesting that the observational picture of the cold and cool wind components across the accretion states is rather similar.

## 6.4 Structure, mass content and impact

In the above, we have discussed how winds of different ionisation components are preferentially observed at high orbital inclination, and how this can be reasonably interpreted within the framework of an equatorial geometry. These gas components, observed through similar signatures in both NS and BH systems, show velocities of up to  $\sim 4000 \text{ km s}^{-1}$ , although they can also appear static. We have also evaluated the main physical mechanisms proposed to launch winds (i.e. thermal, radiative, and magnetic; see Sec. 5) and how they compare with current observational evidence.

### 6.4.1 Wind structure

Beyond understanding how winds are actually launched (see Sec. 5), some of the most pressing open questions concern their structure (i.e. whether different components coexist, and how) and their mass content. While the presence of winds has been established in more than 20 systems, confirmed detections of both low-ionised and high-ionised winds exist only for three systems (Table 4). Among them, simultaneous observations are available only in the case of V404 Cyg. A combined analysis of these data (Muñoz-Darias and Ponti, 2022) shows that blueshifted absorption features at remarkably similar velocities are observed in both the optical and X-ray spectra. However, they do not appear simultaneously: the X-ray absorption components emerge

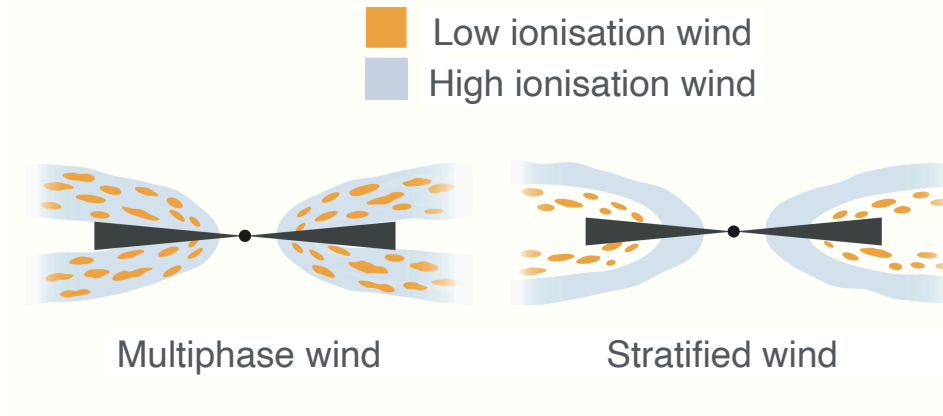


**Fig. 15** Wind structure. Sketch illustrating alternative configurations for a clumpy, low-ionisation wind and a lower-density, highly ionised outflow. An equatorial geometry is assumed in both cases. Adapted from [Muñoz-Darias and Ponti \(2022\)](#).

during the luminous flares, whereas the optical absorptions occur during quieter periods. On the other hand, broad emission lines are observed in both regimes when the source exhibits intermediate behaviour. These components show consistent width between each other, strongly supporting a common (wind) origin for the optical and X-ray emitting regions.

Basic arguments based on the similar kinematical properties of hot and cold winds favour a multiphase wind structure, where both phases coexist spatially, as opposed to a stratified outflow (see sketch in Fig. 15). In the simplest scenario, the multiphase approach explains the observed differences in ionisation parameter ( $\xi$ ) as resulting from variations in the wind density ( $n$  in Eq. 1), that is, the presence of higher-density clumps accounting for the low-ionisation ejecta. In contrast, pure stratification would instead imply different distances from the irradiating source ( $R$  in Eq. 1). However, generalising these results is problematic, as both the 2015 outburst and the wind itself of V404 Cyg are at the extreme end of the population. For instance, the high luminosity of the source during some phases of the outburst suggests a strong contribution of radiation pressure in launching the wind (see e.g. [Motta et al 2017](#); [Casares et al 2019](#)) – a mechanism that is not applicable to other systems unless the line-driven mechanism plays a role (see Sec. 5).

Connected to this, X-ray observations, particularly in the XRISM era, can offer the possibility to simultaneously study different highly-ionised outflow components (e.g. warm and hot winds) within the same dataset. One of the first studies of this class, that of GX 13+1 (Fig. 6; [XRISM collaboration et al 2025](#)), reveals the presence of a relatively slow wind ( $\sim 330 \text{ km s}^{-1}$ ) detected via blue-shifted absorption in dozens of transitions. While these can be generally modelled by a single absorber, a detailed look at the line profiles suggests the presence of different stratified components within the

X-ray outflow. Likewise, the aforementioned study of Her X-1 at different phases of its precession period also supports stratification in the wind: a less ionised and clumpy outflow is found when looking through lines-of-sight sampling the wind further away (vertically) from the equatorial plane (Kosec et al, 2023). On the other hand, a multiphase nature is invoked to explain the properties of the ultraviolet and optical wind (i.e. cold and cool components) detected in Swift J1858.6-0814 (Castro Segura et al, 2022). All considered, both features – that is, multiphase outflows (especially when looking across the full low to high ionisation picture) with some degree of stratification – can likely account for the still limited observational evidence.

#### 6.4.2 Mass outflow rate and wind’s impact

Crude estimations, derived from X-ray observations, of the mass carried by the wind (i.e. the mass outflow rate) exist, particularly for some BH LMXBs. Typical values range from being comparable to the accretion rate, up to exceeding it by a factor of 10–20 (e.g. Lee et al 2002; Neilsen et al 2011; Ponti et al 2012). These figures are derived from the observed absorber column after properly constraining  $\xi$  through spectral modelling. Likewise, it is necessary to assume a particular wind geometry (e.g. equatorial, with a  $30^\circ$  opening angle), as well as an accretion efficiency (i.e. the mass-to-radiation conversion; 10 percent is a typical value).

Proper modelling of low-ionised winds remains to be done, although new radiative transfer codes have recently become available to the community (e.g. *Sirocco*; Matthews et al 2025). The first attempt (Ambrifi et al., to be submitted) indicates that similarly large mass outflow rates, in addition to significant clumping, are required to reproduce the standard optical P-Cyg line profiles detected during regular hard states, such as those seen in MAXI J1820+070 (Muñoz-Darias et al, 2019).

Focussing on individual systems, mass outflow rate estimates have been calculated for the aforementioned case of V404 Cyg. This is possible thanks to the broad phenomenology displayed by the source, which allows the application of different methods. In particular, the evolution of the conspicuous optical nebular phase observed after the abrupt end of the outburst enabled an estimate of the ejected mass. This was done using both the diffusion and recombination timescales of the nebula (Fig. 4) produced by the expanding shell of ejecta. The total mass was found to lie in the range  $10^{-8}$ – $10^{-6} M_\odot$ , up to 100 times the mass accreted during the outburst (Muñoz-Darias et al, 2016; Casares et al, 2019). This high outflow rate is able to explain the large intrinsic column densities (e.g.  $N_H \sim 10^{23}$ – $10^{24} \text{ cm}^{-2}$ ; e.g. Motta et al 2017) reported in this and other systems with strong outflow signatures. This also suggests that, at least for the four systems showing strong signatures of low-ionised winds (see Sec. 3.2 and Table 1) – which share some similar phenomenology – these outflows are dynamically relevant in terms of mass content. For instance, in the case of the NS transient Swift J1858.6–0814, an outflow rate larger than 0.2 times the accretion rate was derived from the ultraviolet P-Cyg profiles (Castro Segura et al, 2022), while the strong NIR wind detected in GRS 1915+105 offers a viable explanation for the heavily X-ray obscured phases displayed by the system (Sánchez-Sierras et al, 2023b).

Although the above mass estimates for both high- and low-ionised winds carry significant uncertainties, they nonetheless suggest that a large fraction of the mass

involved in the accretion process is carried away by the wind. This is expected to have a strong impact on regulating, in some way, the accretion process. At least for the most extreme cases, there is substantial observational evidence supporting this claim. For instance, the already widely discussed 2015 outburst of V404 Cyg was unusually short given the amount of mass stored in its large accretion disc. This has been attributed to a massive outflow that depleted a significant part of the disc and disrupted its structure, abruptly ending the outburst (Muñoz-Darias et al, 2016). Likewise, in GRS 1915+105, besides the NIR wind detected during its X-ray obscured phases, strong X-ray winds were also observed on multiple occasions. The regulation of the inner accretion flow by such winds has been proposed as the origin of some of the different variability patterns detected in the system (Neilsen et al 2011; see also Vincentelli et al 2023).

Even if winds do not display such extreme phenomenology (i.e. generally implying lower luminosities), their impact might still be significant. Some topics discussed in the literature include the possible role of winds in quenching the radio jet (i.e. triggering the transition to the soft state) and stabilising the disc during soft states (e.g. Neilsen and Lee 2009; Ponti et al 2012). However, these arguments generally rely on a scenario in which winds are absent—or significantly weaker—during hard states (i.e. the X-ray wind view). Thus, they do not account for the low-ionisation winds observed in BH hard states. Winds have also been invoked to explain the persistent nature of some long orbital period NS systems, which would otherwise be expected to be transient. Scattering within a strong wind (typically associated with large accretion discs) would enhance the irradiation of the outer disc, keeping hydrogen fully ionised and hence preventing the transient behaviour (Dubus et al, 2019).

Last but not least, another aspect worth bearing in mind is the possible role of winds in angular momentum removal—a key mechanism required for accretion discs to operate. In the Shakura and Sunyaev (1973) prescription, this is implicitly encoded in the viscosity parameter ( $\alpha$ ), to which several physical processes may contribute. The fast outburst decays observed in some systems suggest high values of  $\alpha$ , which can be explained by different scenarios, including a strong contribution from state-independent winds (i.e. winds that remain active throughout the outburst) in removing angular momentum. Under this interpretation, magnetically launched winds might be favoured, as they are expected to carry away more angular momentum per unit mass (Tetarenko et al 2018; Dubus et al 2019).

## 7 The next decade

Without forgetting earlier detections dating back to the final years of the 20th century (see Sec. 1), we are now entering the third decade of intensive research on disc winds in accreting stellar-mass BHs and NSs, following the first blueshifted line detections discovered by *Chandra*. The first decade (mid-2000s to mid-2010s) established the presence of high-ionisation winds, while observations with the largest ground-based telescopes (mainly *GTC* and *VLT*) in the second decade extended our understanding to lower ionisation outflows (optical and NIR), and even into the ultraviolet using the

*Hubble Space Telescope*. This period also saw significant efforts devoted to modelling, particularly in the X-ray regime.

After these two decades of intense study, winds emerge as a fundamental – perhaps ubiquitous – component of accretion onto BHs and NSs, being widely present during their active phases (i.e. outbursts and persistent sources). Their observational signatures depend critically on the spectral regime: high-ionisation outflows are seen during soft states, while low-ionisation winds are preferentially detected in hard states, when radio jets are also active. The physical properties reveal winds that can be relatively fast (though velocities significantly above  $\sim 1$  per cent of the speed of light require confirmation) and geometrically constrained, with strong observational evidence supporting a preferentially equatorial configuration. Structurally, the limited available studies point towards a multi-phase, clumpy nature with some degree of stratification. Last but not least, winds can be massive compared to the accreted material, with compelling evidence that the most extreme cases substantially impact both the accretion disc dynamics and the source’s observational properties.

The third decade, that we are starting at the time of writing, will most likely bring new surprises that we are not yet able to anticipate. However, we should be able to, at the very least, explore the following topics:

- ***XRISM* as a cornerstone for multiwavelength studies at high velocity resolution:** The arrival of *XRISM* is allowing, for the first time, systematic X-ray studies at high velocity resolution. Among other things, this is expected to provide new insights into the presence of different high ionisation components (e.g. the warm and hot phases discussed in this review). It will also allow us to study the actual shapes of the line profiles, which encode information on the geometry of the wind and perhaps the launching mechanisms. Crucially, it also enables the combination of these X-ray studies with optical, NIR and ultraviolet spectroscopy at similarly high resolution, shedding light on the actual structure of the wind.
- **The NIR and beyond in the era of the *James Webb Space Telescope*:** As discussed in this review, the NIR has proven to be an exciting window for studying winds, as it has revealed rich phenomenology (e.g. Fig. 3) and allows one to track outflows during most parts of the outburst. We are still in an exploratory phase for these type of studies, as NIR spectroscopic campaigns remain scarce. The arrival of new instrumentation such as the *Son-of-X-shooter* spectrograph (Schipani et al, 2018) on the *NTT-ESO* telescope can significantly improve this situation by dramatically increasing the number of observations. In addition, the exceptional spectroscopic capabilities of the *James Webb Space Telescope* will allow us to study winds in lines that are not accessible from ground-based observatories.
- **The role of disc winds in polarisation measurements:** The Imaging X-ray Polarimetry Explorer (Weiskopf et al, 2022) is opening a new window by systematically performing polarisation studies of X-ray binaries and AGN. As a potential source of X-ray scattering, accretion disc winds may contribute to the high levels of polarised emission observed in these systems (see e.g. Nitindala et al 2025). This means we not only need to understand the impact of winds on polarisation measurements, but also that such measurements could, in turn, help reveal the presence and properties of the winds themselves (see e.g. Tomaru et al 2024, 2025).

- **New modelling and simulations:** The past decade has seen major advances in the modelling and numerical simulations of disc winds, mostly focused on the high-ionisation components. Further progress, enhanced by the expected growth in computational power, will likely include the incorporation of low-ionisation components (e.g. the SIROCCO code; Matthews et al 2025), allowing us to achieve a more complete theoretical understanding of the physical properties of wind-type outflows. This, in turn, will enable us to test key aspects such as the range of possible launching mechanisms and their impact on the accretion process and the immediate environment of X-ray binaries.

All the above underscores that disc winds will remain a key focus of observational and theoretical studies in the foreseeable future, as we work towards understanding their main properties and role in the fundamental process of mass accretion onto compact objects.

**Acknowledgements.** T.M.-D. acknowledges support by the Spanish *Agencia estatal de investigación* via PID2021-124879NB-I00 and PID2024-161863NB-I00. T.M.D. thanks Alessandra Ambrifi and Montserrat Armas Padilla for their useful comments and suggestions. T.M.D. also acknowledges Gabriel Pérez (IAC) for developing the sketch presented in Fig. 14. G.P. acknowledges financial support from the European Research Council (ERC) under the European Union’s Horizon 2020 research and innovation program HotMilk (grant agreement No. 865637) and from the Framework per *l’Attrazione e il Rafforzamento delle Eccellenze (FARE) per la ricerca in Italia* (R20L5S39T9).

**Declarations.** The authors declare no competing interests.

## References

- Allen JL, Schulz NS, Homan J, et al (2018) The Disk Wind in the Neutron Star Low-mass X-Ray Binary GX 13+1. *ApJ*861:26. <https://doi.org/10.3847/1538-4357/aac2d1>, [arXiv:1806.08800](https://arxiv.org/abs/1806.08800) [astro-ph.HE]
- Ambrifi A, Mata Sánchez D, Muñoz-Darias T, et al (2025) State-dependent signatures of jets and winds in the optical and infrared spectrum of the black hole transient GX 339?4. *Astronomy and Astrophysics* 694:A109. <https://doi.org/10.1051/0004-6361/202451024>, URL <https://ui.adsabs.harvard.edu/abs/2025A&A...694A.109A>, aDS Bibcode: 2025A&A...694A.109A
- Armas Padilla M, Ueda Y, Hori T, et al (2017) Suzaku spectroscopy of the neutron star transient 4u 1608-52 during its outburst decay. *MNRAS*467:290–297. <https://doi.org/10.1093/mnras/stx020>, URL <http://adsabs.harvard.edu/abs/2017MNRAS.467..290A>, [arXiv:1701.02728](https://arxiv.org/abs/1701.02728) [astro-ph.HE]
- Armas Padilla M, Corral-Santana JM, Borghese A, et al (2023) Ultracompat: A comprehensive catalogue of ultra-compact and short orbital period x-ray binaries. *A&A*677:A186. <https://doi.org/10.1051/0004-6361/202346797>, URL <https://ui.adsabs.harvard.edu/abs/2023A&A...677A.186A>, [arXiv:2305.07691](https://arxiv.org/abs/2305.07691) [astro-ph.HE]

- Avakyan A, Neumann M, Zainab A, et al (2023) XRBCats: Galactic low-mass X-ray binary catalogue. *Astronomy and Astrophysics* 675:A199. <https://doi.org/10.1051/0004-6361/202346522>, URL <https://ui.adsabs.harvard.edu/abs/2023A&A...675A.199A>, aDS Bibcode: 2023A&A...675A.199A
- Baglio MC, Alabarta K, Russell DM, et al (2025) Tracking optical variability and outflows across the accretion states of the black hole transient MAXI J1820+070. arXiv e-prints arXiv:2510.16124. <https://doi.org/10.48550/arXiv.2510.16124>, arXiv:2510.16124 [astro-ph.HE]
- Bahramian A, Degenaar N (2022) Low-mass x-ray binaries. arXiv e-prints arXiv:2206.10053. <https://doi.org/10.48550/arXiv.2206.10053>, URL <https://ui.adsabs.harvard.edu/abs/2022arXiv220610053B>, arXiv:2206.10053 [astro-ph.HE]
- Balbus SA, Hawley JF (1991) A powerful local shear instability in weakly magnetized disks. i. linear analysis. *ApJ*376:214. <https://doi.org/10.1086/170270>, URL <https://ui.adsabs.harvard.edu/abs/1991ApJ...376..214B>
- Bałucińska-Church M, Dotani T, Hirotsu T, et al (2009) Neutral absorber dips in the periodic burster LMXB XB 1323-619 from Suzaku. *A&A*500(2):873–882. <https://doi.org/10.1051/0004-6361/200811215>, arXiv:0905.0618 [astro-ph.HE]
- Bandyopadhyay R, Shahbaz T, Charles PA, et al (1997) Infrared spectroscopy of low-mass x-ray binaries. *MNRAS*285(4):718–724. <https://doi.org/10.1093/mnras/285.4.718>, URL <https://ui.adsabs.harvard.edu/abs/1997MNRAS.285..718B>
- Bandyopadhyay RM, Shahbaz T, Charles PA, et al (1999) Infrared spectroscopy of low-mass X-ray binaries - II. *MNRAS*306:417–426. <https://doi.org/10.1046/j.1365-8711.1999.02547.x>
- Beals CS (1929) On the nature of wolf-rayet emission. *MNRAS*90:202–212. <https://doi.org/10.1093/mnras/90.2.202>, URL <http://adsabs.harvard.edu/abs/1929MNRAS...90..202B>
- Beals CS (1931) The contours of emission bands in novæ and Wolf-Rayet stars. *MNRAS*91:966–977. <https://doi.org/10.1093/mnras/91.9.966>
- Beals CS (1953) The Spectra of the P Cygni Stars. *Publications of the Dominion Astrophysical Observatory Victoria* 9:1. URL <https://ui.adsabs.harvard.edu/abs/1953PDAO....9....1B>, aDS Bibcode: 1953PDAO....9....1B
- Begelman MC, McKee CF (1983) Compton heated winds and coronae above accretion disks. II. Radiativetransfer and observable consequences. *ApJ*271:89–112. <https://doi.org/10.1086/161179>
- Begelman MC, McKee CF, Shields GA (1983) Compton heated winds and coronae above accretion disks. I. Dynamics. *ApJ*271:70–88. <https://doi.org/10.1086/161178>

- Behar E, Sako M, Kahn SM (2001) Soft X-Ray Absorption by  $\text{Fe}^{0+}$  to  $\text{Fe}^{15+}$  in Active Galactic Nuclei. *ApJ*563(2):497–504. <https://doi.org/10.1086/323966>, [arXiv:astro-ph/0109314](https://arxiv.org/abs/astro-ph/0109314) [astro-ph]
- Belloni T, Homan J, Casella P, et al (2005) The evolution of the timing properties of the black-hole transient GX 339-4 during its 2002/2003 outburst. *A&A*440:207–222. <https://doi.org/10.1051/0004-6361:20042457>, [arXiv:astro-ph/0504577](https://arxiv.org/abs/astro-ph/0504577)
- Belloni TM (2010) States and Transitions in Black Hole Binaries. Lecture Notes in Physics, Berlin Springer Verlag 794:53–+. [https://doi.org/10.1007/978-3-540-76937-8\\_3](https://doi.org/10.1007/978-3-540-76937-8_3)
- Bhattacharya S, Bhattacharyya S, Shaw G (2024) XMM-Newton High-resolution Spectroscopy of EXO 0748–676 after Its Reemergence from a Long Quiescence. *ApJ*977(1):L17. <https://doi.org/10.3847/2041-8213/ad9337>, [arXiv:2408.02715](https://arxiv.org/abs/2408.02715) [astro-ph.HE]
- Bianchi S, Ponti G, Muñoz-Darias T, et al (2017) Photoionization instability of the  $\text{Fe k}$  absorbing plasma in the neutron star transient *ax j1745.6-2901*. *MNRAS*472:2454–2461. <https://doi.org/10.1093/mnras/stx2173>, URL <http://adsabs.harvard.edu/abs/2017MNRAS.472.2454B>, [arXiv:1709.00860](https://arxiv.org/abs/1709.00860) [astro-ph.HE]
- Blandford RD, Payne DG (1982) Hydromagnetic flows from accretion disks and the production of radio jets. *MNRAS*199:883–903. <https://doi.org/10.1093/mnras/199.4.883>
- Blum JL, Miller JM, Cackett E, et al (2010) Suzaku Observations of the Black Hole H1743-322 in Outburst. *ApJ*713(2):1244–1248. <https://doi.org/10.1088/0004-637X/713/2/1244>, [arXiv:1003.3417](https://arxiv.org/abs/1003.3417) [astro-ph.HE]
- Blundell KM, Schmidtobreick L, Trushkin S (2011) SS433’s accretion disc, wind and jets: before, during and after a major flare. *Monthly Notices of the Royal Astronomical Society* 417:2401–2410. <https://doi.org/10.1111/j.1365-2966.2011.18785.x>, URL <https://ui.adsabs.harvard.edu/abs/2011MNRAS.417.2401B>, aDS Bibcode: 2011MNRAS.417.2401B
- Boirin L, Parmar AN (2003) Discovery of narrow X-ray absorption features from the low-mass X-ray binary X 1254-690 with XMM-Newton. *A&A*407:1079–1084
- Boirin L, Parmar AN, Barret D, et al (2004) Discovery of X-ray absorption features from the dipping low-mass X-ray binary XB 1916-053 with XMM-Newton. *A&A*418:1061–1072
- Boirin L, Méndez MM, Díaz Trigo, Parmar AN, et al (2005) A highly-ionised absorber in the X-ray binary 4U 1323–619: a new explanation of the dipping phenomena. *A&A*436:195

- Bozzo E, Pjanka P, Romano P, et al (2016) Igr j17451-3022: A dipping and eclipsing low mass x-ray binary. *A&A*589:A42. <https://doi.org/10.1051/0004-6361/201527501>, URL <https://ui.adsabs.harvard.edu/abs/2016A&A...589A..42B>, arXiv:1603.03353 [astro-ph.HE]
- Brandt WN, Schulz NS (2000) The Discovery of Broad P Cygni X-Ray Lines from Circinus X-1 with the Chandra High-Energy Transmission Grating Spectrometer. *ApJ*544(2):L123–L127. <https://doi.org/10.1086/317313>, arXiv:astro-ph/0007406 [astro-ph]
- Buisson DJK, Altamirano D, Díaz Trigo M, et al (2020) Soft X-ray emission lines in the X-ray binary Swift J1858.6-0814 observed with XMM-Newton Reflection Grating Spectrometer: disc atmosphere or wind? *Monthly Notices of the Royal Astronomical Society* 498:68–76. <https://doi.org/10.1093/mnras/staa2258>, URL <https://ui.adsabs.harvard.edu/abs/2020MNRAS.498...68B>, aDS Bibcode: 2020MNRAS.498...68B
- Buisson DJK, Altamirano D, Armas Padilla M, et al (2021) Dips and eclipses in the x-ray binary swift j1858.6–0814 observed with nicer. *Monthly Notices of the Royal Astronomical Society* 503(4):5600–5610. <https://doi.org/10.1093/mnras/stab863>
- Carotenuto F, Corbel S, Tremou E, et al (2021) The black hole transient MAXI J1348-630: evolution of the compact and transient jets during its 2019/2020 outburst. *Monthly Notices of the Royal Astronomical Society* 504:444–468. <https://doi.org/10.1093/mnras/stab864>, URL <https://ui.adsabs.harvard.edu/abs/2021MNRAS.504..444C>, aDS Bibcode: 2021MNRAS.504..444C
- Casares J (2015) A FWHM-K2 Correlation in Black Hole Transients. *The Astrophysical Journal* 808:80. <https://doi.org/10.1088/0004-637X/808/1/80>, URL <https://ui.adsabs.harvard.edu/abs/2015ApJ...808...80C>, aDS Bibcode: 2015ApJ...808...80C
- Casares J, Charles PA, Jones DHP, et al (1991) Optical studies of V404 Cyg, the X-ray transient GS2023 + 338. I - The 1989 outburst and decline. *MNRAS*250:712–725
- Casares J, Muñoz-Darias T, Mata Sánchez D, et al (2019) Accretion and outflow in v404 cyg. *MNRAS*488(1):1356–1365. <https://doi.org/10.1093/mnras/stz1793>, URL <https://ui.adsabs.harvard.edu/abs/2019MNRAS.488.1356C>, arXiv:1907.00005 [astro-ph.HE]
- Castor JI (1970) Spectral line formation in Wolf-Rayet envelopes. *Monthly Notices of the Royal Astronomical Society* 149:111. <https://doi.org/10.1093/mnras/149.2.111>, URL <https://ui.adsabs.harvard.edu/abs/1970MNRAS.149..111C>, aDS Bibcode: 1970MNRAS.149..111C
- Castor JI, Lamers HJGLM (1979) An atlas of theoretical p cygni profiles. *ApJS*39:481–511. <https://doi.org/10.1086/190583>, URL <http://adsabs.harvard.edu/abs/1979ApJS...39..481C>

- Castor JI, Abbott DC, Klein RI (1975) Radiation-driven winds in Of stars. *The Astrophysical Journal* 195:157–174. <https://doi.org/10.1086/153315>, URL <https://ui.adsabs.harvard.edu/abs/1975ApJ...195..157C>, aDS Bibcode: 1975ApJ...195..157C
- Castro Segura N, Knigge C, Long KS, et al (2022) A persistent ultraviolet outflow from an accreting neutron star binary transient. *Nature*603(7899):52–57. <https://doi.org/10.1038/s41586-021-04324-2>, URL <https://ui.adsabs.harvard.edu/abs/2022Natur.603...52C>
- Castro Segura N, Knigge C, Matthews JH, et al (2024) Shedding far-ultraviolet light on the donor star and evolutionary state of the neutron-star LMXB Swift J1858.6-0814. *Monthly Notices of the Royal Astronomical Society* 527:2508–2522. <https://doi.org/10.1093/mnras/stad3109>, URL <https://ui.adsabs.harvard.edu/abs/2024MNRAS.527.2508C>, aDS Bibcode: 2024MNRAS.527.2508C
- Chakraborty S, Ratheesh A, Bhattacharyya S, et al (2021) NuSTAR monitoring of MAXI J1348-630: evidence of high density disc reflection. *Monthly Notices of the Royal Astronomical Society* 508:475–488. <https://doi.org/10.1093/mnras/stab2530>, URL <https://ui.adsabs.harvard.edu/abs/2021MNRAS.508..475C>, aDS Bibcode: 2021MNRAS.508..475C
- Chakravorty S, Lee JC, Neilsen J (2013) The effects of thermodynamic stability on wind properties in different low-mass black hole binary states. *MNRAS*436:560–569. <https://doi.org/10.1093/mnras/stt1593>, URL <http://adsabs.harvard.edu/abs/2013MNRAS.436..560C>, [arXiv:1308.4574](https://arxiv.org/abs/1308.4574) [astro-ph.HE]
- Chakravorty S, Petrucci PO, Ferreira J, et al (2016) Absorption lines from magnetically driven winds in X-ray binaries. *A&A*589:A119. <https://doi.org/10.1051/0004-6361/201527163>, [arXiv:1512.09149](https://arxiv.org/abs/1512.09149) [astro-ph.HE]
- Chakravorty S, Petrucci PO, Datta SR, et al (2023) Absorption lines from magnetically driven winds in X-ray binaries - II. High resolution observational signatures expected from future X-ray observatories. *MNRAS*518(1):1335–1351. <https://doi.org/10.1093/mnras/stac2835>, [arXiv:2209.15127](https://arxiv.org/abs/2209.15127) [astro-ph.HE]
- Chandrasekhar S (1961) Hydrodynamic and hydromagnetic stability
- Charles P, Matthews JH, Buckley DAH, et al (2019) Hot, dense He II outflows during the 2017 outburst of the X-ray transient Swift J1357.2-0933. *MNRAS*489(1):L47–L52. <https://doi.org/10.1093/mnras/slz120>
- Chaty S, Charles PA, Martí J, et al (2003) Optical and near-infrared observations of the microquasar v4641 sgr during the 1999 september outburst. *MNRAS*343:169–174. <https://doi.org/10.1046/j.1365-8711.2003.06651.x>, URL <http://adsabs.harvard.edu/abs/2003MNRAS.343..169C>

- Church MJ, Reed D, Dotani T, et al (2005) Discovery of absorption features of the accretion disc corona and systematic acceleration of the X-ray burst rate in XB1323-619. *MNRAS*359:1336–1344. <https://doi.org/10.1111/j.1365-2966.2005.08728.x>
- Contopoulos J, Lovelace RVE (1994) Magnetically Driven Jets and Winds: Exact Solutions. *ApJ*429:139. <https://doi.org/10.1086/174307>
- Corral-Santana JM, Casares J, Muñoz-Darias T, et al (2013) A black hole nova obscured by an inner disk torus. *Science* 339:1048–1051. [arXiv:1303.0034](https://arxiv.org/abs/1303.0034) [astro-ph.GA]
- Corral-Santana JM, Casares J, Muñoz-Darias T, et al (2016) BlackCAT: A catalogue of stellar-mass black holes in X-ray transients. *A&A*587:A61. <https://doi.org/10.1051/0004-6361/201527130>, [arXiv:1510.08869](https://arxiv.org/abs/1510.08869) [astro-ph.HE]
- Costantini E, Pinto C, Kaastra JS, et al (2012) XMM-Newton observation of 4U 1820-30. Broad band spectrum and the contribution of the cold interstellar medium. *A&A*539:A32. <https://doi.org/10.1051/0004-6361/201117818>, [arXiv:1112.4349](https://arxiv.org/abs/1112.4349) [astro-ph.GA]
- Cottam J, Kahn SM, Brinkman AC, et al (2001) High-resolution spectroscopy of the low-mass X-ray binary <ASTROBJ>EXO 0748-67</ASTROBJ>. *A&A*365:L277–L281
- Cúneo VA, Muñoz-Darias T, Sánchez-Sierras J, et al (2020) Discovery of optical outflows and inflows in the black hole candidate grs 1716-249. *MNRAS*498(1):25–32. <https://doi.org/10.1093/mnras/staa2241>, URL <https://ui.adsabs.harvard.edu/abs/2020MNRAS.498...25C>
- Cúneo VA, Muñoz Darias T, Jiménez-Ibarra F, et al (2023) Unveiling optical signatures of outflows in accreting white dwarfs. *Astronomy and Astrophysics* 679:A85. <https://doi.org/10.1051/0004-6361/202347265>, URL <https://ui.adsabs.harvard.edu/abs/2023A&A...679A..85C>, aDS Bibcode: 2023A&A...679A..85C
- D’Aí A, Iaria R, Di Salvo T, et al (2007) A Complex Environment around Circinus X-1. *ApJ*671(2):2006–2016. <https://doi.org/10.1086/522565>
- Datta SR, Chakravorty S, Ferreira J, et al (2024) Impact of disc magnetisation on MHD disc wind signature. *A&A*687:A2. <https://doi.org/10.1051/0004-6361/202349129>, [arXiv:2403.13077](https://arxiv.org/abs/2403.13077) [astro-ph.HE]
- Degenaar N, Maitra D, Cackett EM, et al (2014) Multi-wavelength coverage of state transitions in the new black hole x-ray binary swift j1910.2-0546. *ApJ*784(2):122. <https://doi.org/10.1088/0004-637X/784/2/122>, URL <https://ui.adsabs.harvard.edu/abs/2014ApJ...784..122D>, [arXiv:1403.0939](https://arxiv.org/abs/1403.0939) [astro-ph.HE]

- Degenaar N, Altamirano D, Parker M, et al (2016) Disc reflection and a possible disc wind during a soft X-ray state in the neutron star low-mass X-ray binary 1RXS J180408.9-342058. *MNRAS*461(4):4049–4058. <https://doi.org/10.1093/mnras/stw1593>, [arXiv:1607.01780](https://arxiv.org/abs/1607.01780) [astro-ph.HE]
- Degenaar N, Pinto C, Miller JM, et al (2017) An in-depth study of a neutron star accreting at low Eddington rate: on the possibility of a truncated disc and an outflow. *MNRAS*464(1):398–409. <https://doi.org/10.1093/mnras/stw2355>, [arXiv:1609.04816](https://arxiv.org/abs/1609.04816) [astro-ph.HE]
- Del Santo M, Pinto C, Marino A, et al (2023) An ultrafast outflow in the black hole candidate MAXI J1810-222? *Monthly Notices of the Royal Astronomical Society* 523:L15–L20. <https://doi.org/10.1093/mnrasl/slad048>, URL <https://ui.adsabs.harvard.edu/abs/2023MNRAS.523L..15D>, aDS Bibcode: 2023MNRAS.523L..15D
- Díaz Trigo M, Boirin L (2016) Accretion disc atmospheres and winds in low-mass x-ray binaries. *Astronomische Nachrichten* 337:368. <https://doi.org/10.1002/asna.201612315>, URL <http://adsabs.harvard.edu/abs/2016AN....337..368D>, [arXiv:1510.03576](https://arxiv.org/abs/1510.03576) [astro-ph.HE]
- Díaz Trigo M, Parmar AN, Boirin L, et al (2006) Spectral changes during dipping in low-mass X-ray binaries due to highly-ionized absorbers. *A&A*445:179–195. <https://doi.org/10.1051/0004-6361:20053586>
- Díaz Trigo M, Parmar AN, Miller J, et al (2007) XMM-Newton and INTEGRAL spectroscopy of the microquasar GRO J1655-40 during its 2005 outburst. *A&A*462(2):657–666. <https://doi.org/10.1051/0004-6361:20065406>, [arXiv:astro-ph/0610873](https://arxiv.org/abs/astro-ph/0610873) [astro-ph]
- Díaz Trigo M, Parmar AN, Boirin L, et al (2009) Variations in the dip properties of the low-mass X-ray binary XB 1254-690 observed with XMM-Newton and INTEGRAL. *A&A*493:145–157. <https://doi.org/10.1051/0004-6361/200810154>, [arXiv:0810.0432](https://arxiv.org/abs/0810.0432)
- Díaz Trigo M, Sidoli L, Boirin L, et al (2012) XMM-Newton observations of GX 13 + 1: correlation between photoionised absorption and broad line emission. *A&A*543:A50. <https://doi.org/10.1051/0004-6361/201219049>
- Díaz Trigo M, Migliari S, Miller-Jones JCA, et al (2014) XMM-Newton observations reveal the disappearance of the wind in 4U 1630-47. *A&A*571:A76. <https://doi.org/10.1051/0004-6361/201424554>, [arXiv:1409.3406](https://arxiv.org/abs/1409.3406) [astro-ph.HE]
- Done C, Gierlinski M, Kubota A (2007) Modelling the behaviour of accretion flows in x-ray binaries. everything you always wanted to know about accretion but were afraid to ask. *Astron. Astrophys. Rev.*15(1):1–66. <https://doi.org/10.1007/s00159-007-0006-1>, URL <https://ui.adsabs.harvard.edu/abs/2007A&ARv..15....1D>, [arXiv:0708.0148](https://arxiv.org/abs/0708.0148) [astro-ph]

- Done C, Tomaru R, Takahashi T (2018) Thermal winds in stellar mass black hole and neutron star binary systems. *MNRAS*473(1):838–848. <https://doi.org/10.1093/mnras/stx2400>, [arXiv:1612.09377](https://arxiv.org/abs/1612.09377) [astro-ph.HE]
- Drew JE, Verbunt F (1988) Regular orbital variations in the ultraviolet resonance lines of YZ Cnc. *Monthly Notices of the Royal Astronomical Society* 234:341–351. <https://doi.org/10.1093/mnras/234.2.341>, URL <https://ui.adsabs.harvard.edu/abs/1988MNRAS.234..341D>, aDS Bibcode: 1988MNRAS.234..341D
- Dubus G, Kim RSJ, Menou K, et al (2001) Optical spectroscopy of the x-ray transient xte j1118+480 in outburst. *ApJ*553:307–320. <https://doi.org/10.1086/320648>, URL <http://adsabs.harvard.edu/abs/2001ApJ...553..307D>, astro-ph/0009148
- Dubus G, Done C, Tetarenko BE, et al (2019) The impact of thermal winds on the outburst lightcurves of black hole x-ray binaries. *Astronomy & Astrophysics* 632:A40. <https://doi.org/10.1051/0004-6361/201936333>
- Dunn RJH, Fender RP, Körding EG, et al (2010) A global spectral study of black hole X-ray binaries. *MNRAS*403:61–82. <https://doi.org/10.1111/j.1365-2966.2010.16114.x>, [arXiv:0912.0142](https://arxiv.org/abs/0912.0142) [astro-ph.HE]
- Eggum GE, Coroniti FV, Katz JI (1988) Radiation Hydrodynamic Calculation of Super-Eddington Accretion Disks. *ApJ*330:142. <https://doi.org/10.1086/166462>
- van den Eijnden J, Degenaar N, Russell TD, et al (2020) The variable radio counterpart of Swift J1858.6-0814. *Monthly Notices of the Royal Astronomical Society* 496:4127–4140. <https://doi.org/10.1093/mnras/staa1704>, URL <https://ui.adsabs.harvard.edu/abs/2020MNRAS.496.4127V>, aDS Bibcode: 2020MNRAS.496.4127V
- El Mellah I, Sundqvist JO, Keppens R (2018) Accretion from a clumpy massive-star wind in supergiant X-ray binaries. *MNRAS*475(3):3240–3252. <https://doi.org/10.1093/mnras/stx3211>, [arXiv:1711.08709](https://arxiv.org/abs/1711.08709) [astro-ph.HE]
- Erkal J, Manara CF, Schneider PC, et al (2022) The he i  $\lambda 10830\text{\AA}$  line as a probe of winds and accretion in young stars in lupus and upper scorpius. *Astronomy and Astrophysics* 666:A188. <https://doi.org/10.1051/0004-6361/202244254>, URL <https://ui.adsabs.harvard.edu/abs/2022A&A...666A.188E>, aDS Bibcode: 2022A&A...666A.188E
- Fabian AC, Buisson DJ, Kosec P, et al (2020) The soft state of the black hole transient source MAXI J1820+070: emission from the edge of the plunge region? *Monthly Notices of the Royal Astronomical Society* 493:5389–5396. <https://doi.org/10.1093/mnras/staa564>, URL <https://ui.adsabs.harvard.edu/abs/2020MNRAS.493.5389F>, aDS Bibcode: 2020MNRAS.493.5389F
- Fabrika S (2004) The jets and supercritical accretion disk in SS433. *Astrophys. Space Phys. Res.*12:1–152. <https://doi.org/10.48550/arXiv.astro-ph/0603390>,

[arXiv:astro-ph/0603390](https://arxiv.org/abs/astro-ph/0603390) [astro-ph]

- Fender R, Belloni T (2012) Stellar-Mass Black Holes and Ultraluminous X-ray Sources. *Science* 337:540–. <https://doi.org/10.1126/science.1221790>, [arXiv:1208.1138](https://arxiv.org/abs/1208.1138) [astro-ph.HE]
- Fender R, Muñoz-Darias T (2016) The balance of power: Accretion and feedback in stellar mass black holes. In: Haardt F, Gorini V, Moschella U, et al (eds) *Lecture Notes in Physics*, Berlin Springer Verlag, p 65, [https://doi.org/10.1007/978-3-319-19416-5\\_3](https://doi.org/10.1007/978-3-319-19416-5_3), URL <http://adsabs.harvard.edu/abs/2016LNP...905...65F>, 1505.03526
- Fender RP, Belloni TM, Gallo E (2004) Towards a unified model for black hole X-ray binary jets. *MNRAS*355:1105–1118. <https://doi.org/10.1111/j.1365-2966.2004.08384.x>, [arXiv:astro-ph/0409360](https://arxiv.org/abs/astro-ph/0409360)
- Ferland GJ, Chatzikos M, Guzmán F, et al (2017) The 2017 Release Cloudy. *Rev. Mex. Astron. Astrofis.*53:385–438. <https://doi.org/10.48550/arXiv.1705.10877>, [arXiv:1705.10877](https://arxiv.org/abs/1705.10877) [astro-ph.GA]
- Ferreira J (1997) Magnetically-driven jets from Keplerian accretion discs. *A&A*319:340–359. <https://doi.org/10.48550/arXiv.astro-ph/9607057>, [arXiv:astro-ph/9607057](https://arxiv.org/abs/astro-ph/9607057) [astro-ph]
- Ferreira J, Pelletier G (1995) Magnetized accretion-ejection structures. III. Stellar and extragalactic jets as weakly dissipative disk outflows. *A&A*295:807
- Fijma S, Castro Segura N, Degenaar N, et al (2023) A transient ultraviolet outflow in the short-period x-ray binary uw crb. *MNRAS*526(1):L149–L154. <https://doi.org/10.1093/mnrasl/slad125>, URL <https://ui.adsabs.harvard.edu/abs/2023MNRAS.526L.149F>, [arXiv:2305.10793](https://arxiv.org/abs/2305.10793) [astro-ph.HE]
- Fijma S, Degenaar N, Castro Segura N, et al (2025) A multi-wavelength view of the outflowing short-period X-ray binary UW CrB. *MNRAS*<https://doi.org/10.1093/mnras/staf1790>
- Folha DFM, Emerson JP (2001) Near infrared hydrogen lines as diagnostic of accretion and winds in T Tauri stars. *Astronomy and Astrophysics* 365:90–109. <https://doi.org/10.1051/0004-6361:20000018>, URL <https://ui.adsabs.harvard.edu/abs/2001A&A...365...90F>, aDS Bibcode: 2001A&A...365...90F
- Frank J, King A, Raine D (1992) *Accretion Power in Astrophysics*. *Accretion Power in Astrophysics*, ISBN 0521408636, Cambridge University Press, 1992.
- Fukumura K, Kazanas D, Contopoulos I, et al (2010) Magnetohydrodynamic Accretion Disk Winds as X-ray Absorbers in Active Galactic Nuclei. *ApJ*715(1):636–650. <https://doi.org/10.1088/0004-637X/715/1/636>, [arXiv:0910.3001](https://arxiv.org/abs/0910.3001) [astro-ph.HE]

- Fukumura K, Tombesi F, Kazanas D, et al (2015) Magnetically Driven Accretion Disk Winds and Ultra-fast Outflows in PG 1211+143. *ApJ*805(1):17. <https://doi.org/10.1088/0004-637X/805/1/17>, [arXiv:1503.04074](https://arxiv.org/abs/1503.04074) [astro-ph.HE]
- Fukumura K, Kazanas D, Shrader C, et al (2017) Magnetic origin of black hole winds across the mass scale. *Nature Astronomy* 1:0062. <https://doi.org/10.1038/s41550-017-0062>, [arXiv:1702.02197](https://arxiv.org/abs/1702.02197) [astro-ph.HE]
- Gambino AF, Iaria R, Di Salvo T, et al (2019) Spectral analysis of the dipping LMXB system XB 1916-053. *A&A*625:A92. <https://doi.org/10.1051/0004-6361/201832984>, [arXiv:1904.05770](https://arxiv.org/abs/1904.05770) [astro-ph.HE]
- Gatuzz E, García JA, Kallman TR, et al (2016) Oxygen, neon, and iron X-ray absorption in the local interstellar medium. *A&A*588:A111. <https://doi.org/10.1051/0004-6361/201527752>, [arXiv:1602.06955](https://arxiv.org/abs/1602.06955) [astro-ph.HE]
- Gatuzz E, Díaz Trigo M, Miller-Jones JCA, et al (2019) Chandra high-resolution spectra of 4u 1630-47: the disappearance of the wind. *MNRAS*482:2597–2611. <https://doi.org/10.1093/mnras/sty2850>, URL <http://adsabs.harvard.edu/abs/2019MNRAS.482.2597G>, [arXiv:1810.09464](https://arxiv.org/abs/1810.09464) [astro-ph.HE]
- Gatuzz E, Díaz Trigo M, Miller-Jones JCA, et al (2020) Simultaneous detection of an intrinsic absorber and a compact jet emission in the X-ray binary IGR J17091-3624 during a hard accretion state. *MNRAS*491(4):4857–4868. <https://doi.org/10.1093/mnras/stz3385>, [arXiv:1912.02180](https://arxiv.org/abs/1912.02180) [astro-ph.HE]
- Gavriil FP, Strohmayer TE, Bhattacharyya S (2012) An Fe XXIV Absorption Line in the Persistent Spectrum of the Dipping Low-mass X-Ray Binary 1A 1744-361. *ApJ*753(1):2. <https://doi.org/10.1088/0004-637X/753/1/2>, [arXiv:0909.1607](https://arxiv.org/abs/0909.1607) [astro-ph.HE]
- Gilfanov M (2010) X-Ray Emission from Black-Hole Binaries. In: T. Belloni (ed) *Lecture Notes in Physics*, Berlin Springer Verlag, pp 17–+, [https://doi.org/10.1007/978-3-540-76937-8\\_2](https://doi.org/10.1007/978-3-540-76937-8_2), 0909.2567
- Gu L, Raassen AJJ, Mao J, et al (2019) X-ray spectra of the Fe-L complex. *A&A*627:A51. <https://doi.org/10.1051/0004-6361/201833860>, [arXiv:1905.07871](https://arxiv.org/abs/1905.07871) [astro-ph.HE]
- Gunasekera CM, van Hoof PAM, Chatzikos M, et al (2023) The 23.01 Release of Cloudy. *Research Notes of the American Astronomical Society* 7(11):246. <https://doi.org/10.3847/2515-5172/ad0e75>, [arXiv:2311.10163](https://arxiv.org/abs/2311.10163) [astro-ph.GA]
- Hasinger G, van der Klis M (1989) Two patterns of correlated X-ray timing and spectral behaviour in low-mass X-ray binaries. *A&A*225:79–96

- Herrero A, Garcia M, Puls J, et al (2012) A peculiar of star in the local group galaxy ic 1613. *Astronomy & Astrophysics* 543:A85. <https://doi.org/10.1051/0004-6361/201118383>
- Higginbottom N, Proga D (2015) Coronae and Winds from Irradiated Disks in X-Ray Binaries. *ApJ*807(1):107. <https://doi.org/10.1088/0004-637X/807/1/107>, [arXiv:1504.03328](https://arxiv.org/abs/1504.03328) [astro-ph.HE]
- Higginbottom N, Proga D, Knigge C, et al (2014) Line-driven Disk Winds in Active Galactic Nuclei: The Critical Importance of Ionization and Radiative Transfer. *ApJ*789(1):19. <https://doi.org/10.1088/0004-637X/789/1/19>, [arXiv:1402.1849](https://arxiv.org/abs/1402.1849) [astro-ph.GA]
- Higginbottom N, Proga D, Knigge C, et al (2017) Thermal Disk Winds in X-Ray Binaries: Realistic Heating and Cooling Rates Give Rise to Slow, but Massive, Outflows. *ApJ*836(1):42. <https://doi.org/10.3847/1538-4357/836/1/42>, [arXiv:1612.08996](https://arxiv.org/abs/1612.08996) [astro-ph.HE]
- Higginbottom N, Knigge C, Long KS, et al (2018) Radiation-hydrodynamic simulations of thermally driven disc winds in X-ray binaries: a direct comparison to GRO J1655-40. *MNRAS*479(3):3651–3662. <https://doi.org/10.1093/mnras/sty1599>, [arXiv:1806.04887](https://arxiv.org/abs/1806.04887) [astro-ph.HE]
- Higginbottom N, Knigge C, Long KS, et al (2019) The luminosity dependence of thermally driven disc winds in low-mass x-ray binaries. *MNRAS*484(4):4635–4644. <https://doi.org/10.1093/mnras/stz310>, URL <https://ui.adsabs.harvard.edu/abs/2019MNRAS.484.4635H>, [arXiv:1901.09684](https://arxiv.org/abs/1901.09684) [astro-ph.HE]
- Higginbottom N, Knigge C, Sim SA, et al (2020) Thermal and radiation driving can produce observable disc winds in hard-state x-ray binaries. *MNRAS*492(4):5271–5279. <https://doi.org/10.1093/mnras/staa209>, URL <https://ui.adsabs.harvard.edu/abs/2020MNRAS.492.5271H>, [arXiv:2001.08547](https://arxiv.org/abs/2001.08547) [astro-ph.HE]
- Higginbottom N, Scepi N, Knigge C, et al (2024) State-of-the-art simulations of line-driven accretion disc winds: realistic radiation hydrodynamics leads to weaker outflows. *MNRAS*527(3):9236–9249. <https://doi.org/10.1093/mnras/stad3830>, [arXiv:2312.06042](https://arxiv.org/abs/2312.06042) [astro-ph.HE]
- Homan J, Wijnands R, van der Klis M, et al (2001) Correlated X-Ray Spectral and Timing Behavior of the Black Hole Candidate XTE J1550-564: A New Interpretation of Black Hole States. *ApJS*132:377–402. <https://doi.org/10.1086/318954>, [arXiv:astro-ph/0001163](https://arxiv.org/abs/astro-ph/0001163)
- Homan J, van der Klis M, Fridriksson JK, et al (2010) XTE J1701-462 and Its Implications for the Nature of Subclasses in Low-magnetic-field Neutron Star Low-mass X-ray Binaries. *ApJ*719:201–212. <https://doi.org/10.1088/0004-637X/719/1/201>, [arXiv:1005.3210](https://arxiv.org/abs/1005.3210) [astro-ph.HE]

- Homan J, Neilsen J, Allen JL, et al (2016) Evidence for simultaneous jets and disk winds in luminous low-mass x-ray binaries. *ApJ*830:L5. <https://doi.org/10.3847/2041-8205/830/1/L5>, URL <http://adsabs.harvard.edu/abs/2016ApJ...830L...5H>
- Hori T, Ueda Y, Done C, et al (2018) Evolution of Thermally Driven Disk Wind in the Black Hole Binary 4U 1630-47 Observed with Suzaku and NuSTAR. *ApJ*869(2):183. <https://doi.org/10.3847/1538-4357/aaca5e>
- Hyodo Y, Ueda Y, Yuasa T, et al (2009) Timing and Spectral Study of AXJ1745.6-2901 with Suzaku. *PASJ*61:S99. <https://doi.org/10.1093/pasj/61.sp1.S99>
- Iaria R, Di Salvo T, Lavagetto G, et al (2006) Chandra Observation of the Persistent Emission from the Dipping Source XB 1916-053. *ApJ*647(2):1341–1348. <https://doi.org/10.1086/505616>, [arXiv:astro-ph/0605055](https://arxiv.org/abs/astro-ph/0605055) [astro-ph]
- Iaria R, di Salvo T, Lavagetto G, et al (2007a) Chandra observation of the dipping source XB 1254-690. *A&A*464:291–297. <https://doi.org/10.1051/0004-6361:20065644>, [astro-ph/0612592](https://arxiv.org/abs/astro-ph/0612592)
- Iaria R, Lavagetto G, D’Aí A, et al (2007b) Chandra observation of the Big Dipper X 1624-490. *A&A*463(1):289–295. <https://doi.org/10.1051/0004-6361:20065862>, [arXiv:astro-ph/0612269](https://arxiv.org/abs/astro-ph/0612269) [astro-ph]
- Iaria R, D’Aí A, Lavagetto G, et al (2008) Chandra Observation of Cir X-1 near the Periastron Passage: Evidence for an X-Ray Jet? *ApJ*673(2):1033–1043. <https://doi.org/10.1086/524311>
- Iaria R, Di Salvo T, D’Aí A, et al (2013) X-ray spectroscopy of the ADC source X1822-371 with Chandra and XMM-Newton. *A&A*549:A33. <https://doi.org/10.1051/0004-6361/201015305>, [arXiv:1210.0874](https://arxiv.org/abs/1210.0874) [astro-ph.HE]
- Iaria R, Mazzola SM, Bassi T, et al (2019) Broadband spectral analysis of MXB 1659-298 in its soft and hard state. *A&A*630:A138. <https://doi.org/10.1051/0004-6361/201833982>, [arXiv:1807.11431](https://arxiv.org/abs/1807.11431) [astro-ph.HE]
- Igo Z, Parker ML, Matzeu GA, et al (2020) Searching for ultra-fast outflows in agn using variability spectra. *MNRAS*493(1):1088–1108. <https://doi.org/10.1093/mnras/staa265>, URL <https://ui.adsabs.harvard.edu/abs/2020MNRAS.493.1088I>, [arXiv:2001.08208](https://arxiv.org/abs/2001.08208) [astro-ph.HE]
- Iijima T, Esenoglu HH (2003) Spectral evolution of nova (v1494) aql and its high velocity jets. *A&A*404:997–1009. <https://doi.org/10.1051/0004-6361:20030528>, URL <http://adsabs.harvard.edu/abs/2003A%26A...404..997I>
- Ji L, Schulz N, Nowak M, et al (2009) The Photoionized Accretion Disk in Her X-1. *ApJ*700(2):977–988. <https://doi.org/10.1088/0004-637X/700/2/977>, [arXiv:0905.3773](https://arxiv.org/abs/0905.3773) [astro-ph.HE]

- Ji L, Schulz NS, Nowak MA, et al (2011) Implications of X-ray Line Variations for 4U1822-371. *ApJ*729(2):102. <https://doi.org/10.1088/0004-637X/729/2/102>, [arXiv:1007.3839](https://arxiv.org/abs/1007.3839) [astro-ph.HE]
- Jiang YF, Stone JM, Davis SW (2014) A Global Three-dimensional Radiation Magneto-hydrodynamic Simulation of Super-Eddington Accretion Disks. *ApJ*796(2):106. <https://doi.org/10.1088/0004-637X/796/2/106>, [arXiv:1410.0678](https://arxiv.org/abs/1410.0678) [astro-ph.HE]
- Jimenez-Garate MA, Hailey CJ, den Herder JW, et al (2002) High-Resolution X-Ray Spectroscopy of Hercules X-1 with the XMM-Newton Reflection Grating Spectrometer: CNO Element Abundance Measurements and Density Diagnostics of a Photoionized Plasma. *ApJ*578(1):391–404. <https://doi.org/10.1086/342348>, [arXiv:astro-ph/0206181](https://arxiv.org/abs/astro-ph/0206181) [astro-ph]
- Jimenez-Garate MA, Schulz NS, Marshall HL (2003) Discrete X-Ray Signatures of a Photoionized Plasma above the Accretion Disk of the Neutron Star EXO 0748-676. *ApJ*590:432–444
- Jimenez-Garate MA, Raymond JC, Liedahl DA, et al (2005) Identification of an Extended Accretion Disk Corona in the Hercules X-1 Low State: Moderate Optical Depth, Precise Density Determination, and Verification of CNO Abundances. *ApJ*625(2):931–950. <https://doi.org/10.1086/426702>, [arXiv:astro-ph/0411780](https://arxiv.org/abs/astro-ph/0411780) [astro-ph]
- Jiménez-Ibarra F, Muñoz-Darias T, Casares J, et al (2019) An equatorial outflow in the black hole optical dipper swift j1357.2-0933. *MNRAS*489:3420–3426. <https://doi.org/10.1093/mnras/stz2393>, URL <https://ui.adsabs.harvard.edu/abs/2019MNRAS.489.3420J>, [arXiv:1908.00356](https://arxiv.org/abs/1908.00356) [astro-ph.HE]
- Juett A, Chakrabarty D (2006) Detection of Highly Ionized Metal Absorption Lines in the Ultracompact X-Ray Dipper 4U 1916-05. *ApJ*646:493–498
- Kafka S, Honeycutt RK (2004) Detecting outflows from cataclysmic variables in the optical. *AJ*128:2420–2429. <https://doi.org/10.1086/424618>, URL <http://adsabs.harvard.edu/abs/2004AJ....128.2420K>
- Kallman T, Bautista M (2001) Photoionization and High-Density Gas. *ApJS*133(1):221–253. <https://doi.org/10.1086/319184>
- Kallman TR, McCray R (1982) X-ray nebular models. *ApJS*50:263–317. <https://doi.org/10.1086/190828>, URL <https://ui.adsabs.harvard.edu/abs/1982ApJS...50..263K>
- Kallman TR, Angelini L, Boroson B, et al (2003) Chandra and XMM Observations of the Accretion Disk Corona Source 2S 0921-63. *ApJ*583(2):861–877. <https://doi.org/10.1086/345475>, [arXiv:astro-ph/0209010](https://arxiv.org/abs/astro-ph/0209010) [astro-ph]

- Kallman TR, Palmeri P, Bautista MA, et al (2004) Photoionization Modeling and the K Lines of Iron. *ApJS*155(2):675–701. <https://doi.org/10.1086/424039>, arXiv:astro-ph/0405210 [astro-ph]
- Kallman TR, Bautista MA, Goriely S, et al (2009) Spectrum Synthesis Modeling of the X-Ray Spectrum of GRO J1655-40 Taken During the 2005 Outburst. *ApJ*701(2):865–884. <https://doi.org/10.1088/0004-637X/701/2/865>, arXiv:0905.4206 [astro-ph.HE]
- Kennedy MR, Callanan P, Garnavich PM, et al (2025) Analysis of optical spectroscopy and photometry of the type I X-ray bursting system UW CrB. *The Open Journal of Astrophysics* 8:71. <https://doi.org/10.33232/001c.140729>, URL <https://ui.adsabs.harvard.edu/abs/2025OJAp....8E..71K>, aDS Bibcode: 2025OJAp....8E..71K
- King A, Pounds K (2015) Powerful outflows and feedback from active galactic nuclei. *ARA&A*53:115–154. <https://doi.org/10.1146/annurev-astro-082214-122316>, URL <https://ui.adsabs.harvard.edu/abs/2015ARA&A..53..115K>, arXiv:1503.05206 [astro-ph.GA]
- King AL, Miller JM, Raymond J, et al (2012) An Extreme X-Ray Disk Wind in the Black Hole Candidate IGR J17091-3624. *The Astrophysical Journal* 746:L20. <https://doi.org/10.1088/2041-8205/746/2/L20>, URL <https://ui.adsabs.harvard.edu/abs/2012ApJ...746L..20K>, aDS Bibcode: 2012ApJ...746L..20K
- King AL, Miller JM, Raymond J, et al (2013) Regulation of Black Hole Winds and Jets across the Mass Scale. *ApJ*762(2):103. <https://doi.org/10.1088/0004-637X/762/2/103>, arXiv:1205.4222 [astro-ph.HE]
- King AL, Walton DJ, Miller JM, et al (2014) The Disk Wind in the Rapidly Spinning Stellar-mass Black Hole 4U 1630-472 Observed with NuSTAR. *ApJ*784(1):L2. <https://doi.org/10.1088/2041-8205/784/1/L2>, arXiv:1401.3646 [astro-ph.HE]
- King AL, Miller JM, Raymond J, et al (2015) High-resolution Chandra HETG Spectroscopy of V404 Cygni in Outburst. *ApJ*813:L37. <https://doi.org/10.1088/2041-8205/813/2/L37>, arXiv:1508.01181 [astro-ph.HE]
- Koljonen KII, Long KS, Matthews JH, et al (2023) The origin of optical emission lines in the soft state of X-ray binary outbursts: the case of MAXI J1820+070. *MNRAS*521(3):4190–4206. <https://doi.org/10.1093/mnras/stad809>, arXiv:2303.09242 [astro-ph.HE]
- Kosec P, Fabian AC, Pinto C, et al (2020) An ionized accretion disc wind in Hercules X-1. *MNRAS*491(3):3730–3750. <https://doi.org/10.1093/mnras/stz3200>, arXiv:1910.08337 [astro-ph.HE]
- Kosec P, Kara E, Fabian AC, et al (2023) Vertical wind structure in an X-ray binary revealed by a precessing accretion disk. *Nature Astronomy* 7:715–723. <https://doi.org/10.1038/s41568-023-01400-0>

[org/10.1038/s41550-023-01929-7](https://doi.org/10.1038/s41550-023-01929-7), [arXiv:2304.05490](https://arxiv.org/abs/2304.05490) [astro-ph.HE]

- Kotani T, Ebisawa K, Dotani T, et al (2000) ASCA Observations of the Absorption Line Features from the Superluminal Jet Source GRS 1915+105. *ApJ*539(1):413–423. <https://doi.org/10.1086/309200>, [arXiv:astro-ph/0003237](https://arxiv.org/abs/astro-ph/0003237) [astro-ph]
- Krolik JH, McKee CF, Tarter CB (1981) Two-phase models of quasar emission line regions. *ApJ*249:422–442. <https://doi.org/10.1086/159303>, URL <https://ui.adsabs.harvard.edu/abs/1981ApJ...249..422K>
- Kubota A, Done C (2019) Modelling the spectral energy distribution of super-Eddington quasars. *MNRAS*489(1):524–533. <https://doi.org/10.1093/mnras/stz2140>, [arXiv:1905.02920](https://arxiv.org/abs/1905.02920) [astro-ph.GA]
- Kubota A, Dotani T, Cottam J, et al (2007) Suzaku Discovery of Iron Absorption Lines in Outburst Spectra of the X-Ray Transient 4U 1630-472. *PASJ*59:185–198. <https://doi.org/10.1093/pasj/59.sp1.S185>, [arXiv:astro-ph/0610496](https://arxiv.org/abs/astro-ph/0610496) [astro-ph]
- Kudritzki RP, Puls J (2000) Winds from hot stars. *ARA&A*38:613–666. <https://doi.org/10.1146/annurev.astro.38.1.613>, URL <http://adsabs.harvard.edu/abs/2000ARA%26A..38..613K>
- Kuulkers E, van der Klis M, Oosterbroek T, et al (1994) Spectral and correlated timing behaviour of GX 5-1. *A&A*289:795–821
- Lasota JP (2001) The disc instability model of dwarf novae and low-mass x-ray binary transients. *New Astron. Rev.*45:449–508. [https://doi.org/10.1016/S1387-6473\(01\)00112-9](https://doi.org/10.1016/S1387-6473(01)00112-9), [astro-ph/0102072](https://arxiv.org/abs/astro-ph/0102072)
- Lee JC, Reynolds CS, Remillard R, et al (2002) High-Resolution Chandra HETGS and Rossi X-Ray Timing Explorer Observations of GRS 1915+105: A Hot Disk Atmosphere and Cold Gas Enriched in Iron and Silicon. *ApJ*567:1102–1111. <https://doi.org/10.1086/338588>, [astro-ph/0208187](https://arxiv.org/abs/astro-ph/0208187)
- Lin D, Remillard RA, Homan J (2007) Evaluating Spectral Models and the X-Ray States of Neutron Star X-Ray Transients. *ApJ*667:1073–1086. <https://doi.org/10.1086/521181>, [astro-ph/0702089](https://arxiv.org/abs/astro-ph/0702089)
- Lindstrøm C, Griffin J, Kiss LL, et al (2005) New clues on outburst mechanisms and improved spectroscopic elements of the black hole binary V4641 Sagittarii\*. *MNRAS*363:882–890. <https://doi.org/10.1111/j.1365-2966.2005.09483.x>
- Lovelace RVE, Berk HL, Contopoulos J (1991) Magnetically Driven Jets and Winds. *ApJ*379:696. <https://doi.org/10.1086/170544>
- Luo Y, Fang T (2014) On the Origin of Highly Ionized X-Ray Absorbers Detected in the Galactic X-Ray Binaries. *ApJ*780(2):170. <https://doi.org/10.1088/0004-637X/>

780/2/170, [arXiv:1312.2084](https://arxiv.org/abs/1312.2084) [astro-ph.GA]

- Madej OK, Jonker PG, Díaz Trigo M, et al (2014) Variable Doppler shifts of the thermal wind absorption lines in low-mass X-ray binaries. *MNRAS*438:145–155. <https://doi.org/10.1093/mnras/stt2119>, [arXiv:1311.0874](https://arxiv.org/abs/1311.0874) [astro-ph.HE]
- Manca A, Gambino AF, Sanna A, et al (2023) Spectral analysis of the AMXP IGR J17591-2342 during its 2018 outburst. *MNRAS*519(2):2309–2320. <https://doi.org/10.1093/mnras/stac3707>, [arXiv:2212.07157](https://arxiv.org/abs/2212.07157) [astro-ph.HE]
- Marsh TR, Horne K (1988) Images of accretion discs. II - Doppler tomography. *MNRAS*235:269–286
- Mata Sánchez D, Muñoz-Darias T, Casares J, et al (2015) Mass constraints to sco x-1 from bowen fluorescence and deep near-infrared spectroscopy. *MNRAS*449:L1–L5. <https://doi.org/10.1093/mnrasl/slv002>, [arXiv:1501.02269](https://arxiv.org/abs/1501.02269) [astro-ph.HE]
- Mata Sánchez D, Muñoz-Darias T, Casares J, et al (2018) The 1989 and 2015 outbursts of v404 cygni: a global study of wind-related optical features. *MNRAS*481:2646–2665. <https://doi.org/10.1093/mnras/sty2402>, URL <http://adsabs.harvard.edu/abs/2018MNRAS.481.2646M>
- Mata Sánchez D, Muñoz-Darias T, Cúneo VA, et al (2022) Hard-state optical wind during the discovery outburst of the black hole x-ray dipper maxi j1803-298. *ApJ*926(2):L10. <https://doi.org/10.3847/2041-8213/ac502f>, URL <https://ui.adsabs.harvard.edu/abs/2022ApJ...926L..10M>
- Mata Sánchez D, Muñoz-Darias T, Casares J, et al (2023) Ask the machine: systematic detection of wind-type outflows in low-mass x-ray binaries. *MNRAS*524(1):338–350. <https://doi.org/10.1093/mnras/stad1895>, URL <https://ui.adsabs.harvard.edu/abs/2023MNRAS.524..338M>, [arXiv:2306.12475](https://arxiv.org/abs/2306.12475) [astro-ph.HE]
- Mata Sánchez D, Muñoz-Darias T, Armas Padilla M, et al (2024) Evidence for inflows and outflows in the nearby black hole transient swift j1727.8–162. *A&A*682:L1. <https://doi.org/10.1051/0004-6361/202348754>, URL <https://ui.adsabs.harvard.edu/abs/2024A&A...682L...1M>
- Matthews JH (2016) Disc Winds Matter: Modelling Accretion And Outflow On All Scales. PhD thesis, <https://doi.org/10.5281/zenodo.1256805>, URL <https://ui.adsabs.harvard.edu/abs/2016PhDT.....348M>, aDS Bibcode: 2016PhDT.....348M
- Matthews JH, Knigge C, Long KS, et al (2015) The impact of accretion disc winds on the optical spectra of cataclysmic variables. *MNRAS*450:3331–3344. <https://doi.org/10.1093/mnras/stv867>, URL <http://adsabs.harvard.edu/abs/2015MNRAS.450.3331M>, [arXiv:1504.05590](https://arxiv.org/abs/1504.05590) [astro-ph.SR]

- Matthews JH, Strong-Wright J, Knigge C, et al (2023) A disc wind model for blueshifts in quasar broad emission lines. *Monthly Notices of the Royal Astronomical Society* 526:3967–3986. <https://doi.org/10.1093/mnras/stad2895>, URL <https://ui.adsabs.harvard.edu/abs/2023MNRAS.526.3967M>, aDS Bibcode: 2023MNRAS.526.3967M
- Matthews JH, Long KS, Knigge C, et al (2025) SIROCCO: a publicly available Monte Carlo ionization and radiative transfer code for astrophysical outflows. *Monthly Notices of the Royal Astronomical Society* 536:879–904. <https://doi.org/10.1093/mnras/stae2677>, URL <https://ui.adsabs.harvard.edu/abs/2025MNRAS.536..879M>, aDS Bibcode: 2025MNRAS.536..879M
- Maury AC, Pickering EC (1897) Spectra of bright stars photographed with the 11-inch Draper Telescope as part of the Henry Draper Memorial. *Annals of Harvard College Observatory* 28:1–128
- Menzel DH (1929) The Wolf-Rayet Stars. *Publications of the Astronomical Society of the Pacific* 41:344. <https://doi.org/10.1086/123970>, URL <https://ui.adsabs.harvard.edu/abs/1929PASP...41..344M>, aDS Bibcode: 1929PASP...41..344M
- Miceli C, Mata Sánchez D, Anitra A, et al (2024) Soft-state optical spectroscopy of the black hole MAXI J1305-704. *Astronomy and Astrophysics* 684:A67. <https://doi.org/10.1051/0004-6361/202348482>, URL <https://ui.adsabs.harvard.edu/abs/2024A&A...684A..67M>, aDS Bibcode: 2024A&A...684A..67M
- Migliari S, Fender RP (2006) Jets in neutron star X-ray binaries: a comparison with black holes. *MNRAS* 366:79–91. <https://doi.org/10.1111/j.1365-2966.2005.09777.x>, [astro-ph/0510698](https://arxiv.org/abs/astro-ph/0510698)
- Miller JM (2007) Relativistic X-Ray Lines from the Inner Accretion Disks Around Black Holes. *Annual Review of Astronomy and Astrophysics* 45:441–479. <https://doi.org/10.1146/annurev.astro.45.051806.110555>, URL <https://ui.adsabs.harvard.edu/abs/2007ARA&A..45..441M>, aDS Bibcode: 2007ARA&A..45..441M
- Miller JM, Raymond J, Fabian A, et al (2006) The magnetic nature of disk accretion onto black holes. *Nature* 441:953–955. <https://doi.org/10.1038/nature04912>, [astro-ph/0605390](https://arxiv.org/abs/astro-ph/0605390)
- Miller JM, Raymond J, Homan J, et al (2006) Simultaneous Chandra and RXTE Spectroscopy of the Microquasar H1743-322: Clues to Disk Wind and Jet Formation from a Variable Ionized Outflow. *ApJ* 646(1):394–406. <https://doi.org/10.1086/504673>, [arXiv:astro-ph/0406272](https://arxiv.org/abs/astro-ph/0406272) [astro-ph]
- Miller JM, Raymond J, Reynolds CS, et al (2008) The Accretion Disk Wind in the Black Hole GRO J1655-40. *ApJ* 680(2):1359–1377. <https://doi.org/10.1086/588521>, [arXiv:0802.2026](https://arxiv.org/abs/0802.2026) [astro-ph]

- Miller JM, Maitra D, Cackett EM, et al (2011) A fast x-ray disk wind in the transient pulsar igr j17480-2446 in terzan 5. *ApJ*731(1):L7. <https://doi.org/10.1088/2041-8205/731/1/L7>, URL <https://ui.adsabs.harvard.edu/abs/2011ApJ...731L...7M>, [arXiv:1101.2377](https://arxiv.org/abs/1101.2377) [astro-ph.HE]
- Miller JM, Raymond J, Fabian AC, et al (2012) The Disk-wind-Jet Connection in the Black Hole H 1743-322. *ApJ*759(1):L6. <https://doi.org/10.1088/2041-8205/759/1/L6>, [arXiv:1208.4514](https://arxiv.org/abs/1208.4514) [astro-ph.HE]
- Miller JM, Raymond J, Kallman TR, et al (2014) Chandra spectroscopy of maxi j1305-704: Detection of an infalling black hole disk wind? *ApJ*788:53. <https://doi.org/10.1088/0004-637X/788/1/53>, URL <https://ui.adsabs.harvard.edu/abs/2014ApJ...788...53M>, [arXiv:1306.2915](https://arxiv.org/abs/1306.2915) [astro-ph.HE]
- Miller JM, Fabian AC, Kaastra J, et al (2015) Powerful, Rotating Disk Winds from Stellar-mass Black Holes. *The Astrophysical Journal* 814:87. <https://doi.org/10.1088/0004-637X/814/2/87>, URL <https://ui.adsabs.harvard.edu/abs/2015ApJ...814...87M>, aDS Bibcode: 2015ApJ...814...87M
- Miller JM, Raymond J, Cackett E, et al (2016) An Ultra-fast X-Ray Disk Wind in the Neutron Star Binary GX 340+0. *ApJ*822(1):L18. <https://doi.org/10.3847/2041-8205/822/1/L18>, [arXiv:1604.03329](https://arxiv.org/abs/1604.03329) [astro-ph.HE]
- Miller JM, Zoghbi A, Raymond J, et al (2020) An obscured, seyfert 2-like state of the stellar-mass black hole grs 1915+105 caused by failed disk winds. *ApJ*904(1):30. <https://doi.org/10.3847/1538-4357/abb31>, URL <https://ui.adsabs.harvard.edu/abs/2020ApJ...904...30M>, [arXiv:2007.07005](https://arxiv.org/abs/2007.07005) [astro-ph.HE]
- Miller JM, Mizumoto M, Shidatsu M, et al (2025) XRISM Spectroscopy of the Stellar-Mass Black Hole 4U 1630-472 in Outburst. *arXiv e-prints* [arXiv:2506.07319](https://arxiv.org/abs/2506.07319). <https://doi.org/10.48550/arXiv.2506.07319>, [arXiv:2506.07319](https://arxiv.org/abs/2506.07319) [astro-ph.HE]
- Mirabel IF, Rodriguez LF (1999) Sources of relativistic jets in the galaxy. *Ann Rev Astron Astrophys* 37:409–443. <https://doi.org/10.1146/annurev.astro.37.1.409>, [arXiv:astro-ph/9902062](https://arxiv.org/abs/astro-ph/9902062) [astro-ph]
- Miyamoto S, Kitamoto S, Iga S, et al (1992) Canonical time variations of X-rays from black hole candidates in the low-intensity state. *ApJ*391:L21–L24. <https://doi.org/10.1086/186389>
- Miyamoto S, Iga S, Kitamoto S, et al (1993) Another canonical time variation of X-rays from black hole candidates in the very high flare state? *ApJ*403:L39–L42. <https://doi.org/10.1086/186716>
- Mizumoto M, Nomura M, Done C, et al (2021) UV line-driven disc wind as the origin of UltraFast Outflows in AGN. *MNRAS*503(1):1442–1458. <https://doi.org/10.1093/mnras/staa3282>, [arXiv:2003.01137](https://arxiv.org/abs/2003.01137) [astro-ph.HE]

- Mondal AS, Raychaudhuri B, Dewangan GC (2024) Relativistic X-ray reflection and highly ionized absorption in the spectrum of NS LMXB 1A 1744-361. *MNRAS*527(2):2362–2370. <https://doi.org/10.1093/mnras/stad3326>, [arXiv:2309.12637](https://arxiv.org/abs/2309.12637) [astro-ph.HE]
- Morris SL, Liebert J, Stocke JT, et al (1990) MS 1603.6+2600, an Unusual X-Ray Selected Binary System at High Galactic Latitude. *The Astrophysical Journal* 365:686. <https://doi.org/10.1086/169523>, URL <https://ui.adsabs.harvard.edu/abs/1990ApJ...365..686M>, aDS Bibcode: 1990ApJ...365..686M
- Motta SE, Kajava JJE, Sánchez-Fernández C, et al (2017) The black hole binary v404 cygni: a highly accreting obscured agn analogue. *MNRAS*468:981–993. <https://doi.org/10.1093/mnras/stx466>, URL <http://adsabs.harvard.edu/abs/2017MNRAS.468..981M>, [arXiv:1607.02255](https://arxiv.org/abs/1607.02255) [astro-ph.HE]
- Motta SE, Kajava JJE, Giustini M, et al (2021) Observations of a radio-bright, X-ray obscured GRS 1915+105. *MNRAS*503(1):152–161. <https://doi.org/10.1093/mnras/stab511>, [arXiv:2101.01187](https://arxiv.org/abs/2101.01187) [astro-ph.HE]
- Muñoz-Darias T, Motta S, Belloni TM (2011) Fast variability as a tracer of accretion regimes in black hole transients. *MNRAS*410:679–684. <https://doi.org/10.1111/j.1365-2966.2010.17476.x>, [arXiv:1008.0558](https://arxiv.org/abs/1008.0558) [astro-ph.HE]
- Muñoz-Darias T, Coriat M, Plant DS, et al (2013) Inclination and relativistic effects in the outburst evolution of black hole transients. *MNRAS*432:1330–1337. <https://doi.org/10.1093/mnras/stt546>, [arXiv:1304.2072](https://arxiv.org/abs/1304.2072) [astro-ph.HE]
- Muñoz-Darias T, Fender RP, Motta SE, et al (2014) Black hole-like hysteresis and accretion states in neutron star low-mass X-ray binaries. *MNRAS*443:3270–3283. <https://doi.org/10.1093/mnras/stu1334>, [arXiv:1407.1318](https://arxiv.org/abs/1407.1318) [astro-ph.HE]
- Muñoz-Darias T, Ponti G (2022) Simultaneous x-ray and optical spectroscopy of v404 cygni supports the multi-phase nature of x-ray binary accretion disc winds. *A&A*664:A104. <https://doi.org/10.1051/0004-6361/202243769>, URL <https://ui.adsabs.harvard.edu/abs/2022A&A...664A.104M>, [arXiv:2205.14162](https://arxiv.org/abs/2205.14162) [astro-ph.HE]
- Muñoz-Darias T, Casares J, Mata Sánchez D, et al (2016) Regulation of black-hole accretion by a disk wind during a violent outburst of V404 Cygni. *Nature*534:75–78. <https://doi.org/10.1038/nature17446>
- Muñoz-Darias T, Casares J, Mata Sánchez D, et al (2017) Flares, wind and nebulae: the 2015 december mini-outburst of v404 cygni. *MNRAS*465:L124–L128. <https://doi.org/10.1093/mnrasl/slw222>
- Muñoz-Darias T, Torres MAP, Garcia MR (2018) The low-luminosity accretion disc wind of the black hole transient v4641 sagittarii. *MNRAS*479:3987–3995. <https://doi.org/10.1093/mnras/sty1711>, URL <http://adsabs.harvard.edu/>

[abs/2018MNRAS.479.3987M](https://arxiv.org/abs/2018MNRAS.479.3987M)

- Muñoz-Darias T, Jiménez-Ibarra F, Panizo-Espinar G, et al (2019) Hard-state accretion disk winds from black holes: The revealing case of maxi j1820+070. *ApJ*879:L4. <https://doi.org/10.3847/2041-8213/ab2768>, URL <https://ui.adsabs.harvard.edu/abs/2019ApJ...879L...4M>
- Muñoz-Darias T, Armas Padilla M, Jiménez-Ibarra F, et al (2020) The changing-look optical wind of the flaring x-ray transient swift j1858.6-0814. *ApJ*893(1):L19. <https://doi.org/10.3847/2041-8213/ab8381>, URL <https://ui.adsabs.harvard.edu/abs/2020ApJ...893L..19M>
- Narayan R, Igumenshchev IV, Abramowicz MA (2003) Magnetically Arrested Disk: an Energetically Efficient Accretion Flow. *PASJ*55:L69–L72. <https://doi.org/10.1093/pasj/55.6.L69>, [arXiv:astro-ph/0305029](https://arxiv.org/abs/astro-ph/0305029) [astro-ph]
- Neilsen J, Degenaar N (2023) High-Resolution Spectroscopy of X-ray Binaries. *arXiv e-prints* [arXiv:2304.05412](https://arxiv.org/abs/2304.05412). <https://doi.org/10.48550/arXiv.2304.05412>, [arXiv:2304.05412](https://arxiv.org/abs/2304.05412) [astro-ph.HE]
- Neilsen J, Homan J (2012) A Hybrid Magnetically/Thermally Driven Wind in the Black Hole GRO J1655-40? *ApJ*750(1):27. <https://doi.org/10.1088/0004-637X/750/1/27>, [arXiv:1202.6053](https://arxiv.org/abs/1202.6053) [astro-ph.HE]
- Neilsen J, Lee JC (2009) Accretion disk winds as the jet suppression mechanism in the microquasar GRS 1915+105. *Nature*458:481–484. <https://doi.org/10.1038/nature07680>
- Neilsen J, Remillard RA, Lee JC (2011) The Physics of the "Heartbeat" State of GRS 1915+105. *ApJ*737:69. <https://doi.org/10.1088/0004-637X/737/2/69>, [arXiv:1106.0298](https://arxiv.org/abs/1106.0298) [astro-ph.HE]
- Neilsen J, Coriat M, Fender R, et al (2014) A Link between X-Ray Emission Lines and Radio Jets in 4U 1630-47? *The Astrophysical Journal* 784:L5. <https://doi.org/10.1088/2041-8205/784/1/L5>, URL <https://ui.adsabs.harvard.edu/abs/2014ApJ...784L...5N>, aDS Bibcode: 2014ApJ...784L...5N
- Ng M, Hughes AK, Homan J, et al (2024) X-Ray and Radio Monitoring of the Neutron Star Low-mass X-Ray Binary 1A 1744-361: Quasiperiodic Oscillations, Transient Ejections, and a Disk Atmosphere. *ApJ*966(2):232. <https://doi.org/10.3847/1538-4357/ad35bd>, [arXiv:2310.01511](https://arxiv.org/abs/2310.01511) [astro-ph.HE]
- Nitindala AP, Veledina A, Poutanen J (2025) X-ray polarization from accretion disk winds. *Astronomy and Astrophysics* 694:A230. <https://doi.org/10.1051/0004-6361/202453188>, URL <https://ui.adsabs.harvard.edu/abs/2025A&A...694A.230N>, aDS Bibcode: 2025A&A...694A.230N

- Nomura M, Ohsuga K, Takahashi HR, et al (2016) Radiation hydrodynamic simulations of line-driven disk winds for ultra-fast outflows. PASJ68(1):16. <https://doi.org/10.1093/pasj/psv124>, [arXiv:1511.08815](https://arxiv.org/abs/1511.08815) [astro-ph.HE]
- Nowak MA, Paizis A, Jaisawal GK, et al (2019) Chandra-HETGS Characterization of an Outflowing Wind in the Accreting Millisecond Pulsar IGR J17591-2342. ApJ874(1):69. <https://doi.org/10.3847/1538-4357/ab0a71>, [arXiv:1902.09577](https://arxiv.org/abs/1902.09577) [astro-ph.HE]
- Ohsuga K, Mori M, Nakamoto T, et al (2005) Supercritical Accretion Flows around Black Holes: Two-dimensional, Radiation Pressure-dominated Disks with Photon Trapping. ApJ628(1):368–381. <https://doi.org/10.1086/430728>, [arXiv:astro-ph/0504168](https://arxiv.org/abs/astro-ph/0504168) [astro-ph]
- Pahari M, Bhattacharyya S, Rao AR, et al (2018) AstroSat and Chandra View of the High Soft State of 4U 1630-47 (4U 1630-472): Evidence of the Disk Wind and a Rapidly Spinning Black Hole. ApJ867(2):86. <https://doi.org/10.3847/1538-4357/aae53b>, [arXiv:1810.01275](https://arxiv.org/abs/1810.01275) [astro-ph.HE]
- Paice JA, Gandhi P, Dhillon VS, et al (2018) Blue Oscillations and Rapid Red Flares in Swift J1858.6-0814 Observed with ULTRACAM/NTT. The Astronomer’s Telegram 12197:1
- Panizo-Espinar G, Muñoz-Darias T, Armas Padilla M, et al (2021) Optical nebular emission following the most luminous outburst of aquila x-1. A&A650:A135. <https://doi.org/10.1051/0004-6361/202140323>, URL <https://ui.adsabs.harvard.edu/abs/2021A&A...650A.135P>
- Panizo-Espinar G, Armas Padilla M, Muñoz-Darias T, et al (2022) Discovery of optical and infrared accretion disc wind signatures in the black hole candidate maxi j1348-630. A&A664:A100. <https://doi.org/10.1051/0004-6361/202243426>, URL <https://ui.adsabs.harvard.edu/abs/2022A&A...664A.100P>
- Panizo-Espinar G, Muñoz-Darias T, Armas Padilla M, et al (2024) The omnipresent flux-dependent optical dips of the black hole transient swift j1357.2–0933. A&A682:A19. <https://doi.org/10.1051/0004-6361/202347955>, URL <https://ui.adsabs.harvard.edu/abs/2024A&A...682A..19P>, [arXiv:2311.03460](https://arxiv.org/abs/2311.03460) [astro-ph.HE]
- Parmar AN, Oosterbroek T, Boirin L, et al (2002) Discovery of narrow X-ray absorption features from the dipping low-mass X-ray binary X 1624-490 with XMM-Newton. A&A386:910–915. URL [http://cdsads.u-strasbg.fr/cgi-bin/nph-bib\\_query?bibcode=2002A%26A...386..910P&db\\_key=AST](http://cdsads.u-strasbg.fr/cgi-bin/nph-bib_query?bibcode=2002A%26A...386..910P&db_key=AST)
- Parra M, Petrucci PO, Bianchi S, et al (2024) The current state of disk wind observations in bhlmxbs through x-ray absorption lines in the iron band. A&A681:A49. <https://doi.org/10.1051/0004-6361/202346920>, URL <https://ui.adsabs.harvard.edu/abs/2024A&A...681A..49P>

[ui.adsabs.harvard.edu/abs/2024A&A...681A..49P](https://ui.adsabs.harvard.edu/abs/2024A&A...681A..49P), arXiv:2308.00691 [astro-ph.HE]

- Payne CH (1930) On the Spectra of the Wolf-Rayet Stars. Harvard College Observatory Bulletin 874:23–30. URL <https://ui.adsabs.harvard.edu/abs/1930BHarO.874..23P>, aDS Bibcode: 1930BHarO.874...23P
- Petrov B, Vink JS, Gräfener G (2014) On the  $h\alpha$  behaviour of blue supergiants: rise and fall over the bi-stability jump. *Astronomy and Astrophysics* 565:A62. <https://doi.org/10.1051/0004-6361/201322754>, URL <https://ui.adsabs.harvard.edu/abs/2014A&A...565A..62P>, aDS Bibcode: 2014A&A...565A..62P
- Ponti G, Fender RP, Begelman MC, et al (2012) Ubiquitous equatorial accretion disc winds in black hole soft states. *MNRAS*422:L11. <https://doi.org/10.1111/j.1745-3933.2012.01224.x>
- Ponti G, Muñoz-Darias T, Fender RP (2014) A connection between accretion state and Fe K absorption in an accreting neutron star: black hole-like soft-state winds? *MNRAS*444:1829–1834. <https://doi.org/10.1093/mnras/stu1742>, arXiv:1407.4468 [astro-ph.HE]
- Ponti G, Bianchi S, Muñoz-Darias T, et al (2015) On the Fe K absorption - accretion state connection in the Galactic Centre neutron star X-ray binary AX J1745.6-2901. *MNRAS*446:1536–1550. <https://doi.org/10.1093/mnras/stu1853>, arXiv:1409.3224 [astro-ph.HE]
- Ponti G, Bianchi S, Muñoz-Darias T, et al (2016) High ionisation absorption in low mass x-ray binaries. *Astronomische Nachrichten* 337:512–517. <https://doi.org/10.1002/asna.201612339>, URL <http://adsabs.harvard.edu/abs/2016AN....337..512P>, arXiv:1510.08902 [astro-ph.HE]
- Ponti G, Bianchi S, Muñoz-Darias T, et al (2018) Measuring masses in low mass x-ray binaries via x-ray spectroscopy: the case of mxb 1659-298. *MNRAS*481(1):L94–L99. <https://doi.org/10.1093/mnrasl/sly120>, URL <https://ui.adsabs.harvard.edu/abs/2018MNRAS.481L..94P>, arXiv:1807.04757 [astro-ph.HE]
- Ponti G, Bianchi S, De Marco B, et al (2019) Evolution of the disc atmosphere in the X-ray binary MXB 1659-298, during its 2015-17 outburst. *MNRAS*487(1):858–870. <https://doi.org/10.1093/mnras/stz1245>, arXiv:1905.01308 [astro-ph.HE]
- Poutanen J, Lipunova G, Fabrika S, et al (2007) Supercritically accreting stellar mass black holes as ultraluminous X-ray sources. *MNRAS*377(3):1187–1194. <https://doi.org/10.1111/j.1365-2966.2007.11668.x>, arXiv:astro-ph/0609274 [astro-ph]
- Prabhakar G, Mandal S, Bhuvana GR, et al (2023) Wideband study of the brightest black hole X-ray binary 4U 1543-47 in the 2021 outburst: signature of disc-wind regulated accretion. *Monthly Notices of the Royal Astronomical Society* 520:4889–4901. <https://doi.org/10.1093/mnras/stad080>, URL <https://ui.adsabs.harvard.edu/>

[abs/2023MNRAS.520.4889P](https://ui.adsabs.harvard.edu/abs/2023MNRAS.520.4889P), aDS Bibcode: 2023MNRAS.520.4889P

- Prinja RK, Fullerton AW (1994) Low-velocity variability in the stellar wind of hd 152408 (o8: Iafpe). *ApJ*426:345–356. <https://doi.org/10.1086/174070>, URL <http://adsabs.harvard.edu/abs/1994ApJ...426..345P>
- Prinja RK, Ringwald FA, Wade RA, et al (2000) HST ultraviolet observations of rapid variability in the accretion-disc wind of BZ Cam. *Monthly Notices of the Royal Astronomical Society* 312:316–326. <https://doi.org/10.1046/j.1365-8711.2000.03111.x>, URL <https://ui.adsabs.harvard.edu/abs/2000MNRAS.312..316P>, aDS Bibcode: 2000MNRAS.312..316P
- Proga D, Kallman TR (2002) On the Role of the Ultraviolet and X-Ray Radiation in Driving a Disk Wind in X-Ray Binaries. *ApJ*565(1):455–470. <https://doi.org/10.1086/324534>, [arXiv:astro-ph/0109064](https://arxiv.org/abs/astro-ph/0109064) [astro-ph]
- Proga D, Stone JM, Drew JE (1998) Radiation-driven winds from luminous accretion discs. *MNRAS*295(3):595–617. <https://doi.org/10.1046/j.1365-8711.1998.01337.x>, [arXiv:astro-ph/9710305](https://arxiv.org/abs/astro-ph/9710305) [astro-ph]
- Proga D, Stone JM, Kallman TR (2000) Dynamics of Line-driven Disk Winds in Active Galactic Nuclei. *ApJ*543(2):686–696. <https://doi.org/10.1086/317154>, [arXiv:astro-ph/0005315](https://arxiv.org/abs/astro-ph/0005315) [astro-ph]
- Proga D, Kallman TR, Drew JE, et al (2002) Resonance Line Profile Calculations Based on Hydrodynamical Models of Cataclysmic Variable Winds. *The Astrophysical Journal* 572:382–391. <https://doi.org/10.1086/340339>, URL <https://ui.adsabs.harvard.edu/abs/2002ApJ...572..382P>, aDS Bibcode: 2002ApJ...572..382P
- Psaradaki I, Costantini E, Mehdipour M, et al (2018) Modelling the disc atmosphere of the low mass X-ray binary EXO 0748-676. *A&A*620:A129. <https://doi.org/10.1051/0004-6361/201834000>, [arXiv:1809.06864](https://arxiv.org/abs/1809.06864) [astro-ph.HE]
- Pudritz RE, Norman CA (1986) Bipolar Hydromagnetic Winds from Disks around Protostellar Objects. *ApJ*301:571. <https://doi.org/10.1086/163924>
- Puls J, Kudritzki RP, Santolaya-Rey AE, et al (1998) Spectral Diagnostics of Blue Stars with Winds. p 245, URL <https://ui.adsabs.harvard.edu/abs/1998ASPC..131..245P>, aDS Bibcode: 1998ASPC..131..245P
- Rahoui F, Coriat M, Corbel S, et al (2012) Optical and near-infrared spectroscopy of the black hole GX 339-4 - I. A focus on the continuum in the low/hard and high/soft states. *Monthly Notices of the Royal Astronomical Society* 422:2202–2212. <https://doi.org/10.1111/j.1365-2966.2012.20763.x>, URL <https://ui.adsabs.harvard.edu/abs/2012MNRAS.422.2202R>, aDS Bibcode: 2012MNRAS.422.2202R

- Rahoui F, Coriat M, Lee JC (2014) Optical and near-infrared spectroscopy of the black hole gx 339-4 - ii. the spectroscopic content in the low/hard and high/soft states. *MNRAS*442:1610–1618. <https://doi.org/10.1093/mnras/stu977>, URL <http://adsabs.harvard.edu/abs/2014MNRAS.442.1610R>
- Rahoui F, Tomsick JA, Gandhi P, et al (2017) The nova-like nebular optical spectrum of v404 cygni at the beginning of the 2015 outburst decay. *MNRAS*465:4468–4481. <https://doi.org/10.1093/mnras/stw2890>, URL <http://adsabs.harvard.edu/abs/2017MNRAS.465.4468R>, [arXiv:1611.02278](https://arxiv.org/abs/1611.02278) [astro-ph.HE]
- Raman G, Maitra C, Paul B (2018) Observation of variable pre-eclipse dips and disc winds in the eclipsing LMXB XTE J1710-281. *MNRAS*477(4):5358–5366. <https://doi.org/10.1093/mnras/sty918>, [arXiv:1804.06073](https://arxiv.org/abs/1804.06073) [astro-ph.HE]
- Ratheesh A, Tombesi F, Fukumura K, et al (2021) A variable magnetic disc wind in the black hole X-ray binary GRS 1915+105? *A&A*646:A154. <https://doi.org/10.1051/0004-6361/202038621>, [arXiv:2012.09023](https://arxiv.org/abs/2012.09023) [astro-ph.HE]
- Reeves JN, O’Brien PT, Braito V, et al (2009) A Compton-thick Wind in the High-luminosity Quasar, PDS 456. *The Astrophysical Journal* 701:493–507. <https://doi.org/10.1088/0004-637X/701/1/493>, URL <https://ui.adsabs.harvard.edu/abs/2009ApJ...701..493R>, aDS Bibcode: 2009ApJ...701..493R
- Reis RC, Fabian AC, Ross RR, et al (2009) Determining the spin of two stellar-mass black holes from disc reflection signatures. *MNRAS*395(3):1257–1264. <https://doi.org/10.1111/j.1365-2966.2009.14622.x>
- Richards GT, Vanden Berk DE, Reichard TA, et al (2002) Broad Emission-Line Shifts in Quasars: An Orientation Measure for Radio-Quiet Quasars? *The Astronomical Journal* 124:1–17. <https://doi.org/10.1086/341167>, URL <https://ui.adsabs.harvard.edu/abs/2002AJ....124....1R>, aDS Bibcode: 2002AJ....124....1R
- Richards GT, Kruczek NE, Gallagher SC, et al (2011) Unification of Luminous Type 1 Quasars through C IV Emission. *The Astronomical Journal* 141:167. <https://doi.org/10.1088/0004-6256/141/5/167>, URL <https://ui.adsabs.harvard.edu/abs/2011AJ....141..167R>, aDS Bibcode: 2011AJ....141..167R
- Rogantini D, Costantini E, Zeegers ST, et al (2020) Magnesium and silicon in interstellar dust: X-ray overview. *A&A*641:A149. <https://doi.org/10.1051/0004-6361/201936805>, [arXiv:2007.03329](https://arxiv.org/abs/2007.03329) [astro-ph.HE]
- Rogantini D, Homan J, Plotkin RM, et al (2025) A persistent disk wind and variable jet outflow in the neutron-star low-mass X-ray binary GX 13+1. *arXiv e-prints* [arXiv:2504.05452](https://arxiv.org/abs/2504.05452). <https://doi.org/10.48550/arXiv.2504.05452>, [arXiv:2504.05452](https://arxiv.org/abs/2504.05452) [astro-ph.HE]

- Rózańska A, Madej J, Bagińska P, et al (2014) Disk emission and atmospheric absorption lines in black hole candidate 4U 1630-472. *Astronomy and Astrophysics* 562:A81. <https://doi.org/10.1051/0004-6361/201321567>, URL <https://ui.adsabs.harvard.edu/abs/2014A&A...562A..81R>, aDS Bibcode: 2014A&A...562A..81R
- Sadowski A, Narayan R, McKinney JC, et al (2014) Numerical simulations of supercritical black hole accretion flows in general relativity. *MNRAS*439(1):503–520. <https://doi.org/10.1093/mnras/stt2479>, [arXiv:1311.5900](https://arxiv.org/abs/1311.5900) [astro-ph.HE]
- Sala G, Greiner J, Ajello M, et al (2007) XMM-Newton and INTEGRAL observations of the black hole candidate <ASTROBJ>XTE J1817-330</ASTROBJ>. *A&A*473:561–568. <https://doi.org/10.1051/0004-6361:20077360>, [arXiv:0707.4155](https://arxiv.org/abs/0707.4155)
- Sánchez-Sierras J, Muñoz-Darias T (2020) Near-infrared emission lines trace the state-independent accretion disc wind of the black hole transient maxi j1820+070. *A&A*640:L3. <https://doi.org/10.1051/0004-6361/202038406>, URL <https://ui.adsabs.harvard.edu/abs/2020A&A...640L...3S>
- Sánchez-Sierras J, Muñoz-Darias T, Casares J, et al (2023a) Optical and near-infrared spectroscopy of the black hole transient 4u 1543-47 during its 2021 ultra-luminous state. *A&A*673:A104. <https://doi.org/10.1051/0004-6361/202245682>, URL <https://ui.adsabs.harvard.edu/abs/2023A&A...673A.104S>, [arXiv:2303.08837](https://arxiv.org/abs/2303.08837) [astro-ph.HE]
- Sánchez-Sierras J, Muñoz-Darias T, Motta SE, et al (2023b) Fast infrared winds during the radio-loud and x-ray obscured stages of the black hole transient grs 1915+105. *A&A*680:L16. <https://doi.org/10.1051/0004-6361/202348184>, URL <https://ui.adsabs.harvard.edu/abs/2023A&A...680L..16S>, [arXiv:2311.12933](https://arxiv.org/abs/2311.12933) [astro-ph.HE]
- Sasano M, Makishima K, Sakurai S, et al (2014) Suzaku view of the neutron star in the dipping source 4U 1822-37. *PASJ*66(2):35. <https://doi.org/10.1093/pasj/psu002>, [arXiv:1311.4618](https://arxiv.org/abs/1311.4618) [astro-ph.HE]
- Schipani P, Campana S, Claudi R, et al (2018) SOXS: a wide band spectrograph to follow up transients. eprint: [arXiv:1807.08828](https://arxiv.org/abs/1807.08828), p 107020F, <https://doi.org/10.1117/12.2307349>, URL <https://ui.adsabs.harvard.edu/abs/2018SPIE10702E..0FS>, aDS Bibcode: 2018SPIE10702E..0FS
- Schulz NS, Brandt WN (2002) Variability of the X-Ray P Cygni Line Profiles from Circinus X-1 near Zero Phase. *ApJ*572:971–983
- Schulz NS, Kallman TE, Galloway DK, et al (2008) The Variable Warm Absorber in Circinus X-1. *ApJ*672:1091–1102. <https://doi.org/10.1086/523809>, [arXiv:0709.3336](https://arxiv.org/abs/0709.3336)
- Schulz NS, Kallman TE, Heinz S, et al (2020) Origins of X-Ray Line Emissions in Circinus X-1 at Very Low X-Ray Flux. *ApJ*891(2):150. <https://doi.org/10.3847/1538-4357/ab6dc8>, [arXiv:2001.05638](https://arxiv.org/abs/2001.05638) [astro-ph.HE]

- Shakura NI, Sunyaev RA (1973) Black holes in binary systems. Observational appearance. *A&A*24:337–355
- Shidatsu M, Done C (2019) Application of the Thermal Wind Model to Absorption Features in the Black Hole X-Ray Binary H1743-322. *ApJ*885(2):112. <https://doi.org/10.3847/1538-4357/ab46b3>, [arXiv:1906.02469](https://arxiv.org/abs/1906.02469) [astro-ph.HE]
- Shidatsu M, Ueda Y, Nakahira S, et al (2013) The accretion disk and ionized absorber of the 9.7 hr dipping black hole binary maxi j1305-704. *ApJ*779(1):26. <https://doi.org/10.1088/0004-637X/779/1/26>, URL <https://ui.adsabs.harvard.edu/abs/2013ApJ...779...26S>, [arXiv:1310.0019](https://arxiv.org/abs/1310.0019) [astro-ph.HE]
- Shidatsu M, Done C, Ueda Y (2016) An optically thick disk wind in gro j1655-40? *ApJ*823:159. <https://doi.org/10.3847/0004-637X/823/2/159>, URL <http://adsabs.harvard.edu/abs/2016ApJ...823..159S>, [arXiv:1604.04346](https://arxiv.org/abs/1604.04346) [astro-ph.HE]
- Sidoli L, Oosterbroek T, Parmar AN, et al (2001) An XMM-Newton study of the X-ray binary MXB 1659-298 and the discovery of narrow X-ray absorption lines. *A&A*379:540–550. URL [http://cdsads.u-strasbg.fr/cgi-bin/nph-bib\\_query?bibcode=2001A%26A...379..540S&db\\_key=AST](http://cdsads.u-strasbg.fr/cgi-bin/nph-bib_query?bibcode=2001A%26A...379..540S&db_key=AST)
- Sidoli L, Parmar AN, Oosterbroek T, et al (2002) Discovery of complex narrow X-ray absorption features from the low-mass X-ray binary GX 13+1 with XMM-Newton. *A&A*385:940–946
- Soria R, Wu K, Johnston HM (1999) Optical spectroscopy of gx 339-4 during the high-soft and low-hard states - i. *MNRAS*310(1):71–77. <https://doi.org/10.1046/j.1365-8711.1999.02933.x>, URL <https://ui.adsabs.harvard.edu/abs/1999MNRAS.310...71S>
- Soria R, Wu K, Hunstead RW (2000) Optical spectroscopy of gro j1655-40. *ApJ*539:445–462. <https://doi.org/10.1086/309194>, URL <http://adsabs.harvard.edu/abs/2000ApJ...539..445S>
- Spencer RE (1979) A radio jet in SS433. *Nature* 282:483–484. <https://doi.org/10.1038/282483a0>, URL <https://ui.adsabs.harvard.edu/abs/1979Natur.282..483S>, aDS Bibcode: 1979Natur.282..483S
- Tetarenko BE, Lasota JP, Heinke CO, et al (2018) Strong disk winds traced throughout outbursts in black-hole x-ray binaries. *Nature*554:69–72. <https://doi.org/10.1038/nature25159>, URL <http://adsabs.harvard.edu/abs/2018Natur.554..69T>, [arXiv:1801.07203](https://arxiv.org/abs/1801.07203) [astro-ph.HE]
- Tomaru R, Done C, Odaka H, et al (2018) Monte Carlo simulations of the detailed iron absorption line profiles from thermal winds in X-ray binaries. *MNRAS*476(2):1776–1784. <https://doi.org/10.1093/mnras/sty336>, [arXiv:1802.07019](https://arxiv.org/abs/1802.07019) [astro-ph.HE]

- Tomaru R, Done C, Ohsuga K, et al (2019) The thermal-radiative wind in low-mass X-ray binary H1743-322: radiation hydrodynamic simulations. *MNRAS*490(3):3098–3111. <https://doi.org/10.1093/mnras/stz2738>, [arXiv:1905.11763](https://arxiv.org/abs/1905.11763) [astro-ph.HE]
- Tomaru R, Done C, Ohsuga K, et al (2020a) The thermal-radiative wind in low-mass X-ray binary H1743-322 - II. Iron line predictions from Monte Carlo radiation transfer. *MNRAS*494(3):3413–3421. <https://doi.org/10.1093/mnras/staa961>, [arXiv:1911.01660](https://arxiv.org/abs/1911.01660) [astro-ph.HE]
- Tomaru R, Done C, Ohsuga K, et al (2020b) The thermal-radiative wind in the neutron star low-mass X-ray binary GX 13 + 1. *MNRAS*497(4):4970–4980. <https://doi.org/10.1093/mnras/staa2254>, [arXiv:2007.14607](https://arxiv.org/abs/2007.14607) [astro-ph.HE]
- Tomaru R, Done C, Mao J (2023) What powers the wind from the black hole accretion disc in gro j1655-40? *MNRAS*518(2):1789–1801. <https://doi.org/10.1093/mnras/stac3210>, URL <https://ui.adsabs.harvard.edu/abs/2023MNRAS.518.1789T>
- Tomaru R, Done C, Odaka H, et al (2023) A different view of wind in X-ray binaries: the accretion disc corona source 2S 0921-630. *MNRAS*523(3):3441–3449. <https://doi.org/10.1093/mnras/stad1637>, [arXiv:2302.12638](https://arxiv.org/abs/2302.12638) [astro-ph.HE]
- Tomaru R, Done C, Odaka H (2024) X-ray polarization properties of thermal-radiative disc winds in binary systems. *MNRAS*527(3):7047–7054. <https://doi.org/10.1093/mnras/stad3649>, [arXiv:2308.07237](https://arxiv.org/abs/2308.07237) [astro-ph.HE]
- Tomaru R, Done C, Odaka H (2025) The detection of high X-ray polarization from an accretion disc corona source and its modelling via Monte Carlo radiation transfer simulation. *arXiv e-prints* [arXiv:2509.26147](https://arxiv.org/abs/2509.26147). <https://doi.org/10.48550/arXiv.2509.26147>, [arXiv:2509.26147](https://arxiv.org/abs/2509.26147) [astro-ph.HE]
- Tominaga M, Tsujimoto M, Ebisawa K, et al (2023) X-Ray Spectral Variations of Circinus X-1 Observed with NICER throughout an Entire Orbital Cycle. *ApJ*958(1):52. <https://doi.org/10.3847/1538-4357/ad0034>, [arXiv:2310.07158](https://arxiv.org/abs/2310.07158) [astro-ph.HE]
- Trueba N, Miller JM, Kaastra J, et al (2019) A Comprehensive Chandra Study of the Disk Wind in the Black Hole Candidate 4U 1630-472. *ApJ*886(2):104. <https://doi.org/10.3847/1538-4357/ab4f70>, [arXiv:1910.11243](https://arxiv.org/abs/1910.11243) [astro-ph.HE]
- Trueba N, Miller JM, Fabian AC, et al (2020) A Redshifted Inner Disk Atmosphere and Transient Absorbers in the Ultracompact Neutron Star X-Ray Binary 4U 1916-053. *ApJ*899(1):L16. <https://doi.org/10.3847/2041-8213/aba9de>, [arXiv:2008.01083](https://arxiv.org/abs/2008.01083) [astro-ph.HE]
- Trueba N, Miller JM, Fabian AC, et al (2022) A Spectroscopic Angle on Central Engine Size Scales in Accreting Neutron Stars. *ApJ*925(2):113. <https://doi.org/10.3847/1538-4357/ac3766>, [arXiv:2111.04764](https://arxiv.org/abs/2111.04764) [astro-ph.HE]

- Tsujimoto M, Enoto T, Díaz Trigo M, et al (2025) Outflowing photoionized plasma in Circinus X-1 using the high-resolution X-ray spectrometer Resolve onboard XRISM and the radiative transfer code cloudy. PASJ <https://doi.org/10.1093/pasj/psaf022>, [arXiv:2503.08254](https://arxiv.org/abs/2503.08254) [astro-ph.HE]
- Ueda Y, Inoue H, Tanaka Y, et al (1998) Detection of absorption-line features in the x-ray spectra of the galactic superluminal source gro j1655-40. ApJ492:782–787. <https://doi.org/10.1086/305063>, URL <http://adsabs.harvard.edu/abs/1998ApJ...492..782U>
- Ueda Y, Asai K, Yamaoka K, et al (2001) Discovery of an Iron K Absorption Line in the Low-Mass X-Ray Binary GX 13+1. ApJ556:L87–L90
- Ueda Y, Murakami H, Yamaoka K, et al (2004) Chandra High-Resolution Spectroscopy of the Absorption-Line Features in the Low-Mass X-Ray Binary GX 13+1. ApJ609:325–334
- Ueda Y, Yamaoka K, Remillard R (2009) GRS 1915+105 in “Soft State”: Nature of Accretion Disk Wind and Origin of X-ray Emission. ApJ695(2):888–899. <https://doi.org/10.1088/0004-637X/695/2/888>, [arXiv:0901.1982](https://arxiv.org/abs/0901.1982) [astro-ph.HE]
- van den Eijnden J, Degenaar N, Pinto C, et al (2018) The very faint X-ray binary IGR J17062-6143: a truncated disc, no pulsations, and a possible outflow. MNRAS475(2):2027–2044. <https://doi.org/10.1093/mnras/stx3224>
- van der Klis M (2006) Rapid X-ray Variability. Cambridge Astrophysics Series pp 39–112
- van Peet JCA, Costantini E, Méndez M, et al (2009) Properties of the ionised plasma in the vicinity of the neutron-star X-ray binary EXO 0748-676. A&A497(3):805–813. <https://doi.org/10.1051/0004-6361/200811181>, [arXiv:0902.4470](https://arxiv.org/abs/0902.4470) [astro-ph.GA]
- Vincentelli FM, Muñoz-Darias T (2025) Accretion disc winds imprint distinct signatures in the optical variability spectrum of black hole transients. A&A695:A181. <https://doi.org/10.1051/0004-6361/202452634>, [arXiv:2501.04087](https://arxiv.org/abs/2501.04087) [astro-ph.HE]
- Vincentelli FM, Neilsen J, Tetarenko AJ, et al (2023) A shared accretion instability for black holes and neutron stars. Nature615(7950):45–49. <https://doi.org/10.1038/s41586-022-05648-3>, URL <https://ui.adsabs.harvard.edu/abs/2023Natur.615...45V>, [arXiv:2303.00020](https://arxiv.org/abs/2303.00020) [astro-ph.HE]
- Wang J, Kara E, García JA, et al (2024) The 2022 Outburst of IGR J17091?3624: Connecting the Exotic GRS 1915+105 to Standard Black Hole X-Ray Binaries. The Astrophysical Journal 963:14. <https://doi.org/10.3847/1538-4357/ad1595>, URL <https://ui.adsabs.harvard.edu/abs/2024ApJ...963...14W>, aDS Bibcode: 2024ApJ...963...14W

- Wang Y, Méndez M (2016) The XMM-Newton spectra of the 2012 outburst of the black hole candidate 4U 1630-47 revisited. *MNRAS*456(2):1579–1586. <https://doi.org/10.1093/mnras/stv2814>, [arXiv:1512.00512](https://arxiv.org/abs/1512.00512) [astro-ph.HE]
- Wang Y, Ji L, García JA, et al (2021) A Variable Ionized Disk Wind in the Black Hole Candidate EXO 1846-031. *ApJ*906(1):11. <https://doi.org/10.3847/1538-4357/abc55e>, [arXiv:2010.14662](https://arxiv.org/abs/2010.14662) [astro-ph.HE]
- Waters T, Proga D, Dannen R (2021) Multiphase AGN Winds from X-Ray-irradiated Disk Atmospheres. *ApJ*914(1):62. <https://doi.org/10.3847/1538-4357/abf6e6>, [arXiv:2101.09273](https://arxiv.org/abs/2101.09273) [astro-ph.GA]
- Weisskopf MC, Soffitta P, Baldini L, et al (2022) The Imaging X-Ray Polarimetry Explorer (IXPE): Pre-Launch. *Journal of Astronomical Telescopes, Instruments, and Systems* 8:026002. <https://doi.org/10.1117/1.JATIS.8.2.026002>, URL <https://ui.adsabs.harvard.edu/abs/2022JATIS...8b6002W>, aDS Bibcode: 2022JATIS...8b6002W
- Woods DT, Klein RI, Castor JI, et al (1996) X-Ray-heated Coronae and Winds from Accretion Disks: Time-dependent Two-dimensional Hydrodynamics with Adaptive Mesh Refinement. *ApJ*461:767. <https://doi.org/10.1086/177101>
- Wu H, Wang W, Sai N (2023) Accretion disk wind during the outburst of the stellar-mass black hole MAXI J1348-630. *Journal of High Energy Astrophysics* 37:25–33. <https://doi.org/10.1016/j.jheap.2022.12.001>, URL <https://ui.adsabs.harvard.edu/abs/2023JHEAp..37...25W>, aDS Bibcode: 2023JHEAp..37...25W
- Xiang J, Lee JC, Nowak MA, et al (2009) The Accretion Disk Corona and Disk Atmosphere of 4U 1624-490 as Viewed by the Chandra-High Energy Transmission Grating Spectrometer. *ApJ*701:984–993. <https://doi.org/10.1088/0004-637X/701/2/984>, [arXiv:0905.3925](https://arxiv.org/abs/0905.3925) [astro-ph.HE]
- XRISM collaboration (2025) Structured ionized winds shooting out from a quasar at relativistic speeds. arXiv e-prints [arXiv:2505.09171](https://arxiv.org/abs/2505.09171). <https://doi.org/10.48550/arXiv.2505.09171>, [arXiv:2505.09171](https://arxiv.org/abs/2505.09171) [astro-ph.HE]
- XRISM collaboration, Audard M, Awaki H, et al (2025) Stratified wind from a super-Eddington X-ray binary is slower than expected. *Nature* in press [arXiv:2509.14555](https://arxiv.org/abs/2509.14555). <https://doi.org/10.48550/arXiv.2509.14555>, [arXiv:2509.14555](https://arxiv.org/abs/2509.14555) [astro-ph.HE]
- Xu Y, Harrison FA, Tomsick JA, et al (2020) Studying the Reflection Spectra of the New Black Hole X-Ray Binary Candidate MAXI J1631-479 Observed by NuSTAR: A Variable Broad Iron Line Profile. *The Astrophysical Journal* 893:30. <https://doi.org/10.3847/1538-4357/ab7dc0>, URL <https://ui.adsabs.harvard.edu/abs/2020ApJ...893...30X>, aDS Bibcode: 2020ApJ...893...30X

- Yoneyama T, Dotani T (2023) X-ray spectroscopy of the accretion disk corona source 2S 0921-630 with Suzaku archival data. PASJ75(1):30–36. <https://doi.org/10.1093/pasj/psac086>, [arXiv:2210.10792](https://arxiv.org/abs/2210.10792) [astro-ph.HE]
- Younes G, Kouveliotou C, Grefenstette BW, et al (2015) Simultaneous NuSTAR/Chandra Observations of the Bursting Pulsar GRO J1744-28 during Its Third Reactivation. ApJ804(1):43. <https://doi.org/10.1088/0004-637X/804/1/43>, [arXiv:1502.05982](https://arxiv.org/abs/1502.05982) [astro-ph.HE]
- Zeegers ST, Costantini E, Rogantini D, et al (2019) Dust absorption and scattering in the silicon K-edge. A&A627:A16. <https://doi.org/10.1051/0004-6361/201935050>, [arXiv:1905.06560](https://arxiv.org/abs/1905.06560) [astro-ph.GA]
- Zhang L, Stone JM, Mullen PD, et al (2025) Radiation GRMHD Models of Accretion onto Stellar-Mass Black Holes: I. Survey of Eddington Ratios. arXiv e-prints arXiv:2506.02289. <https://doi.org/10.48550/arXiv.2506.02289>, [arXiv:2506.02289](https://arxiv.org/abs/2506.02289) [astro-ph.HE]
- Zhang SN, Liao J, Yao Y (2012) Measuring the black hole masses in accreting X-ray binaries by detecting the Doppler orbital motion of their accretion disc wind absorption lines. MNRAS421(4):3550–3556. <https://doi.org/10.1111/j.1365-2966.2012.20579.x>, [arXiv:1201.3451](https://arxiv.org/abs/1201.3451) [astro-ph.HE]
- Zhang Z, Makishima K, Sakurai S, et al (2014) Probing the accretion scheme of the dipping X-ray binary 4U 1915-05 with Suzaku. PASJ66(6):120. <https://doi.org/10.1093/pasj/psu117>, [arXiv:1409.2091](https://arxiv.org/abs/1409.2091) [astro-ph.HE]
- Zhang Z, Bambi C, Liu H, et al (2024) Variable Ionized Disk Winds in MAXI J1803-298 Revealed by NICER. The Astrophysical Journal 975:22. <https://doi.org/10.3847/1538-4357/ad7b29>, URL <https://ui.adsabs.harvard.edu/abs/2024ApJ...975...22Z>, aDS Bibcode: 2024ApJ...975...22Z
- Zoghbi A, Miller JM, King AL, et al (2016) Disk-Wind Connection during the Heartbeats of GRS 1915+105. ApJ833(2):165. <https://doi.org/10.3847/1538-4357/833/2/165>, [arXiv:1610.05772](https://arxiv.org/abs/1610.05772) [astro-ph.HE]